Final Technical Progress Report,
Reporting Period: October 1, 1997 through September 30, 1998

IMPROVED METHODS FOR WATER SHUTOFF

Submitted to

BDM-OKLAHOMA/
THE U.S. DEPARTMENT OF ENERGY

by

Randall S. Seright

New Mexico Petroleum Recovery Research Center
New Mexico Institute of Mining and Technology
Socorro, New Mexico 87801

September 30, 1998

Prime Contract Number: DE-AC22-94PC91008
Subcontract Number: G4S60330

BDM Subcontract Administrator: David Fuqua
BDM Program Manager: Mike Madden

NM PRRC Contributors: Jenn-Tai Liang, Richard Schrader,
John Hagstrom II, Jin Liu, Kathryn Wavrik

PRRC Report 98-26

DISCLAIMER

This report was prepared as an account of work sponsored by an agency of the United States Government. Neither the United States Government nor any agency thereof, nor any of their employees, makes any warranty, expressed or implied, or assumes any legal liability or responsibility for the accuracy, completeness, or usefulness of any information, apparatus, product, or process disclosed, or represents that its use would not infringe privately owned rights. Reference herein to any specific commercial product, process, or service by trade name, trademark, manufacturer, or otherwise does not necessarily constitute or imply its endorsement, recommendation, or favoring by the United States Government or any agency thereof. The views and opinions of authors expressed herein do not necessarily state or reflect those of the United States Government.

ABSTRACT

In the United States, more than 20 billion barrels of salt water are produced each year during oilfield operations. A tremendous economic incentive exists to reduce water production if that can be accomplished without significantly sacrificing hydrocarbon production. For each 1% reduction in water production, the cost-savings to the oil industry could be between $50,000,000 and $100,000,000 per year. Reduced water production would result directly in improved oil recovery efficiency in addition to reduced oil-production costs. A substantial positive environmental impact could also be realized if significant reductions are achieved in the amount of water produced during oilfield operations.

This three-year research project had three objectives. The first objective was to identify chemical blocking agents that will (a) during placement, flow readily through fractures without penetrating significantly into porous rock and without "screening out" or developing excessive pressure gradients and (b) at a predictable and controllable time, become immobile and resist breakdown upon exposure to moderate to high pressure gradients. The second objective was to identify schemes that optimize placement of the above blocking agents. The third objective was to explain why gels and other chemical blocking agents reduce permeability to one phase (e.g., water) more than that to another phase (e.g., oil or gas). We also wanted to identify conditions that maximize this phenomenon. This project consisted of three tasks, each of which addressed one of the above objectives. This report describes work performed during the third and final period of the project.

During this three-year project, we:

1. Developed a procedure and software for sizing gelant treatments in hydraulically fractured production wells.
2. Developed a method (based on interwell tracer results) to determine the potential for applying gel treatments in naturally fractured reservoirs.
3. Characterized gel properties during extrusion through fractures.
4. Developed a method to predict gel placement in naturally fractured reservoirs.
5. Made progress in elucidating the mechanism for why some gels can reduce permeability to water more than that to oil.
6. Demonstrated the limitations of using WOR diagnostic plots to distinguish between channeling and coning.
7. Proposed a philosophy for diagnosing and attacking water-production problems.

The Executive Summary provides a brief description of our accomplishments in each of the above areas. This project was supported financially by BDM-Oklahoma, the U.S. Department of Energy (National Petroleum Technology Office), and a consortium of 17 oil and service companies. Technology transfer activities are detailed in Appendix C.

TABLE OF CONTENTS

TABLE OF FIGURES

LIST OF TABLES

ACKNOWLEDGMENTS

Financial support for this work is gratefully acknowledged from the United States Department of Energy (National Petroleum Technology Office), BDM-Oklahoma, ARCO, British Petroleum, Chevron, Chinese Petroleum Corporation, Conoco, Exxon, Halliburton, Marathon, Norsk Hydro, Phillips Petroleum, Saga, Schlumberger-Dowell, Shell, Statoil, and Texaco. I greatly appreciate the efforts of those individuals who contributed to this project. Richard Schrader performed most of the experimental work described in Chapters 2 and 3. During this work, Kathryn Wavrik and John Hagstrom determined the polymer concentrations, and the New Mexico Bureau of Mines Chemistry Laboratory determined the chromium concentrations. Dr. Jenn-Tai Liang played the major role for the work described in Chapters 4 and 5. John Hagstrom performed the experiments described in Chapter 5. I especially appreciate the thorough review of this manuscript by Julie Ruff.

EXECUTIVE SUMMARY

This report describes work performed during the third and final period of the project, "Improved Methods for Water Shutoff." This project had three general objectives. The first objective was to identify chemical blocking agents that will (a) during placement, flow readily through fractures without penetrating significantly into porous rock and without "screening out" or developing excessive pressure gradients and (b) at a predictable and controllable time, become immobile and resist breakdown upon exposure to moderate to high pressure gradients. The second objective was to identify schemes that optimize placement of the above blocking agents. The third objective was to explain why gels and other chemical blocking agents reduce permeability to one phase (e.g., water) more than that to another phase (e.g., oil or gas). We also wanted to identify conditions that maximize this phenomenon.

SUMMARY OF TECHNICAL ACCOMPLISHMENTS

In this project, we:

1. Developed a procedure and software for sizing gelant treatments in hydraulically fractured production wells.
2. Developed a method (based on interwell tracer results) to determine the potential for applying gel treatments in naturally fractured reservoirs.
3. Characterized gel properties during extrusion through fractures.
4. Developed a method to predict gel placement in naturally fractured reservoirs.
5. Made progress in elucidating the mechanism for why some gels can reduce permeability to water more than that to oil.
6. Demonstrated the limitations of using WOR diagnostic plots to distinguish between channeling and coning.
7. Proposed a philosophy for diagnosing and attacking water-production problems.

Sizing Gelant Treatments in Hydraulically Fractured Production Wells

One-third of all newly drilled wells are intentionally fractured. Often, when hydraulic fracturing stimulates production wells, the fracture unintentionally extends through shale or calcite barriers into water zones, causing substantially increased water production. Gelant treatments have frequently been applied in an attempt to correct this problem. However, the design of the gelant volumes for these applications has been strictly empirical, and consequently, the success rates for these treatments have been erratic. We developed a sound engineering basis for sizing gelant treatments. We presented a simple 11-step procedure for sizing gelant treatments in hydraulically fractured production wells. We incorporated this procedure in user-friendly graphical-user-interface software. Details can be found in SPE paper 38835 and in our second annual report (DOE/PC/91008-4). The software can be downloaded from our web site at http://baervan.nmt.edu/ResSweepEffic/reservoir.htm. We hope that our method will increase confidence in and applications of gel technology for reducing water production in hydraulically fractured production wells.

Potential for Gel Treatments in Naturally Fractured Reservoirs

We considered some of the reservoir variables that affect the severity of channeling and the potential of gel treatments for reducing channeling through naturally fractured reservoirs. We

performed extensive tracer and gel placement studies using two different simulators. We showed that gel treatments have the greatest potential when the conductivities of fractures that are aligned with direct flow between an injector-producer pair are at least 10 times the conductivity of off-trend fractures. Gel treatments also have their greatest potential in reservoirs with moderate to large fracture spacing. Produced tracer concentrations from interwell tracer studies can help identify reservoirs that are predisposed to successful gel applications. Our simulation studies also show how tracer transit times can be used to estimate the conductivity of the most direct fracture. The effectiveness of gel treatments should be insensitive to fracture spacing for fractures that are aligned with the direct flow direction. The effectiveness of gel treatments increases with increased fracture spacing for fractures that are not aligned with the direct flow direction. Details of this work can be found in SPE paper 39802 and our second annual report (DOE/PC/91008-4). After further development and testing, we hope this work will lead to the first reliable method to quantify the type of naturally fractured reservoir where gel treatments will be effective.

Gel Properties in Fractures

Some of the most successful water-shutoff treatments in fractured reservoirs used relatively large volumes of gel that extruded through fractures during the gel placement process. To determine gel properties in fractures, we performed many experiments where one-day-old Cr(III)-acetate-HPAM gels were extruded through 2.7- to 4-ft-long fractures. These experiments showed that gel extrusion through fractures occurs at an unexpectedly low rate if the fracture conductivity or width is sufficiently small. We demonstrated that this low rate of gel propagation occurs because the gel dehydrates as it extrudes through fractures. Our experiments used a Cr(III)-acetate-HPAM gel that is commonly injected during field applications. In fractures with conductivities between 1 and 242 darcy-ft (effective average widths between 0.006 and 0.04 in.), the gel was concentrated (or dehydrated) and gel propagation was delayed by factors typically between 20 and 40 during the extrusion process. The gel dehydration effect became less pronounced as the fracture width increased. However, a fracture width around 0.4 in. was required to completely eliminate the effect.

For a given fracture conductivity, a minimum pressure gradient (i.e., a yield stress) was necessary to extrude gel through the fracture. A correlation was developed that provides a good estimate of the required pressure gradient for gel extrusion for a wide range of fracture conductivity and width values. For example, to extrude the gel with a pressure gradient less than 1 psi/ft, the fracture width should be at least 0.1 in. During gel extrusion through fractures of a given width, the pressure gradient and degree of gel dehydration were nearly independent of position and velocity during both radial and linear flow. During brine injection after gel placement, no significant gel washout occurred for fracture widths up to 0.4 in. For fractures with widths greater than 0.1 inches, the gel did not completely heal the fracture (i.e., reduce its flow capacity to near zero). However, the fracture conductivities were reduced substantially.

Various studies were performed to understand the mechanism for gel propagation through fractures. For example, when compressing a gel against a filter, some free chromium and HPAM left the gel and passed through the filter along with water. However, expressed relative to the chromium and HPAM concentrations in the original gel, the relative chromium concentration in the filtrate was greater than the relative HPAM concentration. We also found that the pressure

gradients and dehydration factors during extrusion of gel through fractures were effectively the same for fractures in 650-md Berea sandstone as in 50-md sandstone. The gel effluent from a fracture had the same composition and appearance as that for the injected gel, even though a concentrated gel was found in the fracture. During gel extrusion, measurements of water leakoff along a fracture suggested that a filter cake of concentrated gel formed gradually along the length of the fracture. The gel could extrude through a 28-darcy (20-30 mesh) quartz sandpack, but the pressure gradient was quite high (~200 psi/ft). Gel produced from the first two taps in the sandpack had the same composition and appearance as that for the injected gel. In contrast, a rubbery gel was found on the inlet face of the sandpack that was about 10 times more concentrated than the injected gel. A model was proposed to explain how gel propagates through fractures. Basically, this model assumed that elements of gel experience repeated sequences where the gel elements (a) elastically deform to a critical point, (b) experience failure at or near the fracture wall, and (c) after failure, jump ahead along the fracture, while the elastic forces relax. This model was shown to account for several aspects of gel behavior during extrusion through fractures. A relationship was found between final gel composition in the fracture and the pressure gradient required for gel extrusion through a fracture. The final chromium and HPAM concentrations varied with the one-third power of the applied pressure gradient. For a given concentrated gel, the final HPAM/chromium concentration ratio was consistent with stoichiometric HPAM/chromium crosslinking, assuming that the HPAM had an 8% degree of hydrolysis and two carboxylate groups were tied to each chromium atom.

Details of this work can be found in SPE paper 39957, *SPEPF* (Feb. 1997) 59-65, in our previous annual reports (DOE/PC/91008-1 and DOE/PC/91008-4), and in Chapter 3 of this report. Characterization of gel properties during extrusion through fractures is crucial in order to develop models to predict gel placement in fractured reservoirs.

Gel Placement in Naturally Fractured Injection Wells

A model was developed that predicts areal gel front profiles and distances of gel penetration as a function of gel volume injected into naturally fractured wells. This model incorporates several key features of gel extrusion through fractures, including yield-stress and gel dehydration phenomena. Important input parameters for the model include pressure drop between wells and fracture conductivities and spacings for both on-trend and off-trend fractures. Our model predicts that the general outline or shape of the areal gel front profiles depends primarily on the ratio of conductivity of on-trend fractures to the conductivity of off-trend fractures. A laboratory experiment was performed to test the model. Significant deviations were noted between the predicted and experimental shapes of the gel profiles. However, the volume of gel required for breakthrough was reasonably close to the predicted value. Details of our work can be found in Chapter 2 of this report. Prediction of gel placement is crucial to assess whether a gel treatment will ultimately improve sweep efficiency. Also, prediction of gel placement is a necessary step toward determining the proper volume of gel to inject in a given application.

Disproportionate Permeability Reduction

The ability of blocking agents to reduce the permeability to water much more than to oil is critical to the success of water-shutoff treatments in production wells if hydrocarbon-productive zones

cannot be protected during placement. Results from the literature and our own experimental work have shown that many polymers and gels exhibit this disproportionate permeability reduction.

During our project, we examined several mechanisms that were proposed to explain the disproportionate permeability reduction. At present, the most promising mechanism combines the "wall-effect" mechanism of Zaitoun *et al.*[55] and the "gel-droplet" model of Nilsson *et al.*[56] Additional work is needed to test the validity of this model.

Other mechanisms showed some promise, but various experimental results argue against them as a general explanation for the disproportionate permeability reduction. For example, wettability can play an important role in the phenomenon. Hydrophilic polymers or gel components can make porous media more water-wet, thus altering relative permeability characteristics.[55,56] However, the disproportionate permeability reduction occurs even without wettability changes. Therefore, wettability effects do not provide a general explanation for the phenomenon.

Another promising mechanism was the "segregated-pathway" mechanism.[48,53] This mechanism relied on oil and water basically following separate pathways on a microscopic scale in porous media. The mechanism was consistent with many experimental observations. However, it incorrectly predicted that simultaneous injection of oil and a water-based gelant should generally enhance the disproportionate permeability reduction.

In another mechanism, we speculated that a balance between capillary forces and gel elasticity might contribute to disproportionate permeability reduction.[53] However, experimental results indicated that this mechanism is valid only in micromodels and small glass tubes, not in porous rock.

Our studies[48] ruled out gravity effects as a viable mechanism because the disproportionate permeability reduction was insensitive to core orientation and water-oil density differences. Also, lubrication effects were judged not to be the underlying cause of the phenomenon because it could occur to the same extent over a wide range of non-wetting-phase viscosities (using fluids ranging from low-viscosity gases to 31-cp oils).[48,50] Furthermore, several experiments demonstrated that gel shrinking and swelling are not the underlying cause of the disproportionate permeability reduction.[48,53] A few other mechanisms were also examined and discounted.[1,2,48,53]

Additional work is needed to predict and maximize the disproportionate-permeability-reduction phenomenon, especially for field applications. Details of our work to date can be found in our annual reports (DOE/PC/91008-1 and DOE/PC/91008-4) and Chapter 5 of this report. With an understanding of the disproportionate permeability reduction, we hope to identify ways to achieve maximum permeability reduction to water and minimum permeability reduction to hydrocarbon. Also, it will improve our ability to predict and control the phenomenon. These achievements, in turn, will dramatically increase the applicability of gel treatments for water shutoff in production wells because concern about gel placement should be diminished.

Water/Oil Ratio Diagnostic Plots

Water/oil ratio (WOR) diagnostic plots were proposed (by others) as a method to diagnose excessive water-production mechanisms. This method was said to be capable of distinguishing whether a production well is experiencing premature water breakthrough caused by water coning or channeling through high-permeability layers. According to this method, gradually increasing WOR curves with negative derivative slopes are unique for coning problems, and rapidly increasing WOR curves with positive derivative slopes are indicative of a channeling problem. To investigate whether diagnostic plots can be applied generally or if they have limitations, reservoir models were built for water coning and channeling, respectively, and a sensitivity analysis was performed using numerical simulation. Reservoir and fluid parameters were varied to examine WOR and WOR derivative behavior for both coning and channeling production problems. The results from this study demonstrated that multilayer channeling problems can easily be mistaken as bottomwater coning, and vice versa, if WOR diagnostic plots are used alone to identify an excessive water-production mechanism. Hence, WOR diagnostic plots can easily be misinterpreted and should therefore not be used alone to diagnose the specific cause of a water-production problem. Details of this work can be found in our second annual report (DOE/PC/91008-4).

In a previous study using analytical coning models, we showed that gels are rarely expected to be effective in suppressing water coning in unfractured production wells.[20,21] A critical examination of published field cases and simulation studies using numerical coning models confirms our earlier findings. Details of this work can be found in Chapter 4 of this report.

Proposed Philosophy for Diagnosing and Attacking Water-Production Problems

An important development from our project was a philosophy toward approaching water-shutoff problems. This philosophy recognizes that (1) many types of water-production problems exist, (2) no single water-shutoff method will solve all problems, and (3) producers have limited resources for diagnosing water-production problems. The two key elements of our philosophy are (1) diagnose and solve the easiest water problems first and (2) start the diagnosis process using information that you already have. Implementing this philosophy requires a priority listing of types of water problems, from least difficult to most difficult. Based on work in this and previous DOE-sponsored projects, we developed that prioritization. (It can be found on our web site at http://baervan.nmt.edu/ResSweepEffic/reservoir.htm. It is also described in Ref. 51 of this report.) Since our introduction of this philosophy at an SPE Workshop in Dunkeld, Scotland in May, 1997, talks on this topic have been requested and presented at Anchorage (August 1997), Houston (August and September 1997), Calgary (October 1997), Dallas (November 1997), and Leipzig (June 1998). This philosophy also is a central theme of our newly developed SPE Short Course, “Water Shutoff,” which was first presented at the 1998 SPE/DOE IOR Symposium.

When deciding whether or not to apply a gel treatment, a chronic problem for oil companies is limited resources to properly diagnosis the cause of water production. By providing these companies with a prioritization of which diagnostic methods to apply first and which production problems to look for first, our philosophy provides a cost-effective approach to ensure that the problems are correctly identified. In turn, by increasing the frequency for proper diagnosis of

water production problems, we increase the probability that an effective solution will be attempted, and we increase the success rates for those treatments.

Suggestions for Future Work

Three immediate needs become evident from this work. First, a need exists to develop a capability to predict and optimize the ability of gels to reduce permeability to water more than that to oil or gas. Second, a need exists to develop procedures for optimizing blocking-agent placement in wells where hydraulic fractures cause channeling problems. Third, a need exists to develop procedures to optimize blocking-agent placement in naturally fractured reservoirs. These items will be addressed in our next DOE-sponsored research project, “Using Chemicals to Optimize Conformance Control in Fractured Reservoirs.”

1. INTRODUCTION

In the United States, more than 20 billion barrels of water are produced each year during oilfield operations. Today, the cost of water disposal is typically between $0.25 and $0.50 per bbl for pipeline transport and $1.50 per bbl for trucked water. Therefore, a tremendous economic incentive exists to reduce water production if that can be accomplished without significantly sacrificing hydrocarbon production. For each 1% reduction in water production, the cost-savings to the oil industry could be between $50,000,000 and $100,000,000 per year. Reduced water production would result directly in improved oil recovery (IOR) efficiency in addition to reduced oil-production costs. A substantial positive environmental impact could also be realized if significant reductions are achieved in the amount of water produced during oilfield operations.

In an earlier project, we identified fractures (either naturally or artificially induced) as a major factor that causes excess water production and reduced oil recovery efficiency, especially during waterfloods and IOR projects. We found fractures to be a channeling and water-production problem that has a high potential for successful treatment by gels and certain other chemical blocking agents. By analogy, these blocking materials have a high potential for treating narrow channels behind pipe and small casing leaks. We also determined that the ability of blocking agents to reduce permeability to water much more than that to oil is critical to the success of these blocking treatments in production wells if zones are not isolated during placement of the blocking agent.

Objectives

This project had three general objectives. The first objective was to identify chemical blocking agents that will (a) during placement, flow readily through fractures without penetrating significantly into porous rock and without "screening out" or developing excessive pressure gradients and (b) at a predictable and controllable time, become immobile and resist breakdown upon exposure to moderate to high pressure gradients. The second objective was to identify schemes that optimize placement of the above blocking agents. The third objective was to explain why gels and other chemical blocking agents reduce permeability to one phase (e.g., water) more than that to another phase (e.g., oil or gas). We also wanted to identify conditions that maximize this phenomenon.

Report Content

This report describes work performed during the third and final year of the project. Results from the first two periods of the project can be found in Refs. 1 and 2. In Chapter 2, we introduce an engineering-based approach to sizing gel treatments in naturally fractured injection wells. In Chapter 3, we report experimental results from studies of gel properties in fractures. In Chapter 4, we review recent literature to establish whether gel and foam treatments have successfully mitigated water or gas coning in field applications. Finally, in Chapter 5, we investigate the mechanism responsible for gels reducing the permeability to water more than that to oil.

2. GEL PLACEMENT IN NATURALLY FRACTURED RESERVOIRS

Objective

Some of the most successful gel treatments to date were applied in naturally fractured injection wells.[3-6] Reportedly, the most effective treatments involved injection of large volumes of gel. However, optimum sizing procedures for these treatments are currently unknown. The objective of this report is to introduce an engineering-based approach to predict gel placement in naturally fractured injection wells. This represents a first step toward a methodology of treatment sizing.

Review of Previous Findings

In several fields, fairly large volumes of gel were injected—i.e., from 4,000 to 37,000 bbls of gel per injection well. These gel treatments included applications by Marathon in nine fields in the Big Horn Basin of Wyoming,[3] by Amoco in the Wertz field in Wyoming,[4] and by Chevron in the Rangely field in Colorado.[5] (Also, Chevron recently applied gelled foam treatments in the Rangely field using as much as 45,000 barrels of blocking agent per well.[7])

Minimum Pressure Gradient for Extrusion. In developing a methodology to predict gel placement, several laboratory and field observations must be considered. First, in the field applications, the times required to inject the gel were 10 to 100 times greater than the gelation times.[3-5] Therefore, the gels extruded through the fractures during most of the placement process. Second, laboratory studies[8-10] reveal that gels generally require the application of a minimum pressure gradient (i.e., a yield stress) before they will extrude through a given fracture. The pressure gradient required to extrude a given gel through a fracture decreases with increased fracture conductivity and width.[10] Fig. 1 shows this relation for a Cr(III)-acetate-HPAM gel that was typical of that used in the above field applications. (The gel used to generate Fig. 1 contained 0.5% Allied Colloids 935 polyacrylamide crosslinked by 0.0417% Cr(III)-acetate).

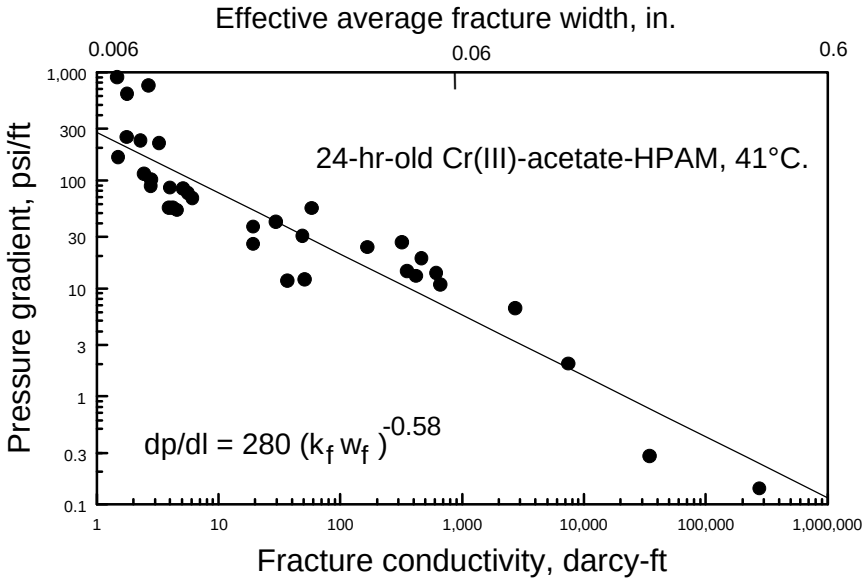

Fig. 1—Pressure gradient required to extrude a gel through fractures.

For the data in Fig. 1, the pressure gradient (*dp/dl*, in psi/ft) required to extrude the gel was correlated to fracture conductivity ($k_f w_f$, in darcy-ft) using Eq. 1:

$$dp/dl = 280\ (k_f w_f)^{-0.58} \quad \text{..... (1)}$$

Pressure gradients in reservoirs are often on the order of 1 psi/ft. The above equation suggests that the fracture conductivity must be at least 15,000 darcy-ft and the fracture width must be at least 0.1 inches in order for the gel to extrude with a pressure gradient of 1 psi/ft or less. Interestingly, injectivity problems were rarely encountered during gel injection for the above field applications.[3-6] This observation coupled with the results from our extrusion experiments suggests that the fractures were fairly wide in these field applications.

Delay for Gel Propagation. Another interesting observation during these field applications was that gel rarely was detected in offset producers even though the gel volume injected was over 10 times the volume associated with breakthrough of a water or gas tracer. In particular, Chevron reported that gel breakthrough was detected in only one of 44 large-volume gel treatments.[5] One can envision several reasons why this result would occur. For example, before gel injection, a water or gas tracer is expected to flow directly from the injector to the producer through the most-direct fracture. In contrast, the viscous gel may be diverted into secondary fractures during the injection process (because of the low mobility ratio associated with gel injection). Thus, a significantly greater gel volume must be injected to achieve breakthrough at the production well.

Another possible explanation can be found in the results from laboratory experiments (see Table 1). We found that gels can concentrate or dehydrate as they extrude through fractures.[10] In other words, much of the water can leave the gel and leak off through the fracture faces, but the crosslinked polymer remains behind in a more concentrated form in the fracture. For example, a Cr(III)-acetate-HPAM gel concentrated by a factor of about 40 during extrusion through a fracture with a conductivity of about 1 darcy-ft and an effective average width of 0.0063 inches.[10] The degree of gel dehydration decreased with increased fracture conductivity and width. However, for this particular gel, the fracture width must be at least 0.4 inches to completely eliminate this dehydration effect. Thus, gel dehydration provides another reason why gel transport through a fracture can be much slower than that for a water or gas tracer.

Table 1—Gel Dehydration During Extrusion Through Fractures

Conductivity, darcy-ft	Width, inches	Pressure gradient, psi/ft	Gel breakthrough, fracture volumes
1.14	0.0063	750	40
4.5	0.0100	65	35
242	0.0376	20	21
568	0.0500	11	7.7
2,730	0.084	6.5	4.8
7,500	0.12	2.0	5.4
34,700	0.2	0.28	1.8
277,000	0.4	0.14	1.1

Incremental Oil Versus Treatment Volume. During field applications of gel treatments in naturally fractured injection wells, incremental oil recovery appeared to increase with increased volume of gel injected (Fig. 2). For Marathon's treatments, incremental oil recoveries ranged from 0 bbls when injecting 37 bbl of gel per foot of net pay (not shown in Fig. 2) to 718,000 bbls when injecting 670 bbl of gel per foot of net pay.[3] For Amoco's treatments, incremental oil recoveries ranged from 35,000 bbls when injecting 23 bbl of gel per foot of net pay to 140,000 bbls when injecting 42 bbl of gel per foot of net pay.[4] For Chevron's treatments, oil recovery data were not provided on a well-by-well basis. However, on average (for 44 treatments), the incremental oil recovery per treatment was 15,600 bbls for an average treatment size of 66 bbls per foot of net pay.[5] Although Marathon, Amoco, and Chevron all noted that larger treatments resulted in greater oil recoveries, we do not have a good understanding of the relation between treatment size and oil recovery. The issue is further complicated in that a variety of responses to gel treatments have been noted. For example, in their Rangely CO_2 flood, Chevron[5] reported eight different types of responses to gel treatments, including (1) no apparent impact on injection or production, (2) production smoothing, (3) oil rate increase, (4) reduction in water production, (5) reduction in gas production, (6) areal sweep improvement, (7) reduction or elimination of oil decline rate, and (8) improved pattern CO_2 retention and utilization.

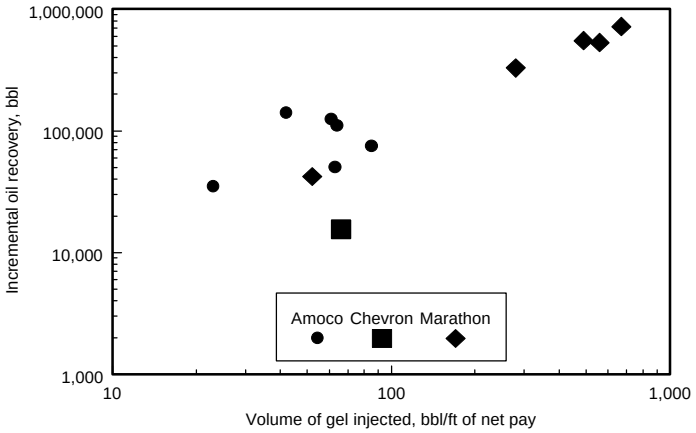

Fig. 2—Incremental oil recovery versus treatment size.

Severity of Channeling. In an earlier paper,[11] we considered some of the reservoir variables that affect the severity of channeling and the potential of gel treatments for reducing channeling through naturally fractured reservoirs. Using numerical studies, we showed that gel treatments have the greatest potential when the conductivities of fractures that are aligned with direct flow between an injector-producer pair are at least 10 times the conductivity of off-trend fractures. Gel treatments also have their greatest potential in reservoirs with moderate to large fracture spacing. Produced tracer concentrations from interwell tracer studies can help identify reservoirs that are predisposed to successful gel applications. Our simulation studies also showed how tracer transit times can be used to estimate the conductivity of the most-direct fracture. The effectiveness of gel treatments should be insensitive to fracture spacing for fractures that are aligned with the direct flow direction. The effectiveness of gel treatments increases with increased fracture spacing for fractures that are not aligned with the direct flow direction.

Most studies described in Ref. 11 assumed an ideal gel placement, where the gel only entered the most-direct fracture between an injector-producer pair. In this report, we extend our analyses to quantify gel placement in naturally fractured reservoirs, using gel properties measured during our extrusion experiments.[10] With this placement knowledge, an opportunity exists to quantify sweep improvement from a gel treatment as a function of the volume of gel injected.

Representation of a Naturally Fractured Reservoir

When modeling naturally fractured reservoirs, the fracture systems generally have been envisioned as slabs (i.e., one set of parallel fractures), columns (i.e., two intersecting sets of parallel vertical fractures), or cubes (i.e., three intersecting sets of parallel fractures—two vertical and one horizontal). Geostatistics have also been used to describe fracture distributions. In this report, we focus on the column model. For simplicity, assume that a naturally fractured reservoir consists of a regular pattern of vertical *x*-direction fractures intersected by vertical *y*-direction fractures (see Fig. 3). The *y*-direction fractures intersect the *x*-direction fractures at an angle, *q*. Following along a given *x*-direction fracture, an intersecting *y*-direction fracture is encountered at a regular interval, DL_x. Similarly, following along a given *y*-direction fracture, an intersecting *x*-direction fracture is encountered at a regular interval, DL_y. Of course, DL_x may be different than DL_y. Also, the shortest distance between adjacent fractures is $DL_y \sin q$ for the *x*-direction fractures and is $DL_x \sin q$ for the *y*-direction fractures.

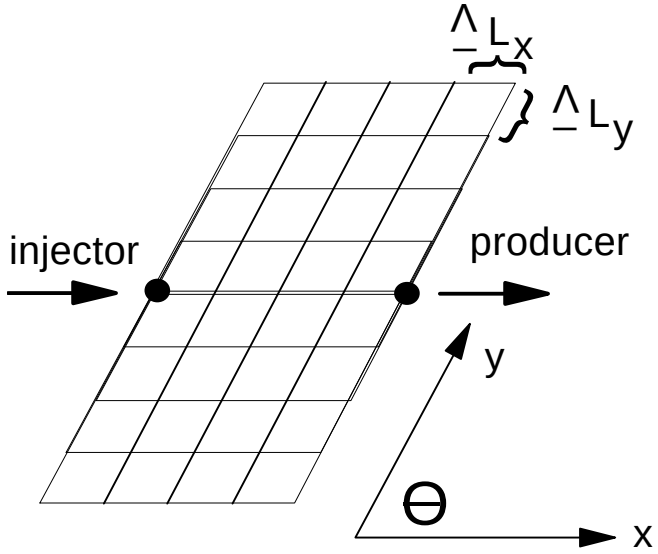

Fig. 3—Plan view of an injector-producer pair in a simple naturally fractured reservoir.

For our base case, one injection well and one production well are located at either end of the central *x*-direction fracture. The distance and pressure drop between the two wells are fixed. We assume that flow through the rock is negligible compared with that through the fractures and that the system is incompressible. Furthermore, fractures pointed in the *y*-direction are assumed to have a conductivity, $(k_f w_f)_y$, and fractures pointed in the *x*-direction are assumed to have a different conductivity, $(k_f w_f)_x$. A conductivity ratio, *R*, is defined using Eq. 2.

$$R = (k_f w_f)_x / (k_f w_f)_y \quad \text{..... (2)}$$

We also assume that the fracture system is initially filled with fluids that have the mobility of water.

Areal Gel Profiles

Our first objective in this analysis is to determine how gel might distribute in our fracture system during a gel treatment. In attacking this problem, we note that during gel injection, the pressure drop in the fracture system is dominated by the pressure drop across the viscous gel bank. Fig. 9 of Ref. 10 indicates that the gel is typically 1,000 to 100,000 times more viscous than water. Therefore, in the vicinity of the gel bank, the pressure differences in parts of the fracture system that do not contain gel (i.e., where only water or hydrocarbon flows) are negligible compared to the pressure drops in the fractures that contain gel. Thus, we assume that the pressure drop is the same from the injection well to any point at the gel front.

In our analysis, we assume that gel only flows through the fracture network. This assumption is consistent with experimental observations—gel does not flow through porous rock.[8-10] We also neglect the effects of gravity in the displacement of fracture fluids (i.e., water) by gel. This assumption is reasonable in view of the large viscosity contrast between gel and water. Ref. 8 demonstrated that viscous forces usually dominate over gravity forces during gel placement in fractures. We also neglect dispersion of the gel bank. This assumption also seems reasonable in view of the large mobility contrast between the gel bank and the displaced water in the fractures.

We note that a minimum pressure gradient is required to extrude the gel through a fracture with a given conductivity.[8-10] Also, once that pressure gradient is achieved, the pressure gradient required for extrusion is effectively independent of gel velocity.[8,9] These observations considerably simplify the flow behavior of gels in fractures. If the pressure gradient is below the minimum or critical value, no flow occurs. If the minimum pressure gradient is met, gel flow occurs at that pressure gradient.

The minimum or critical pressure gradient required for gel extrusion decreases with increased fracture conductivity or width.[10] This relation is quantified by Eq. 1 for the Cr(III)-acetate-HPAM gel that we consider in this work. Thus, for the *x*-direction fractures (i.e., the fractures pointed in the *x*-direction) in Fig. 3, the critical pressure gradient, $(dp/dl)_x$, is related to *x*-direction fracture conductivity, $(k_f w_f)_x$, by Eq. 3.

$$(dp/dl)_x = 280\,[(k_f w_f)_x]^{-0.58} \quad \text{..... (3)}$$

Similarly, for the *y*-direction fractures (i.e., the fractures pointed in the *y*-direction) in Fig. 3, the critical pressure gradient, $(dp/dl)_y$, is related to *y*-direction fracture conductivity, $(k_f w_f)_y$, by Eq. 4.

$$(dp/dl)_y = 280\,[(k_f w_f)_y]^{-0.58} \quad \text{..... (4)}$$

Let the gel penetrate some distance, L_{xo}, along the central *x*-direction fracture that connects the two wells. Then, the pressure drop from the injector to the end of the gel bank in this fracture is given by Eq. 5.

$$Dp = L_{xo}\,(dp/dl)_x = L_{xo}\,280\,[(k_f w_f)_x]^{-0.58} \quad (5)$$

Gel Penetration in *y*-Direction Fractures. When the gel has penetrated the distance, L_{xo}, along the central *x*-direction fracture, gel will have penetrated a distance, L_{y1}, along the first *y*-direction fracture leading away from the injection well. That distance can be estimated using Eq. 6.

$$L_{y1} = Dp / (dp/dl)_y = Dp / \{280\,[(k_f w_f)_y]^{-0.58}\} \quad (6)$$

Combining Eqs. 2 and 6 gives Eq. 7.

$$L_{y1} = Dp / \{280\,[(k_f w_f)_x / R]^{-0.58}\} \quad (7)$$

Combining Eqs. 5 and 7 yields Eq. 8, which can be used to estimate, the ratio, L_{y1}/L_{xo}.

$$L_{y1} / L_{xo} = R^{-0.58} \quad (8)$$

We wish to determine relations like Eq. 8 for the other *y*-direction fractures. In the n^{th} *y*-direction fracture (from the left edge of Fig. 3), we wish to determine the distance of gel penetration, L_{yn}, away from the central *x*-direction fracture. The total pressure drop from the injector to the edge of the gel bank in the n^{th} *y*-direction fracture is the sum of the pressure drop through the gel bank in the *x*-direction, Dp_x, and that in the *y*-direction, Dp_y.

$$Dp = Dp_x + Dp_y = (n\text{-}1)\,DL_x\,(dp/dl)_x + L_{yn}(dp/dl)_y \quad (9)$$

Combining Eqs. 2, 3, 4, 5, and 9 yields Eq. 10.

$$L_{yn} / L_{xo} = R^{-0.58}\,[1 - (n\text{-}1)\,DL_x/L_{xo}] \quad (10)$$

Gel Penetration in *x*-Direction Fractures. We also wish to determine relations like Eq. 10 for the other *x*-direction fractures. In particular, in the m^{th} *x*-direction fracture (up or down from the central *x*-direction fracture of Fig. 3), we wish to determine the distance of gel penetration, L_{xm}. The total pressure drop from the injector to the edge of the gel bank in the m^{th} *x*-direction fracture is the sum of the pressure drop through the gel bank in the *x*-direction, Dp_x, and that in the *y*-direction, Dp_y.

$$Dp = Dp_x + Dp_y = L_{xm}(dp/dl)_x + m\,DL_y(dp/dl)_y \quad (11)$$

Combining Eqs. 2, 3, 4, 5, and 11 yields Eq. 12.

$$L_{xm}/L_{xo} = 1 - R^{0.58}\,m\,DL_y/L_{xo} \quad (12)$$

L_{xm}/L_{xo} must be positive, so

$$1 - R^{0.58}\,m\,DL_y/L_{xo} > 0 \quad (13)$$

Solving for m yields Eq. 14.

$$m < R^{-0.58} L_{xo} / DL_y \quad (14)$$

Since m must be an integer (indicating the row number associated with an *x*-direction fracture), Eq. 15 provides m_{max}, which indicates the last *x*-direction fracture (i.e., the *x*-direction fracture farthest from the central *x*-direction fracture) that will contain gel.

$$m_{max} = \text{INT}\,[R^{-0.58} (L_{xo} / DL_y)] \quad (15)$$

Gel Front Profiles. Eqs. 5, 10, 12, and 15 can be used to determine the areal gel profile in a naturally fractured system. Fig. 4 plots generalized outlines of gel front profiles as a function of the fracture conductivity ratio, *R*. Interestingly, Fig. 4 should be relevant to a wide variety of conditions. Careful consideration of Eqs. 10 and 12 reveals that Fig. 4 can provide gel front positions independent of fracture spacing between adjacent *x*-direction or *y*-direction fractures. Also, the outline of the gel front is independent of gel penetration in the central *x*-direction fracture, L_{xo}.

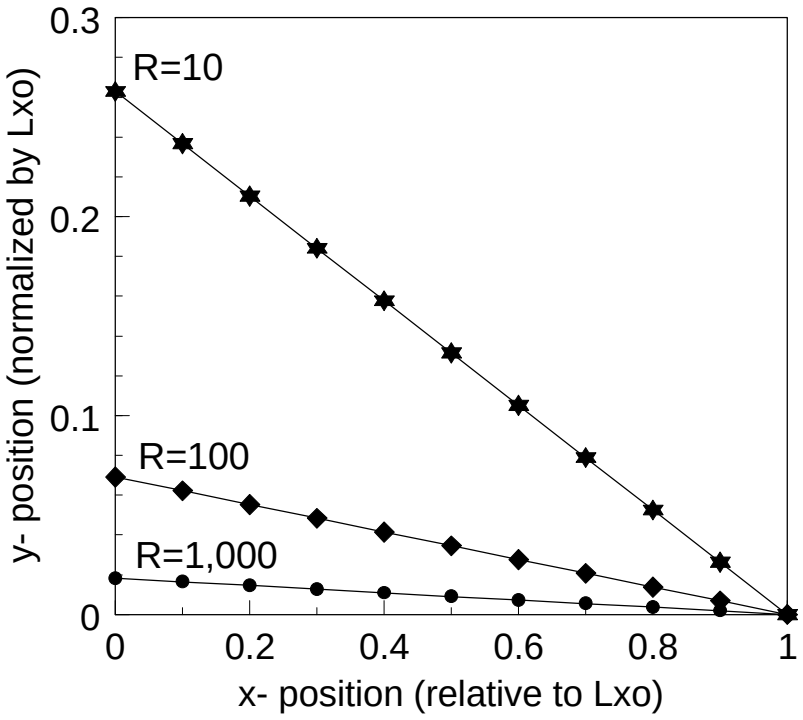

Fig. 4—Generalized outlines of gel front profiles.

To illustrate the above points, consider the three examples shown in Figs. 5-7. These figures show gel front profiles for different spacings between fractures. In each case, the *x*-direction fractures are ten times more conductive than the *y*-direction fractures (R=10). Also, for simplicity in illustration, assume that q is 90°. In Fig. 5, $DL_x=DL_y=L_{xo}/4$. In Fig. 6, $DL_x=DL_y/2.5=L_{xo}/10$. In Fig. 7, $DL_x=DL_y=L_{xo}/10$. In each figure, the bold lines show parts of the fracture system that contain

gel, while the thin lines show parts of the fracture system that do not contain gel. The solid circles show the outline of the outer-most extent of gel penetration in the fracture system. Note that these solid-circle outlines have the same shape and dimensions for all three figures. These outlines are also consistent with the R=10 case shown in Fig. 4.

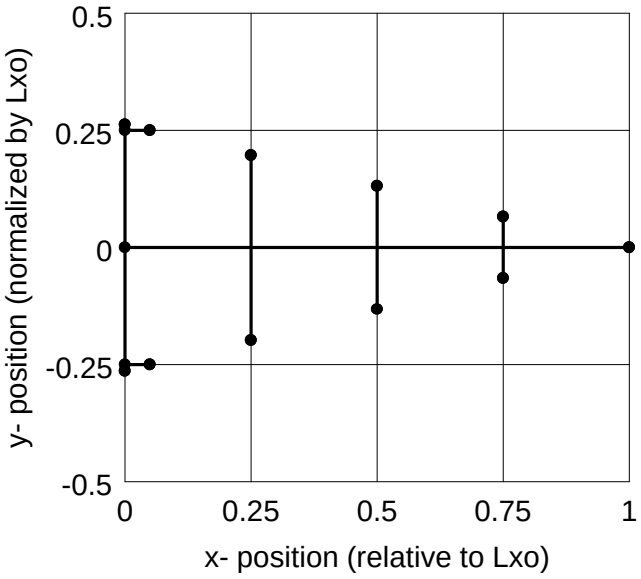

Fig. 5—Gel front profile for $DL_x=DL_y=L_{xo}/4$. R=10.

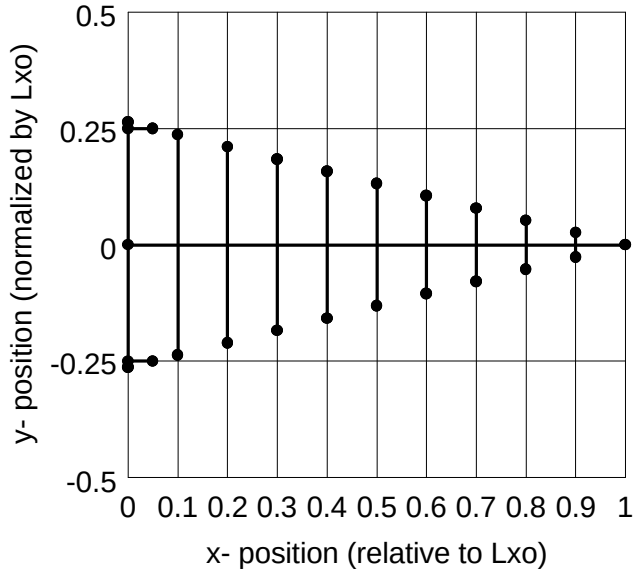

Fig. 6—Gel front profile for $DL_x=DL_y/2.5=L_{xo}/10$. R=10.

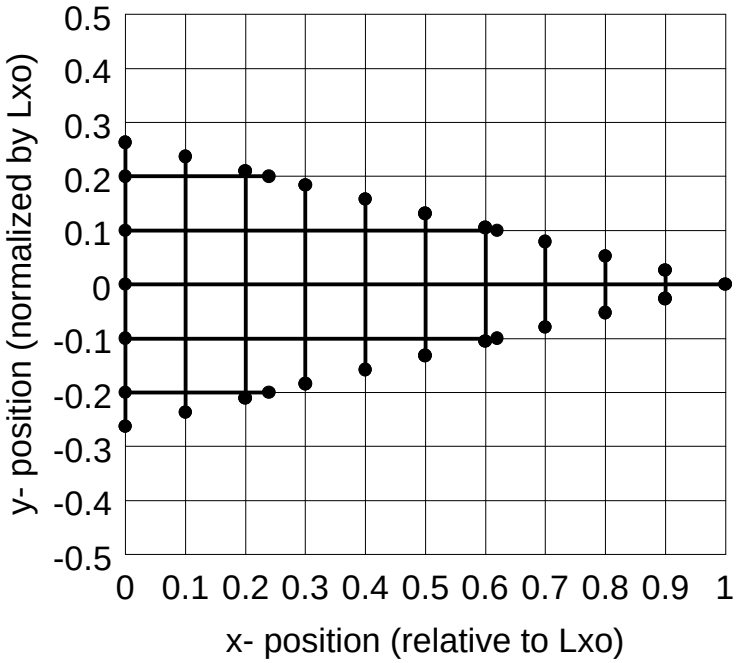

Fig. 7—Gel front profile for $DL_x=DL_y=L_{xo}/10$. R=10.

Gel Volumes

For the pattern between an injector-producer pair (e.g., illustrated in Figs. 5-7), the volume, V_y, occupied by gel in the y-direction fractures is given by Eq. 16,

$$V_y = 2h_f\, w_{fy}\, \Sigma\, L_y \quad \text{.....(16)}$$

where h_f is fracture height and w_{fy} is the width of a y-direction fracture. The factor of 2 in Eq. 16 occurs because the gel penetrates from the central x-direction fracture in both directions along a given y-direction fracture. Combining Eqs. 10 and 16 yields Eq. 17.

$$V_y = 2h_f\, w_{fy}\, L_{xo}\, R^{-0.58}\, \Sigma\, [1-(n\text{-}1)\, DL_x / L_{xo}] \quad \text{.....(17)}$$

This equation can be simplified to form Eq. 18,

$$V_y = h_f\, w_{fy}\, L_{xo}\, R^{-0.58}\, I_y\, [2+(DL_x / L_{xo})(1-I_y)] \quad \text{.....(18)}$$

where I_y is defined by Eq. 19.

$$I_y = \text{INT}\, [L_{xo} / DL_x] \quad \text{.....(19)}$$

The volume, V_x, occupied by gel in the x-direction fractures is given by Eq. 20,

$$V_x = h_f\, w_{fx}\, \Sigma\, L_x \quad \text{.....(20)}$$

where h_f is fracture height and w_{fx} is the width of an x-direction fracture. Combining Eqs. 12 and 20 yields Eq. 21.

$$V_x = h_f\, w_{fx}\, L_{xo}\, [1 + 2\, \Sigma\, (1 - R^{0.58}\, m\, DL_y / L_{xo})] \quad \text{.....(21)}$$

This equation can be simplified to form Eq. 22,

$$V_x = h_f\, w_{fx}\, L_{xo}\, \{1+I_x [2 - (DL_y / L_{xo}) R^{0.58}\, (I_x +1)]\} \quad \text{.....(22)}$$

where I_x is defined by Eq. 23.

$$I_x = \text{INT}\, [R^{-0.58}\, (L_{xo} / DL_y)] \quad \text{.....(23)}$$

The ratio, V_y / V_x, can determined by dividing Eq. 18 by Eq. 22 and recognizing (from Ref. 9) that $w_{fy} / w_{fx} = R^{-1/3}$.

$$V_y / V_x = \{R^{-0.91}\, I_y\, [2+(DL_x/L_{xo})(1- I_y)]\} / \, [1+I_x\, (2 - (DL_y / L_{xo}) R^{0.58}\, (I_x +1))] \quad \text{.....(24)}$$

Fig. 8 plots V_y / V_x versus L_{xo} / DL_y for the case when $DL_x = DL_y$. For a given R-value, note that for high L_{xo} / DL_y values (i.e., dense fracture spacing), the V_y / V_x ratio stabilizes at a fixed value. For R-values of 10, 100, and 1,000, the stabilized V_y / V_x ratios are 0.47, 0.22, and 0.10, respectively. Careful consideration of Eq. 24 reveals that as fracture spacing becomes more dense, the V_y / V_x ratio approaches $R^{-1/3}\, (DL_y / DL_x)$.

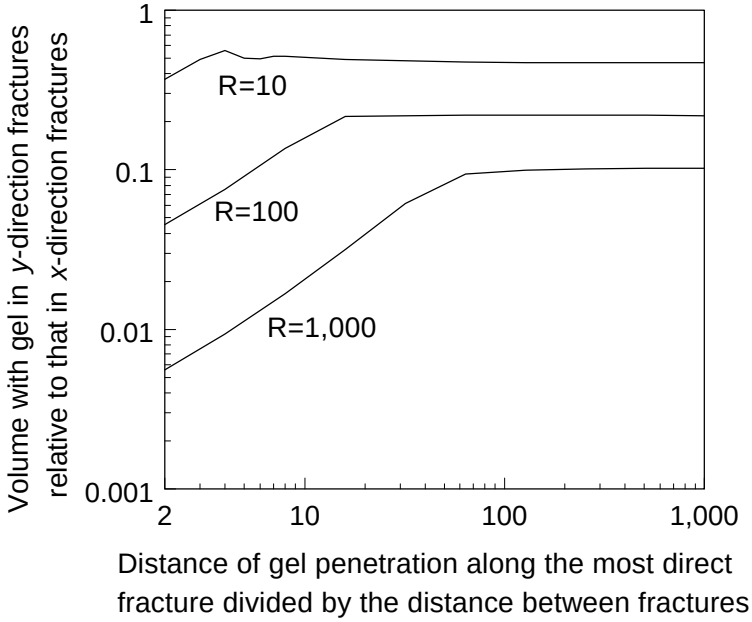

Fig. 8—(V_y / V_x) versus L_{xo} / DL_y. (When $DL_x = DL_y$.)

The total volume associated with gel in the fracture pattern is simply ($V_x + V_y$). This volume can be normalized by the gel volume in the most-direct x-direction fracture, $h_f\, w_{fx}\, L_{xo}$. Fig. 9 provides a plot of $(V_x + V_y) / (h_f\, w_{fx}\, L_{xo})$ versus L_{xo} / DL_y when $DL_x = DL_y$.

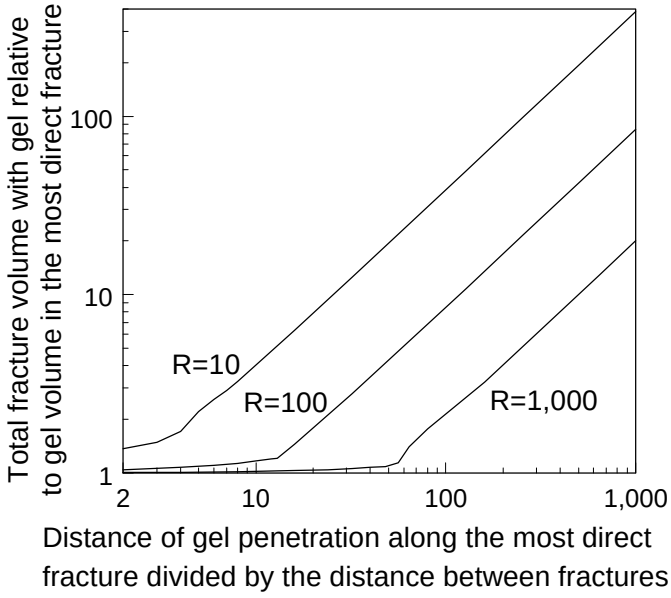

Fig. 9—$(V_x + V_y) / (h_f w_{fx} L_{xo})$ versus L_{xo} / DL_y. (When $DL_x = DL_y$.)

In Fig. 9, for a given R-value, the total fracture volume occupied by gel remains near unity until a critical L_{xo} / DL_y value is reached. For greater L_{xo} / DL_y values, the total fracture volume with gel increases in direct proportion to the L_{xo} / DL_y value. Careful consideration of Eqs. 18-24 reveals that the behavior in Fig. 9 can be approximated fairly closely using Eqs. 25 and 26.

$$(V_x + V_y) / (h_f w_{fx} L_{xo}) = R^{-0.58} (L_{xo} / DL_y) [1 + R^{-0.33} (DL_y / DL_x)] \quad \text{.....(25)}$$

if $(DL_y / L_{xo}) \le R^{-0.58} [1 + R^{-0.33} (DL_y / DL_x)]$ and

$$(V_x + V_y) / (h_f w_{fx} L_{xo}) = 1 \quad \text{.....(26)}$$

if $(DL_y / L_{xo}) > R^{-0.58} [1 + R^{-0.33} (DL_y / DL_x)]$.

Eqs. 25 and 26 suggest that knowledge of the fracture conductivity ratio, R, fracture widths, and fracture spacing should allow one to estimate the volume of the fracture system that will be occupied by gel. Eq. 26, in particular, suggests that most of the injected gel will be confined to the most-direct fracture if $(DL_y / L_{xo}) > R^{-0.58} [1 + R^{-0.33} (DL_y / DL_x)]$. To relate the normalized volumes from Eqs. 25 and 26 to actual gel volumes, the results must be multiplied by the volume associated with gel in the most-direct fracture. In turn, the volume associated with the most-direct fracture can be estimated from interwell tracer studies.[11]

Effect of Gel Dehydration

Table 1 reveals that gels can concentrate or dehydrate during extrusion through fractures. (We define the "degree of dehydration" as the factor by which the gel is concentrated.) How does this phenomenon affect the placement and sizing of the gel bank? With our current understanding, gel

dehydration will certainly affect sizing of the gel bank, but it should have no effect on the relative placement of gel in *x*-direction versus *y*-direction fractures.

Effect on Gel Volume. To understand the above observations, first consider the effects of dehydration on sizing of the gel treatment. To date, our experiments indicate that the degree of gel dehydration is independent of the distance of penetration along a fracture of a given conductivity.[2,10] Therefore, if the degrees of gel dehydration are known for gel in *x*-direction (F_{dx}) and *y*-direction (F_{dy}) fractures, the total volume of gel injected, V_T, can be related to V_x and V_y using Eq. 27.

$$V_T = F_{dx}\, V_x + F_{dy}\, V_y \quad \text{.....(27)}$$

(This equation applies to the fracture pattern illustrated in Fig. 3. If a symmetric pattern exists to the left of the injector, then the total gel volume to be injected must be doubled.) Eqs. 18, 22, and 27 can be combined to relate the total volume of gel injected to the fracture conductivity ratio, fracture spacing, and degree of gel dehydration. Alternatively, using the approximations associated with Eqs. 25 and 26, Eqs. 28 and 29 result.

$$V_T / (h_f\, w_{fx}\, L_{xo}) = R^{-0.58}\, (L_{xo}/DL_y)\, \{[F_{dx} + R^{-0.33}\, (DL_y/DL_x)\, F_{dy}]\} \quad \text{.....(28)}$$

if $(DL_y/L_{xo}) \le R^{-0.58}\, [1 + R^{-0.33}\, (DL_y/DL_x)\, (F_{dy}/F_{dx})]$ and

$$V_T / (h_f\, w_{fx}\, L_{xo}) = F_{dx} \quad \text{.....(29)}$$

if $(DL_y/L_{xo}) > R^{-0.58}\, [1 + R^{-0.33}\, (DL_y/DL_x)\, (F_{dy}/F_{dx})]$. Eq. 29 indicates that most of the gel will be confined to the most-direct fracture if $(DL_y/L_{xo}) > R^{-0.58}\, [1 + R^{-0.33}\, (DL_y/DL_x)\, (F_{dy}/F_{dx})]$.

Effect on Gel Placement. In the development of Eqs. 10 and 12, the distance of gel penetration along a given fracture was completely independent of the degree of dehydration experienced by the gel. This result is a natural consequence of our observation that the gel moves under a fixed pressure gradient if the gel's yield stress is exceeded (Eq. 1). Regardless of the degree of dehydration experienced by the gel, the gel will propagate along a fracture until the pressure gradient falls below the critical yield stress. Then, the gel will stop moving.

Effect of Fracture Orientation (θ). Upon first consideration, one might perceive that our analysis assumes that the angle of fracture intersection (θ in Fig. 3) is 90°. However, the analysis using our column model is valid for any angle. This conclusion follows from our observation that gel propagation in a given fracture depends primarily on the pressure gradient and our assumption that the pressure drop from the injection well to the gel front is independent of position on the gel front. In Figs. 4-7, for convenience of illustration, the angle between the *x*- and *y*-direction fractures is shown to be 90°. However, the analysis is valid for other θ-values. Of course, the shapes of the gel front profiles will be distorted with changing θ-values. However, the distances of gel penetration into *y*-direction fractures (relative to that in the central *x*-direction fracture) are independent of θ-value.

Effect of Gel Injection Rate. As mentioned earlier, in our experimental work, we observed that above the critical yield stress for the gel, the pressure gradient for gel propagation is insensitive to flow rate.[8,9] Consequently, the shapes of the gel front profiles are expected to be independent of gel injection rate. Also, for a given total volume of gel injected, gel placement in the fracture system is expected to be independent of injection rate. However, this conclusion was derived based on gel that was about 24 hours old. Since the gel does become somewhat more rigid with age,[9] one might expect older gels to require greater pressure gradients for extrusion than newer gels—perhaps leading to greater degrees of gel dehydration. Of course, for a given volume of gel, gels injected using rapid flow rates should have a narrower range of gel ages during the placement process than gels injected using slow flow rates. This issue is a topic for future work.

Importance of Gelant Leakoff During Large-Volume Gel Treatments

As mentioned earlier, in large-volume gel treatments, the time required to inject the gel was much longer than the gelation time.[3-5] Thus, we concluded that the gel extruded through the fracture system during most of the placement process. However, the injected blocking agent was probably in a fluid gelant form for a short time after leaving the wellbore. In contrast to the crosslinked polymer (i.e., the gel), this gelant could possibly penetrate into the porous rock during the placement process. This section presents the results from several simple calculations to illustrate the relative importance (or lack thereof) of gelant flow during placement of large-volume gel treatments. Treatments at Chevron's Rangely field in Colorado will be used as an example.[5]

Gelant Volume Relative to Gel Volume. At Rangely, the average treatment size was about 12,000 bbl of blocking agent injected per well.[5] Injection rates were typically 1 bbl/minute. Gelation times for the Cr(III)-acetate-HPAM gel were typically 2 to 3 hours. The HPAM solution was mixed in batches; then, the Cr(III)-acetate crosslinker was added continuously to the polymer injection stream just before the wellhead. The hold-up volume in the tubing in the wellbore was about 30 bbls, so the gelant typically aged for about 30 minutes before reaching the target zones between 5,500 to 6,500 feet.[5] Therefore, the blocking agent may have been in a fluid gelant form for 1.5 to 2.5 hours in the formation before gelation. With an injection rate of 1 bbl/minute, roughly 120 bbl (±30 bbl) is the estimated gelant volume in the formation. (The remainder of the blocking agent should be in gelled form.) This 120-bbl volume amounts to 1% of the average 12,000-bbl gel treatment that was injected. This fact argues that the importance of gelant flow may be very small compared to that for gel extrusion during the placement process.

Gelant Penetration into Porous Rock. If the gelant happened to flow radially from the wellbore through the porous rock, how far would the gelant penetrate before gelation? At Rangely, given an average sandstone porosity of 11% and net pay of 175 ft^3, the radius of gelant penetration would be less than 6 ft.

Of course, since the formation contains natural fractures, we expect the gelant to follow those fractures—possibly leaking off from the fracture faces. The volume of porous rock (11% porosity) occupied by 120 bbl of gelant is 6,120 ft^3. If an injection well at Rangely had a single two-wing fracture in the net pay that was 35 ft long in either direction from the well, gelant leakoff to a distance of 3 inches from the fracture faces would account for 6,120 ft^3 of gelant volume. Once this gelant in the porous rock forms a gel, one could argue that the rock was damaged to inhibit further flow or leakoff. Thereafter, the gelant/gel should be confined to the

fractures. Very few injectivity limitations were encountered during gel injection at Rangely.[5] This observation indicates that the gelant and/or gel did not damage the near wellbore region significantly—implying that the fracture system was still open near the wellbore. Given that the fracture system was still open, any near-wellbore gelant leakoff would appear to have little consequence on either the blocking-agent injectivity or placement.

Gelant Volume in Fractures. High-molecular-weight polymers experience difficulty penetrating into 10-md rock (e.g., that at Rangely), even if no crosslinker is present.[12] Perhaps, essentially all of the gelant or gel will stay in the fractures. A gelant volume of 120 bbls translates to a fracture volume of 673 ft^3 (assuming fracture porosity is 100%). If the fracture width was 0.1 inches and the fracture extended only through the 175 ft of net pay, 673 ft^3 would fill a two-wing fracture out to a distance of 230 ft from the well. If the fracture extended through all 675 ft of gross pay at Rangely, 673 ft^3 would fill a two-wing fracture out to a distance of 60 ft from the well.

(In the above example, we selected a fracture width of 0.1 inches because that represents the minimum width that allows Cr(III)-acetate-HPAM gel extrusion using a typical reservoir pressure gradient—e.g., 1 psi/ft.[10] Since high injection pressures were not observed during gel injection at Rangely, we conclude that the fractures must have been fairly wide—i.e., at least 0.1 inches.)

The above arguments apply to a single, two-wing fracture. In a naturally fractured system, of course, multiple fractures will be present. For comparative purposes, assume that the fracture system consists of two equally spaced, vertical, perpendicular sets of parallel fractures, where each fracture has a width of 0.1 inches and a height of 175 ft. Then, the 673 ft^3 of gelant volume could be contained within a 80-ft by 80-ft square for a fracture spacing of 40 ft; within a 60-ft by 60-ft square for a fracture spacing of 20 ft; or within a 40-ft by 40-ft square for a fracture spacing of 8 ft.

The implication from the above calculations is that the gelant is only likely to be of significance near the injection wellbore. Gel extrusion through fractures (rather than gelant flow) must dominate during the vast majority of the placement process.

One might argue that an injectivity advantage exists if the near-wellbore portions of the fracture are filled with gelant rather than gel. Certainly, for a given length of fracture and for a given flow rate, the pressure drop associated with gelant flow will be much less than that for gel extrusion. Also, with fluids that are not gelled, an injectivity advantage might exist because of relatively low viscosities near-wellbore. However, for gels, a minimum pressure gradient or yield stress is required to move the gel.[8-10] In locations where the gel exists, this minimum pressure gradient must be attained regardless of the radial position of the gel relative to the injection well.[10]

Experimental Verification

To test our predictions, an experiment was performed by extruding a Cr(III)-acetate-HPAM gel through a fracture system. Our fracture system consisted of one-hundred 650-md Berea sandstone cubes that were arranged to form the areal pattern illustrated in Fig. 10. Each sandstone cube had dimensions of 1.5 in. x 1.5 in. x 1.5 in. The cubes were positioned to create nine 0.25-in.-wide "fractures" in one direction (aligned with the injector-producer flow direction) and nine 0.125-in.-

wide “fractures” that were perpendicular to the first set of fractures. Injection and production ports were positioned as indicated in Fig. 10. (Actually, some variation between fracture widths did occur. We believe that these variations ultimately influenced our experimental results, as will be seen shortly.) A clear polycarbonate sheet was epoxied to the tops of the sandstone cubes to allow visualization of the gel front during the experiment. Impermeable boundaries were also epoxied to the bottoms of the sandstone cubes and to the outer perimeter of the composite system. The total fracture volume of the system was about 1,300 cm^3. The volume in the most direct fracture between the injection and production ports was about 90 cm^3. The conductivity of a given fracture that was aligned with flow from the injector to the producer was about 8 times that for the off-trend fractures (i.e., R=8).

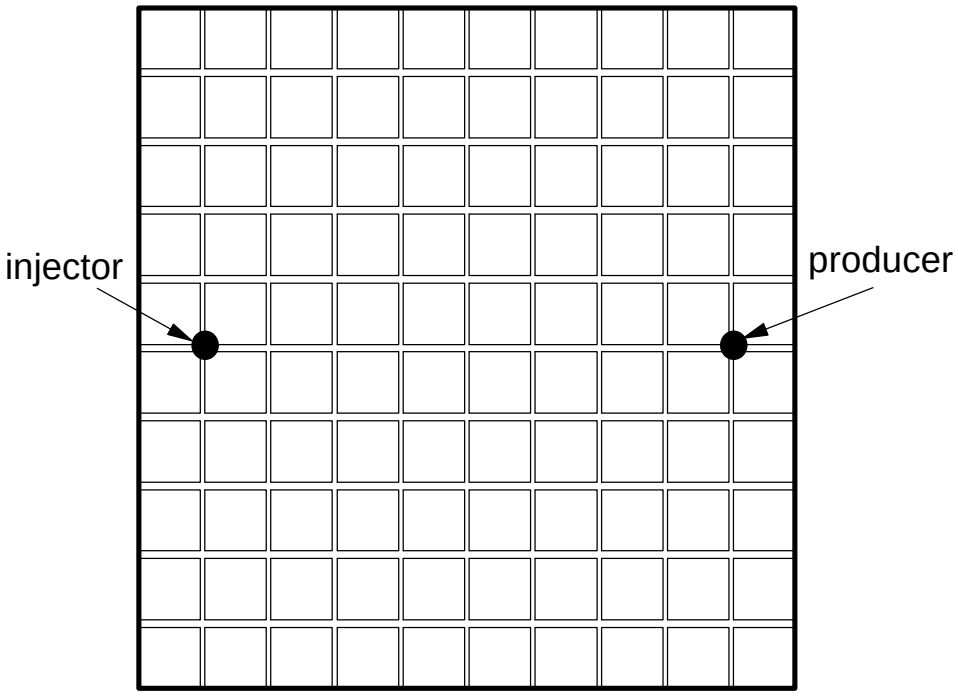

Fig. 10—Areal view of fracture experiment before gel placement.

We used a Cr(III)-acetate-HPAM gel that contained 0.5% Allied Colloids Alcoflood 935 HPAM, 0.0417% Cr(III)-acetate, 1% NaCl, and 0.1% $CaCl_2$ at pH=6. The experiment was performed at 41°C (105°F). The gelant was aged at 41°C for 24 hours (5 times the gelation time) before injection into the fracture system. We injected 400 cm^3 of gel using a fixed rate of 200 cm^3/hr. Gel injection was stopped at this point because the gel arrived at the production port. Fig. 11 shows the shape of the gel front after gel injection. For comparison, Fig. 12 shows the areal front that was predicted by our method.

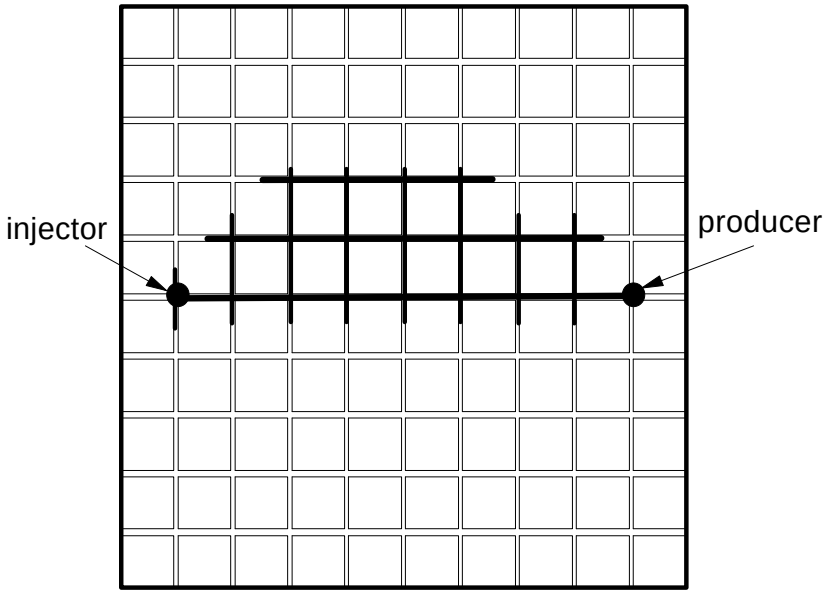

Fig. 11—Actual areal view of fracture experiment after gel placement.

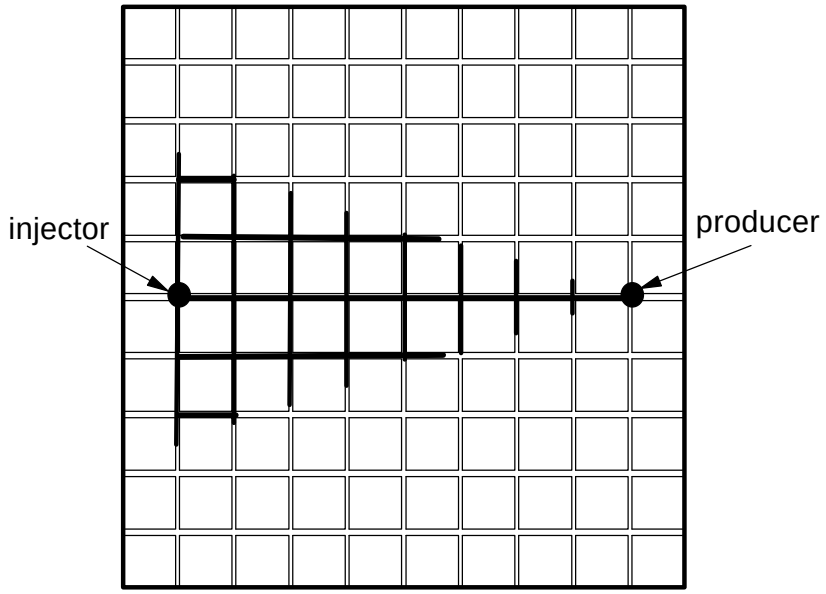

Fig. 12—Predicted areal view after gel placement.

Obviously, significant differences exist between the actual (Fig. 11) and predicted (Fig. 12) profiles. We suspect that these differences occurred because the widths of our fractures varied to some extent from block to block in our pattern. In the top (north) part of the pattern, the maximum distance of gel penetration in the *y*-direction fractures was reasonably consistent with the prediction. However, the physical location of this maximum was significantly off from the prediction. In the bottom (south) part of the pattern, the predicted maximum distance of penetration in the *y*-direction fractures was much greater than the experimental result.

The volume (400 cm^3) of gel required for breakthrough at the production port was reasonably close to the volume predicted by Eq. 25. The predicted breakthrough volume was 325 cm^3 or 3.6 times the volume of the most direct fracture. Note that Eq. 25 does not account for gel dehydration. From Table 1, we expect a gel dehydration factor between 1.1 and 1.8 for fractures with 0.25-in. widths. Thus, after accounting for gel dehydration, the actual breakthrough volume was very consistent with our prediction.

Fig. 13 compares results of tracer tests that were performed during brine injection before versus after gel placement. The aqueous tracer contained 40-ppm KI, 1% NaCl, and 0.1% $CaCl_2$. We monitored the effluent (specifically, the iodide) from the fracture system spectrophotometrically at a wavelength of 230 nm. In Fig. 13, the effluent tracer concentration is reported relative to the injected tracer concentration, C/C_o. For the *x*-axis of Fig. 13, the volume of tracer injected (and produced) is reported relative to the volume associated with the most direct fracture (90 cm^3 in this case). Fig. 13 shows that the tracer breakthrough cures were virtually identical before and after gel placement. This result indicates that the gel treatment did not significantly change sweep efficiency in our fracture pattern.

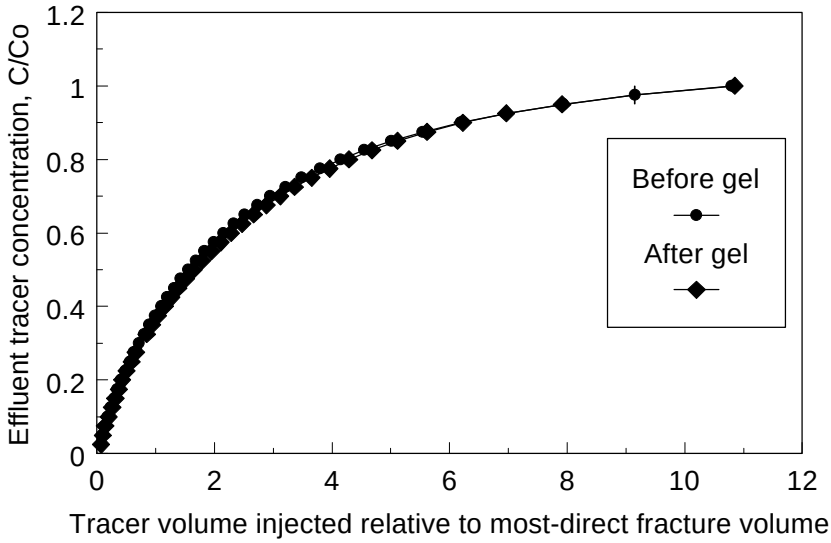

Fig. 13—Tracer results during brine injection before versus after gel placement.

At the end of the experiment, the core was disassembled, and the gel was analyzed at 36 locations in the fracture system. On average, the chromium and polymer concentrations for gel in the fractures were 1.5 times the values in the original gel. No correlation was found between final gel composition and distance of penetration along a given fracture. Interestingly, the final chromium and HPAM concentrations for gel in 0.125-inch-wide fractures were the same as those in the 0.25-inch-wide fractures. In contrast, from Table 1, we might have expected the gel in the narrower fractures to be two to three times more concentrated than that in the wider fractures.

To refine and test our model, we plan to perform more tests of this type in fracture systems.

Conclusions

For fracture systems consisting of a regular pattern of vertical x-direction fractures intersected by vertical y-direction fractures:

1. A model has been developed that predicts areal gel front profiles and distances of gel penetration as a function of gel volume injected into naturally fractured injection wells.
2. Areal gel front profiles can be predicted using Eqs. 8, 10, and 12 of this report.
3. Our model predicts that the general outline or shape of the areal gel front profiles depends primarily on the ratio of conductivity of on-trend fractures to the conductivity of off-trend fractures. This shape is predicted to be insensitive to fracture spacing, injection rate, and degree of dehydration experienced by the gel. However, experimental results suggest that local variations in fracture widths can significantly affect the shape of the gel front.
4. To achieve a given distance of gel penetration into a fracture system, the required volume of gel to be injected can be predicted using Eqs. 18, 22, and 27 of this report. If fracture spacing is fairly dense, these equations simplify so that Eqs. 28 and 29 can be used.
5. In large-volume applications, gel injectivity and placement is governed by gel extrusion properties in the fractures. Flow of fluid gelant (before gelation) is relatively unimportant.

Future Work

In the future, we plan to test the predictions from our model using both laboratory and field data. In the laboratory, additional tests will be performed like those mentioned in the latter part of this chapter. Depending on the outcome of our experimental work, our model may need modification.

We would also like to test our model using field data. To perform a rigorous test, we need some means to assess the locations of the gel fronts in field applications. However, this information is simply not available, especially because gel rarely was detected in offset production wells. Even so, some insights can be gained by performing a few calculations with field data. We may be able to estimate limits of how far the gel penetrated into the reservoir and the distribution of gel in the fracture system. To use our method, we need field information about fracture conductivities, *R*-values, and fracture spacings. In turn, determination of these parameters requires (1) interwell tracer times between an injector and the offset production wells, (2) injection and production rates, (3) downhole pressures for the injector and the offset producers, and (4) gel breakthrough times (or lack of breakthrough).[11] Of course, geologic information about the distribution of fractures (e.g., from cores or logs in deviated wells) would also be very valuable.

Another important step for the future will include predicting sweep improvement that results from a given gel placement. We envision predicting and experimentally verifying tracer transit behavior before and after gel placement in fracture systems.

3. GEL PROPERTIES IN FRACTURES

Gels have often been used to reduce fluid channeling in reservoirs.[13] The objective of these gel treatments is to substantially reduce flow through fractures or high-permeability channels without damaging hydrocarbon-productive zones. The most successful applications for this purpose have occurred when treating linear flow problems—either fractures[3-7,13-15] or flow behind pipe.[16,17] In fractured reservoirs, some of the most successful treatments used relatively large volumes (e.g., 10,000 to 37,000 bbl/well) of Cr(III)-acetate-HPAM gel.[3-5] In these applications, the gel injection times were substantially longer than the gelation time (e.g., by factors ranging from 10 to 100). Since these gels (after gelation) do not flow through porous rock,[8] they must extrude through fractures during the placement process. Therefore, we are investigating the properties of gels during placement in fractures.

Review of Previous Work

Much of our previous work in this area is described in Refs. 8-10. We performed gel-extrusion studies with several gels.[8] However, most of our work used a Cr(III)-acetate-HPAM gel that contained 0.5% Allied Colloids Alcoflood 935 HPAM, 0.0417% Cr(III)-acetate, 1% NaCl, and 0.1% $CaCl_2$ at pH=6. All experiments were performed at 41°C (105°F). The gelant formulations were usually aged at 41°C for 24 hours (5 times the gelation time) before injection into a given fractured core.

Minimum Pressure Gradient for Gel Extrusion. We noted that a certain minimum pressure gradient or yield stress must be applied to extrude a gel through a given fracture. Below this critical pressure gradient, the gel may not enter or propagate through the fracture.[10] Above this critical pressure gradient, the pressure gradient is nearly independent of flow rate.[8,9] Stated another way, gels show an extremely strong apparent shear-thinning behavior when extruding through fractures (and tubes, see Fig. 14). For short tubes with diameters less than 0.035 in. or fractures with estimated widths less than 0.035 in., the resistance factors, F_r, were described fairly well using Eq. 30,

$$F_r = 2 \times 10^6 \, u^{-0.83} \quad \text{if } w_f < 0.035 \text{ in.} \qquad (30)$$

where u was the superficial velocity in ft/d. The solid line in Fig. 14 illustrates Eq. 30. For tubes with diameters greater than 0.035 in., the resistance factors were described using Eq. 31.

$$\begin{aligned} F_r &= 2 \times 10^6 \, u^{-0.83} \quad \text{if } u \le 600 \text{ ft/d} \\ F_r &= 10{,}000 \quad \text{if } 600 < u < 6{,}200 \text{ ft/d} \\ F_r &= 4 \times 10^7 \, u^{-0.95} \quad \text{if } u \ge 6{,}200 \text{ ft/d} \end{aligned} \qquad (31)$$

The dashed curve in Fig. 14 illustrates Eq. 31 for velocities above 600 ft/d. Below 600 ft/d, Eq. 31 predicts the same values as Eq. 30. In Eqs. 30 and 31, a velocity exponent of -1 would demonstrate that the pressure gradient was fixed, independent of velocity. The data in Fig. 14 approaches that behavior.

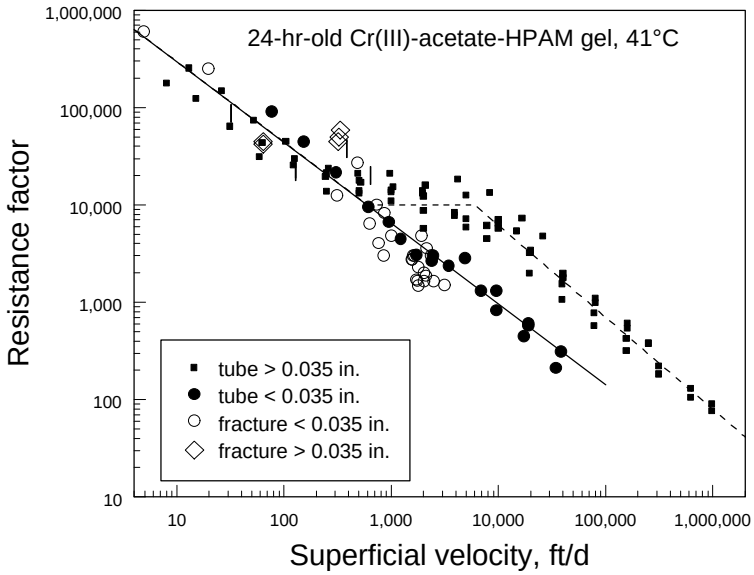

Fig. 14—Strong shear-thinning behavior in short tubes and fractures.

Pressure Gradient Versus Fracture Width. The critical pressure gradient for Cr(III)-acetate-HPAM gel extrusion decreases with increased fracture conductivity or width (Fig. 1, page 2). For fractures with conductivities ($k_f w_f$, in darcy-ft) between 1 and 277,000 darcy-ft (widths between 0.006 and 0.4 inches), the required pressure gradient (dp/dl, in psi/ft) can be estimated using Eq. 1 (page 3). To extrude this gel with a pressure gradient of only 1 psi/ft (a typical pressure gradient in a reservoir), the fracture width (w_f) should be at least 0.1 inches.

Gel Dehydration. Gel extrusion through fractures can occur at an unexpectedly low rate if the fracture conductivity or width is sufficiently small.[9,10] This low rate of gel propagation occurs because the gel dehydrates as it extrudes through the fracture. In other words, water leaves the gel and leaks off into the porous rock or flows through the fracture ahead of the gel, while the crosslinked polymer remains behind in the fracture to propagate at a much slower rate. Fig. 15 illustrates this propagation delay for a Cr(III)-acetate-HPAM gel in a fracture with a conductivity of 1.75 darcy-ft (effective average width of 0.0073 in.). We injected 110 fracture volumes of 24-hr-old Cr(III)-acetate-HPAM gel. Fig. 15 indicates that HPAM and chromium fronts arrived at the core outlet after injecting 30 fracture volumes of gel. Gel taken from the core inlet contained 26 times the original HPAM concentration and 44 times the original chromium concentration.

A similar experiment was performed in a wider, more-conductive fracture (w_f = 0.2 in., $k_f w_f$ = 34,700 darcy-ft). In this case, Fig. 16 shows that gel breakthrough at the fracture outlet did not occur until 1.8 fracture volumes of gel were injected. After gel placement, this fractured core was split apart to reveal a rubbery gel in the fracture. Fig. 17 shows chromium and HPAM concentrations for gel as a function of gel location along the length of the fracture. (These concentrations are reported relative to the chromium and HPAM concentrations in the gel before it was injected.) For gel in the fracture, on average, the HPAM concentration was twice that in original gel, while the chromium concentration was five times that in the original gel.

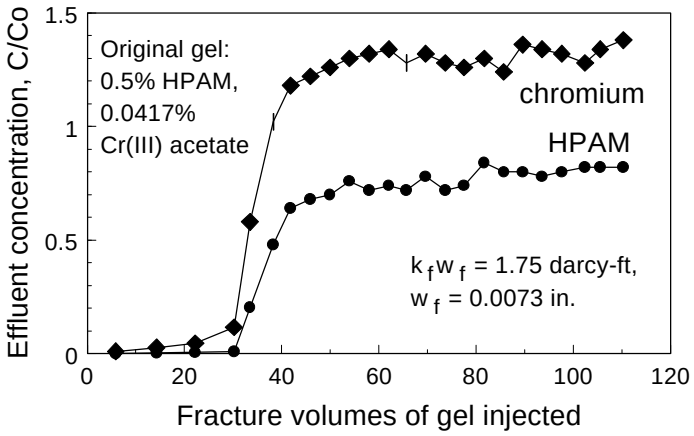

Fig. 15—Chromium and HPAM concentrations in Core 20 effluent.

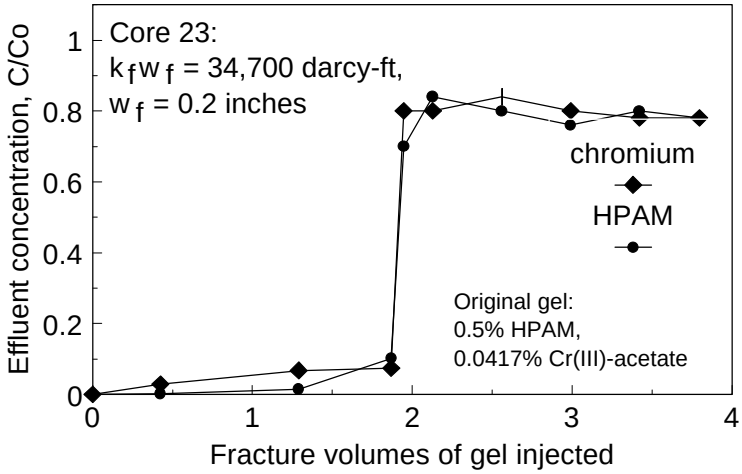

Fig. 16—Chromium and HPAM concentrations in Core 23 effluent.

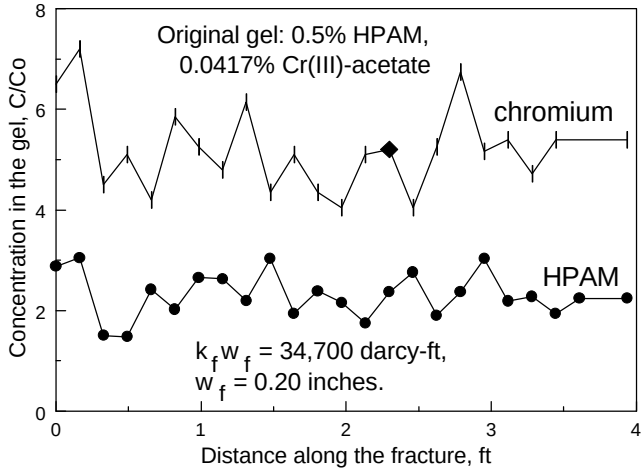

Fig. 17—Gel composition versus fracture length (Core 23).

Table 1 (page 3) shows how the dehydration effect varies with fracture conductivity and width for conductivities ranging from 1.14 to 277,000 darcy-ft (fracture widths ranging from 0.0063 to 0.4 in.).[10]

In fractures with conductivities between 1 and 242 darcy-ft (effective average widths between 0.006 and 0.04 inches), the Cr(III)-acetate-HPAM gel was concentrated (or dehydrated) by a factor typically between 20 and 40 during the extrusion process. This dehydration effect delayed propagation of the gel through fractures by factors ranging from 20 to 40. The gel dehydration effect became less pronounced as the fracture width increased. However, a fracture width around 0.4 inches was required to completely eliminate the effect.

At pressure gradients around 1 psi/ft (typical of far-wellbore pressure gradients), this gel may concentrate (dehydrate) by a factor less than 6. However, since near-wellbore pressure gradients could be much greater than 1 psi/ft, much greater degrees of gel dehydration could be observed near the well.

Gel Washout During Brine Injection. How effectively does the gel reduce fracture conductivity after gel placement? This question is addressed in Fig. 18 for fractures with conductivities ranging from 1 to 277,000 darcy-ft. The brine injection rates during these experiments were generally the same as those used during gel placement (typically 200 cm^3/hr). These studies were routinely performed after the gel injection experiments described above.

For reference, the horizontal line (at a *y*-value of 0.081 darcy-ft) in Fig. 18 gives the conductivity associated with a fresh, unfractured 650-md Berea sandstone core. For fractures with initial conductivities (before gel placement) below 5,000 darcy-ft, the final conductivities (after gel placement) were less than or equal to 0.081 darcy-ft. This result indicates that the gels effectively healed the fractures when the initial conductivities were less than 5,000 darcy-ft (i.e., fracture widths less than about 0.1 inches). We noted (Table 1) that the gel placement process concentrated gel in the fracture by a factor of 5 or more when the initial conductivities were less than 5,000 darcy-ft. These gels may be more resistant to washout than less concentrated gels. Incidentally, final core conductivity values less than 0.081 darcy-ft indicated that the permeability of the porous rock was reduced along with the conductivity losses experienced by the fracture. Much of this damage to the porous rock was simply gel that was not completely removed from the injection sand face before beginning brine injection.

For fractures with initial conductivities greater than 5,000 darcy-ft, Fig. 18 shows that the gel did not completely heal the fracture (because the final conductivities were greater than 0.081 darcy-ft). For these cases, the final conductivity after gel placement increased with increased initial fracture conductivity. Even so, the gel substantially reduced the fracture conductivities for all cases. For the 277,000-darcy-ft fracture, the gel reduced fracture conductivity by a factor of 600,000.

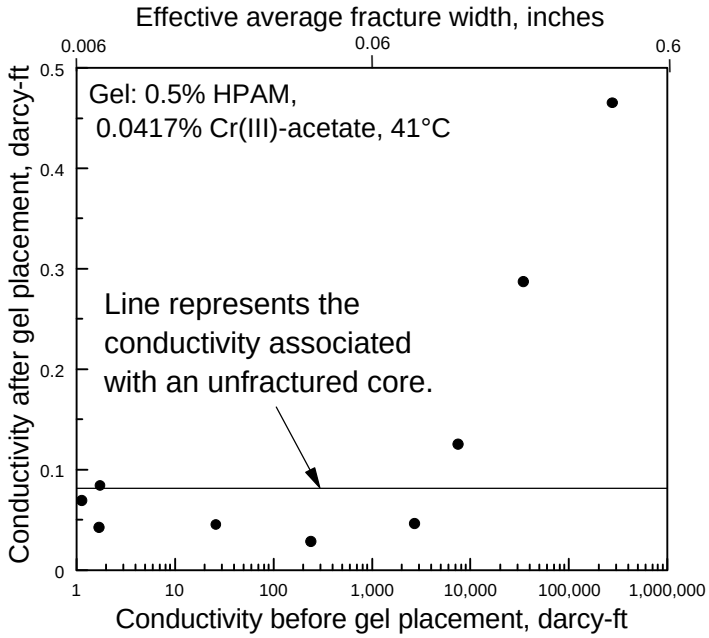

Fig. 18—Core conductivity during brine injection after gel placement versus fracture conductivity before gel placement.

For all tests that we performed to date, virtually no gel, polymer, or chromium was produced from the fractured cores during brine injection after gel placement. This result is demonstrated in Fig. 19 for the three most conductive fractures that we used to date (Cores 23, 24, and 25 with conductivities of 34,700, 277,000, and 7,500 darcy-ft, respectively, and widths of 0.2, 0.4, and 0.12, respectively). Within about 0.2 fracture volumes of brine throughput, the HPAM and chromium concentrations in the effluent were reduced below two percent of the concentrations in the original gel. Thus, we observed virtually no gel washout under the conditions that we tested.

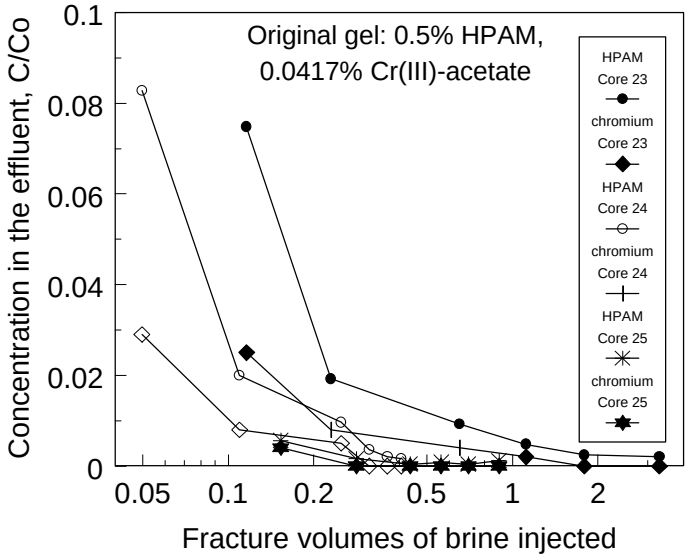

Fig. 19—Chromium and HPAM concentrations produced from Cores 23-25 (relative to the original values) during brine injection after gel placement.

Chromium and HPAM Removed From Gel During Dehydration

Our previous experiments indicated that as much as 95% of the water can leave the gel during extrusion through narrow fractures.[10] How much chromium and HPAM leave the gel during this process? Our analysis of effluent from fractured cores indicated that virtually no chromium or HPAM were produced until gel arrived at the fracture outlet. However, any free chromium or HPAM that left the gel may have been retained by the porous rock during these experiments. Therefore, we performed two experiments where a Cr(III)-acetate-HPAM gel was compressed against a 4.7-cm-diameter, 5-μm Millipore filter. In both experiments, the applied pressure was increased in stages, and the filtrate was analyzed for chromium and/or HPAM. In both experiments, 300 cm^3 of gel were originally placed before the filter. The maximum distance from the filter to the top of the gel column was 7 inches (18 cm). The results from these experiments are shown in Figs. 20 and 21. (Chromium concentrations were determined by atomic absorption, while the starch tri-iodide method was used to determine HPAM concentrations.)

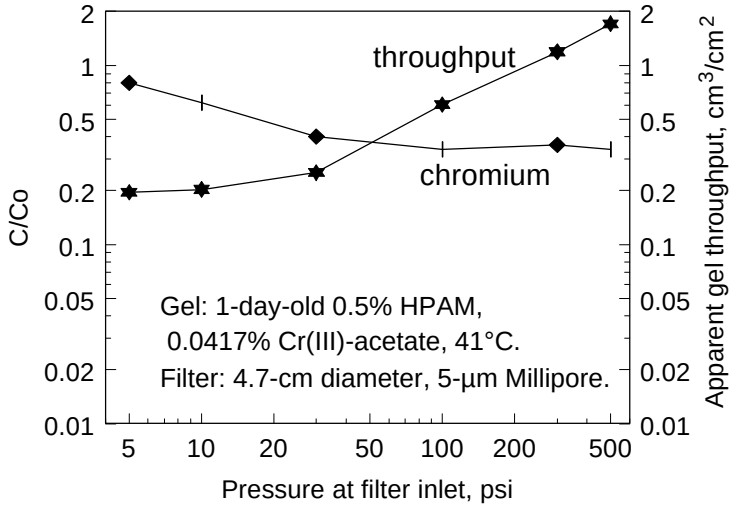

Fig. 20—Chromium in filtrate from first filtration experiment.

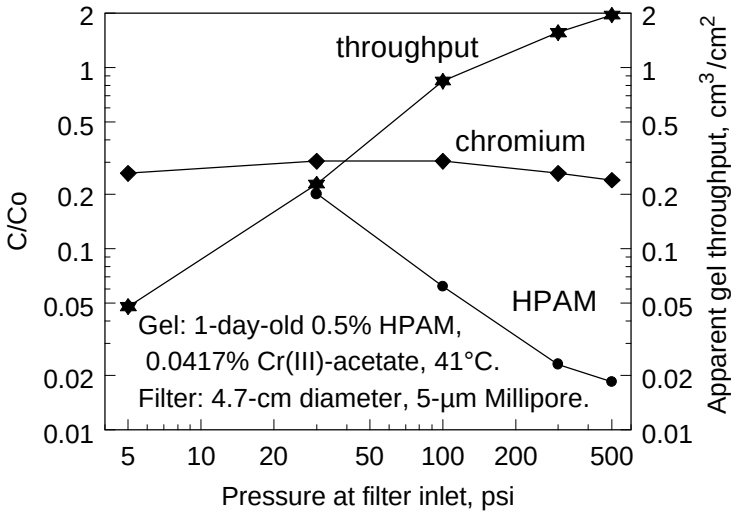

Fig. 21—Chromium and HPAM in filtrate from second filtration experiment.

Figs. 20 and 21 indicate that at moderate to high pressure differences, the chromium concentration in the filtrate stabilized at 25% to 35% of the chromium concentration in the original gel. Fig. 21 indicates that the first filtrate contained 20% of the HPAM concentration in the original gel. However, the HPAM concentration rapidly dropped to low values in subsequent filtrate samples. Thus, under pressure, significantly more free chromium leaves the gel than HPAM. (In these experiments, no gel was ever noted in the filtrate. This observation suggests that the chromium and HPAM in the filtrate were not present as crosslinked material.) For both experiments, the total throughput was slightly less than 2 cm^3 of filtrate per cm^2 of filter surface area. Since the filter area was 17.3 cm^2, the total volume of filtrate was roughly 30 cm^3 or 10% of the original gel volume. Thus, in these experiments, the gel was concentrated by a much smaller factor than that during our gel extrusion experiments in fractures. A rationalization for this result is that the pressure gradients in the filtration experiments were much less than those in the fractured cores. In the filtration experiments, the pressure was applied over about 7 inches (18 cm) of gel (before reaching the filter). In contrast in the fractured cores, the pressure difference occurred between the gel in a narrow fracture and the porous rock just inside the fracture face—a much smaller distance, leading to a much greater pressure gradient.

Effect of Rock Permeability on Gel Extrusion Through Fractures

For all data shown in Fig. 1 (page 2), the core material used was 650-md Berea sandstone. At a recent project review (January 28, 1998), the question was raised: does the performance of the gel during our extrusion experiments depend on the permeability of the porous rock? We will answer this question using both calculations and experimental data.

Preparation of the fractured cores was described earlier.[8,9] The fractured cores (Berea sandstone) were 4 feet (122 cm) in length and 1.5 inches (3.8 cm) in height and width. Each core had four internal pressure taps that were spaced equidistant along the fracture—thus dividing the core into five equal sections. Before gel injection, all fractured cores were completely saturated with brine. All fractures were oriented vertically during our experiments.

Extrusion Through Fractures in 50-md Berea. Four experiments were performed using 50-md Berea sandstone. These 4-ft-long cores had the same dimensions and were prepared and fractured in the same manner as that for the 650-md Berea cores in our earlier work.[8,9] The fractures in the 50-md Berea had conductivities ranging from 5 to 34,700 darcy-ft (Table 2). We extruded a 24-hr-old Cr(III)-acetate-HPAM gel using the same flow rate, temperature, and experimental conditions that were used in our earlier floods. Fig. 22 compares the results for these new experiments (in 50-md Berea) with those from our earlier studies (in 650-md Berea). Fig. 22 shows that within the data scatter, the gel shows the same performance while extruding through fractures in 50-md Berea as through fractures in 650-md Berea. Specifically, using 50-md Berea, the pressure gradient required for gel extrusion through fractures ranged from 131 psi/ft in a fracture with a conductivity of 5.06 darcy-ft to 1.1 psi/ft in a fracture with a conductivity of 34,700 darcy-ft. For a given fracture conductivity, the degree of gel dehydration using 50-md Berea was similar to that using 650-md Berea (compare the fifth column of Table 2 with the fourth column of Table 1, page 3). Figs. 23-26 show gel compositions versus fracture length for the 50-md Berea experiments.

Table 2—Effect of Fracture Conductivity on Gel Propagation (50-md Berea Cores)

Core	Conductivity, darcy-ft	Fracture width, inches	Pressure gradient, psi/ft	Average gel concentration factor
30	5.06	0.010	131	21
31	70.5	0.025	53	21
32	2,220	0.079	4.5	3.8
33	34,700	0.20	1.1	1.2

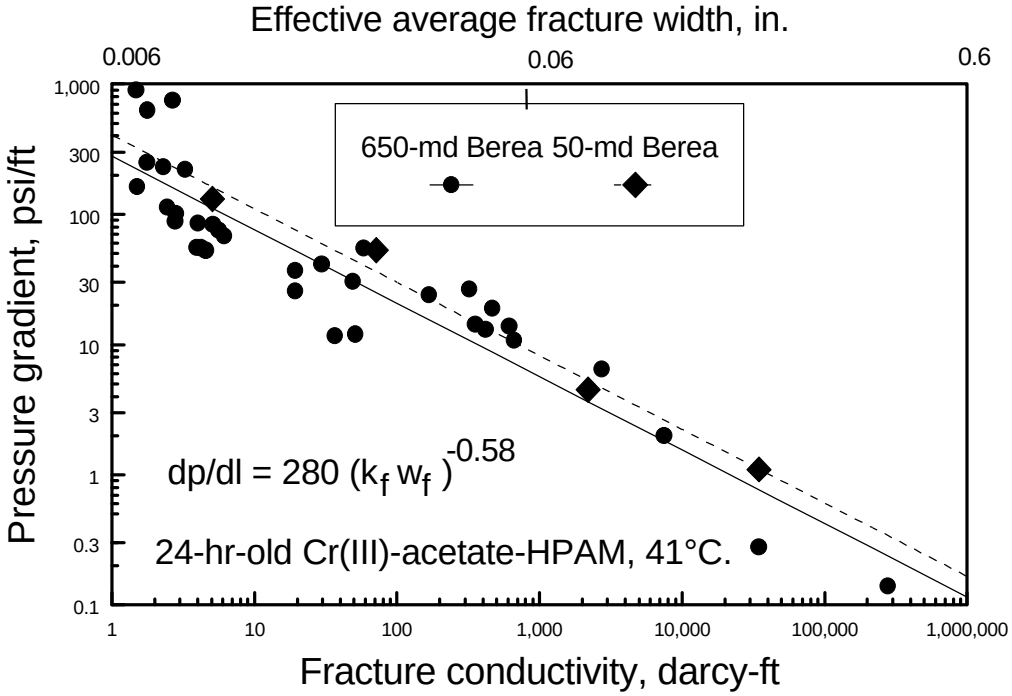

Fig. 22—Pressure gradient versus fracture conductivity.

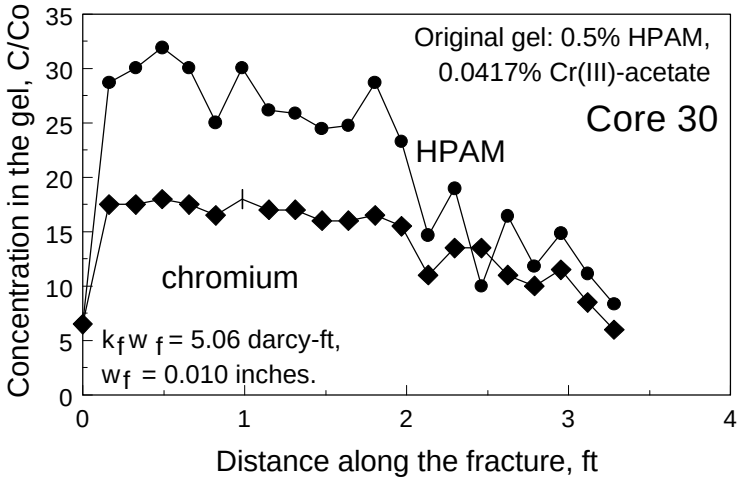

Fig. 23—Gel composition versus fracture length (Core 30).

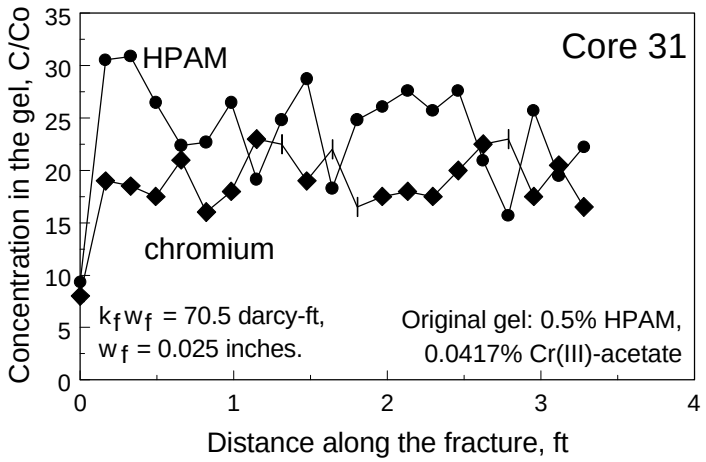

Fig. 24—Gel composition versus fracture length (Core 31).

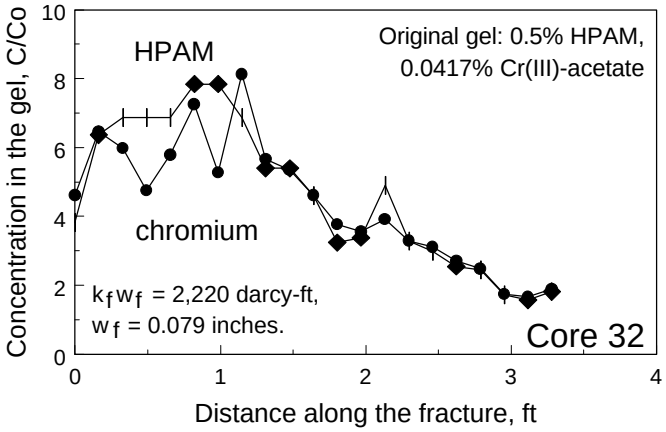

Fig. 25—Gel composition versus fracture length (Core 32).

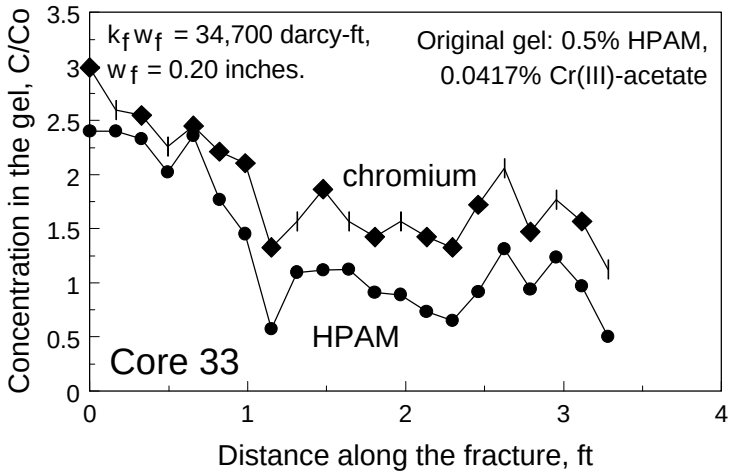

Fig. 26—Gel composition versus fracture length (Core 33).

Calculations. The above issue can also be addressed from a theoretical viewpoint using simple calculations with the Darcy equation. We first ask, what pressure gradient would be observed in the porous rock if all water left the gel and flowed only through the porous rock (i.e., no fracture was present)? To answer this question, we need the maximum water flow rate, the cross-sectional area of the rock, the viscosity of the water (brine), and the rock permeability. Most of the experiments represented in Fig. 22 were performed using a fixed volumetric injection rate of 200 cm^3/hr. The cross-sectional area of most of these cores was 14.5 cm^2 (i.e., the cross-sectional area of the porous rock, not including the fracture). The viscosity of our brine was 0.67 cp at 41°C. From the Darcy equation, one can easily determine that the maximum pressure gradient (*dp/dl*, in psi/ft) in the porous rock is related to rock permeability (*k*, in md) by Eq. 32.

$$dp/dl = 1{,}149 / k \quad \text{.....(32)}$$

Under our experimental conditions, Eq. 32 reveals that the maximum pressure gradient in the porous rock is 1.77 psi/ft if the rock permeability is 650 md. This limit assumes that all water from the dehydrated gel flows through the porous rock rather than through the fracture. Thus, for all data using 650-md Berea in Fig. 22 where pressure gradients were greater than 1.77 psi/ft, the flow capacity of the porous rock was sufficient to handle all water of dehydration from the gel. Actually, Fig. 22 shows that we experimentally observed a pressure gradient around 0.1 psi/ft for an experiment in 650-md sandstone. Thus, Eq. 32 appears to conservatively over-predict the pressure gradient by a factor of at least 17. This conclusion is also supported by the results in the 50-md fractured cores. Eq. 32 predicts that the limiting pressure gradient should be 23 psi/ft in the 50-md fractured cores. However, we experimentally observed a pressure gradient of 1.1 psi/ft for an experiment in 50-md sandstone (Table 2 and Fig. 22). At least two reasons may account for the over-prediction by Eq. 32. First, not all water is removed from the gel during the extrusion process. Second, some free water probably continues to flow through the fracture.

Based on both experiments and calculations, we conclude that our experiments in fractured cores provide accurate indications of gel extrusion properties in fractures. We plan additional experiments in 10-md limestone cores; however, we have experienced difficulty obtaining carbonate cores that are amenable to the creation of 4-ft long fractures. Our efforts in this area will continue.

Gels with Other Concentrations

In all experiments to this point, we injected gels that contained 0.5% HPAM and 0.0417% Cr(III) acetate. (Refer to this composition as our 1X gel.) What would happen if different concentrations were used? This question is relevant to field applications since the gel concentrations are often progressively increased during the course of a gel treatment. In Core 27 (average $k_f w_f$=58.4 darcy-ft), we injected a gel (named our 0.5X gel) that contained one-half the HPAM and Cr(III)-acetate concentrations of our earlier experiments. All other conditions were the same. Gel arrived at the end of the 4-ft-long fracture after injecting roughly twice the volume associated with breakthrough for the 1X gel in earlier, similar experiments. During injection of the 0.5X gel, the pressure gradient along the gel-filled fracture averaged 55 psi/ft. This value is consistent with the trend shown in Fig. 1 (page 2). Furthermore, chemical analysis of gel in the fracture (determined after the fracture was opened) revealed that the gel was concentrated by a factor of 32 (on

average). The final concentrations in the dehydrated gel were about the same as those seen in our previous experiments with our 1X gel (in fractures with similar conductivities). Fig. 27 plots chromium and HPAM concentrations for gel in the fracture relative to the concentrations in the originally injected gel. These results suggest that for a given fracture conductivity and gel system, the gel may concentrate to a fixed level, regardless of the initial gel composition. (Incidentally, in Figs. 27 and 28, the samples were lost from the last quarter of the fracture so those analyses were not available.)

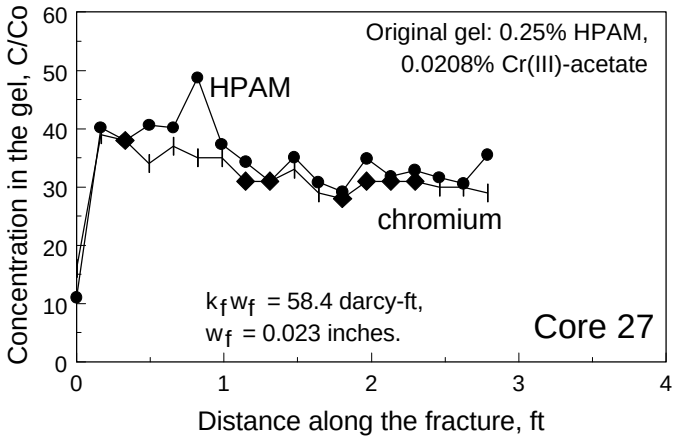

Fig. 27—Gel composition versus fracture length (Core 27).

To further test this idea, we performed another experiment using a gel that initially contained 3% HPAM and 0.25% Cr(III) acetate (named our 6X gel). Our 1X gel experienced a pressure gradient of 6.5 psi/ft and concentrated by a factor of 4.8 when extruded through a 2,730 darcy-ft fracture (Table 1, page 3). Thus, based on the above results, we speculated that our 6X gel might extrude through a similar fracture, exhibiting a low pressure gradient and without dehydrating.

We extruded our 6X gel through a 4-ft-long, 2,220 darcy-ft fractured core (Core 28) using the same conditions as those in our other experiments. Analysis of pressure behavior (during gel injection) and gel in the fracture (after disassembly of the core) revealed that the gel was concentrated, on average, by a factor of 5. Fig. 28 plots chromium and HPAM concentrations for gel in the fracture relative to the concentrations in the originally injected gel. The average pressure gradient was 233 psi/ft during gel extrusion.

Another experiment was performed with our 6X gel in a 4-ft-long, 17,760 darcy-ft fractured core (Core 29) using the same conditions as those in our other experiments. Analysis of pressure behavior (during gel injection) and gel in the fracture (after disassembly of the core) revealed that the gel was concentrated, on average, by a factor of 3. Fig. 29 plots chromium and HPAM concentrations for gel in the fracture relative to the concentrations in the originally injected gel. The average pressure gradient was 70 psi/ft during gel extrusion. This value was 30 to 70 times greater than the pressure gradient expected for a 1X gel (see Fig. 1, page 2). Incidentally, in Fig. 29, unusual gel-concentration behavior was noted at two positions along the fracture—at 1.8 ft and 3.3 ft. At these locations, the chromium/HPAM ratios were anomalous. We have not seen this behavior previously, and we have no explanation for it.

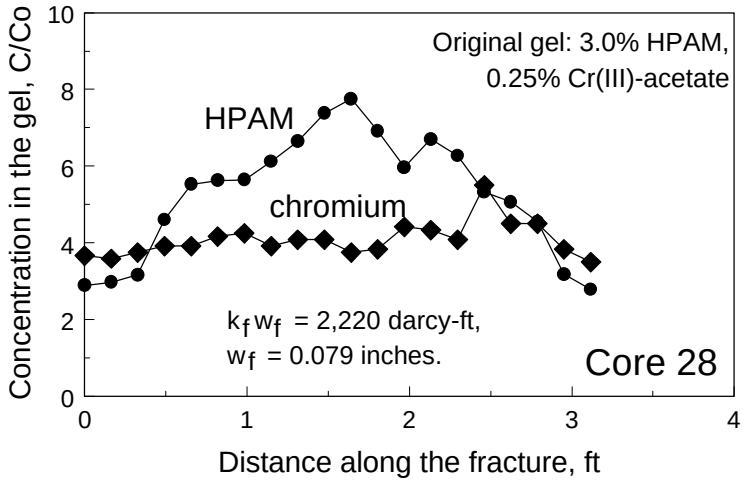

Fig. 28—Gel composition versus fracture length (Core 28).

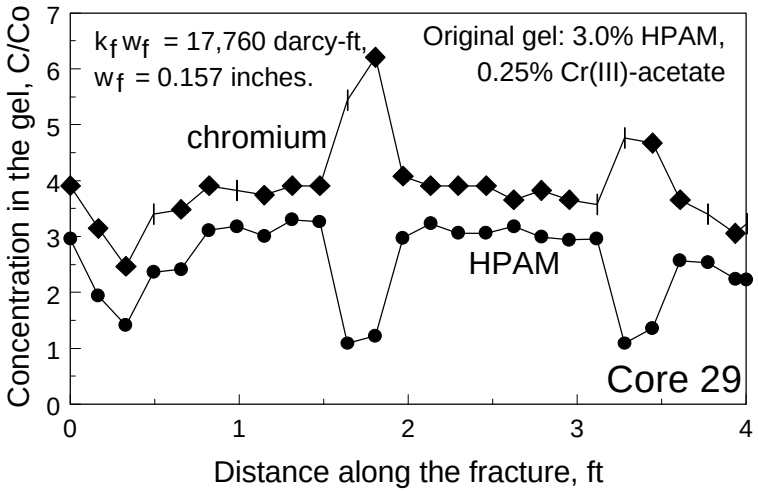

Fig. 29—Gel composition versus fracture length (Core 29).

Gel Extrusion in Radial Flow

Most of the previous discussion is relevant to gel extrusion in linear flow—for example, in vertical fractures that cut through vertical wells. However, in vertical fractures that cut through horizontal wells, the flow geometry is radial (at least, near the well). How does gel extrusion in radial flow compare with that in linear flow?

Eq. 33 gives the Darcy equation for radial flow.

$$dp/dr = u\mu/k_f = u\mu_w F_r / k_f \quad \text{.....(33)}$$

In the proper velocity range, Eqs. 31 and 33 combine to give Eq. 34.

$$dp/dr = c_a u^{n+1} \mu_w / k_f \quad \text{.....(34)}$$

In Eq. 34, c_a is a constant and n is the velocity exponent that varies from -0.83 to -0.95 (from Eq. 31). Since n is close to a value of -1, Eq. 34 suggests that the pressure gradient should be almost constant (i.e., independent of velocity or radial position) during gel extrusion in radial flow. If the pressure gradient is independent of radial position, we expect the degree of gel dehydration also to be independent of radial position.

Radial Fracture H1. To test these ideas, we performed gel extrusion experiments in a horizontally-oriented radial-flow fracture. (We will call this "Radial Fracture H1.") The fracture was formed by placing two 650-md Berea sandstone slabs (each with dimensions, 12 x 12 x 3 in.) together and casting in epoxy. From tracer and conductivity experiments, we estimated that the fracture width was about 0.01 in. Thus, the fracture dimensions were 12 x 12 x 0.01 in. An injection port and a production port were positioned at opposite corners of the fracture, and four internal pressure taps were located along the connecting diagonal.

We injected 1,870 cm^3 of 24-hr-old Cr(III)-acetate-HPAM gel (0.5% HPAM, 0.0417% Cr(III) acetate, 1% NaCl, 0.1% $CaCl_2$) at a rate of 200 cm^3/hr. No chromium or polymer was produced during the gel injection process. Near the end of gel injection, Fig. 30 shows the pressure behavior observed across the radial fracture. For comparison, Fig. 30 also plots the pressure behavior expected for Newtonian radial flow and for Newtonian linear flow. In agreement with the prediction of Eq. 34, Fig. 30 shows that the behavior during gel extrusion in radial flow was more similar to that for Newtonian linear flow than for Newtonian radial flow. In other words, during gel extrusion through fractures, the pressure gradient was nearly independent of position in both linear and radial flow.

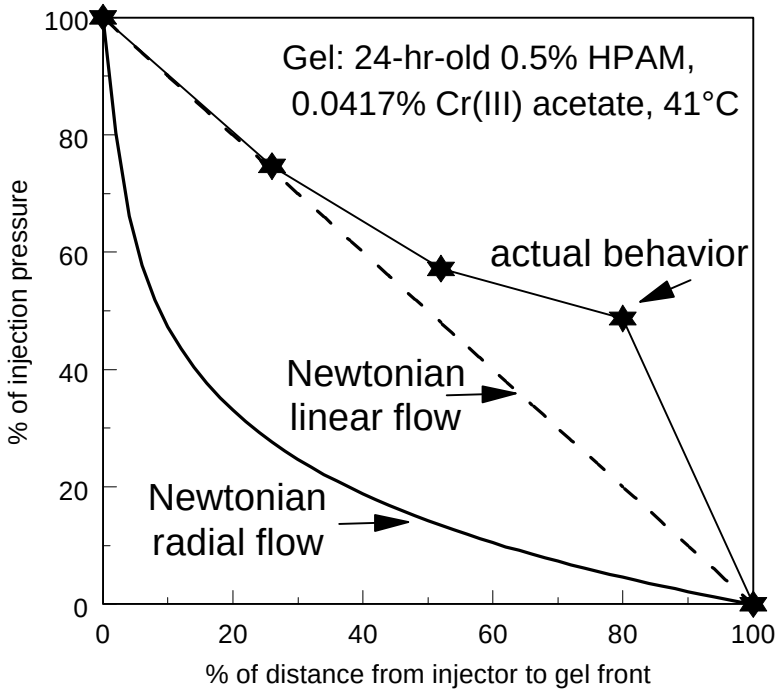

Fig. 30—Pressure behavior observed during gel injection into Radial Fracture H1.

After gel injection, the core was opened to expose the gel in the fracture. Fig. 31 shows the extent of gel propagation in this horizontal fracture. The fracture area was divided into 36 equal 2-inch x 2-inch squares, and the composition of each square was determined. The numbers in the squares in Fig. 31 indicate the chromium concentrations relative to the chromium concentration in the originally injected gel. Fig. 31 reveals that on average, the gel was concentrated by a factor of 21 (standard deviation: ± 6) during the extrusion process. The gel was often slightly less concentrated near the gel-water front. However, in general, the degree of dehydration was independent of radial position from the injection point.

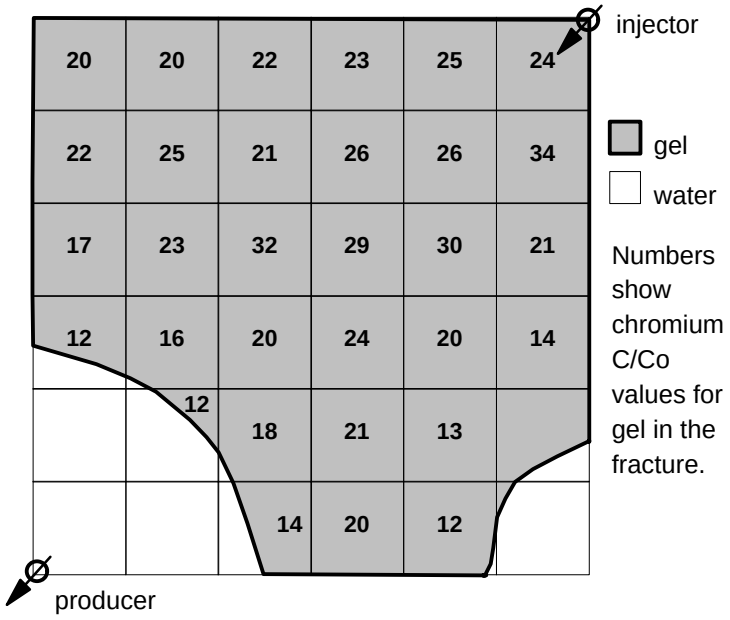

Fig. 31—Relative chromium concentrations in Radial Fracture H1.
(Fracture dimensions: 12 in. x 12 in. x ~0.01 in.)

Radial Fracture H3. The above experiment was repeated using Radial Fracture H3, which had a fracture width of about 0.04 in. (rather than 0.01 in. associated with Radial Fracture H1 above). The fracture volume in this case was 93 cm^3. (For comparison, the total pore volume of the rock-matrix system was 2,973 cm^3.) We injected about 19 fracture volumes (1,750 cm^3) of 1-day-old Cr(III)-acetate-HPAM gel using an injection rate of 200 cm^3/hr. During gel injection, Fig. 32 shows the chromium and HPAM concentrations in the core effluent relative to the concentrations in the original gel. The first chromium and HPAM were detected in the effluent after injecting about 9 fracture volumes of gel. These concentrations gradually increased over the course of injecting the next 9-10 fracture volumes of gel, until the final relative chromium and HPAM concentrations were 0.80 and 0.56, respectively.

Radial Fracture H3 had 12 pressure taps. The solid circles in Fig. 33 illustrate the locations of the 12 pressure taps that were monitored during this experiment. The numbers between the solid circles indicate the pressure gradients that were observed between the various taps near the end of

gel injection. Figs. A1 to A3 in Appendix A show the details of the pressure behavior for the various taps during the course of gel injection.

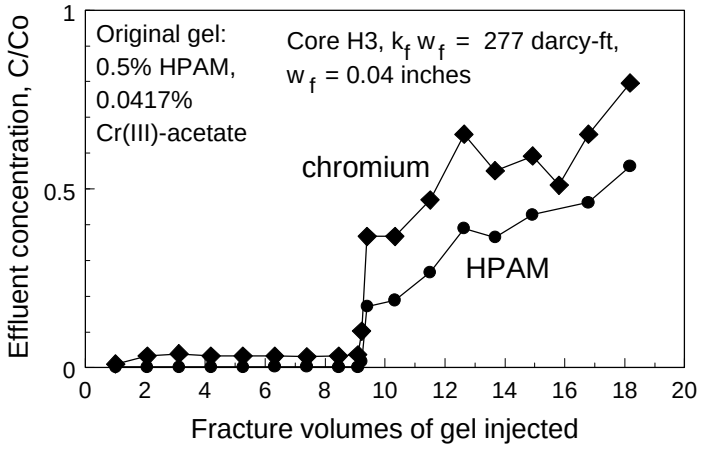

Fig. 32—Chromium and HPAM concentrations in effluent from Radial Fracture H3.

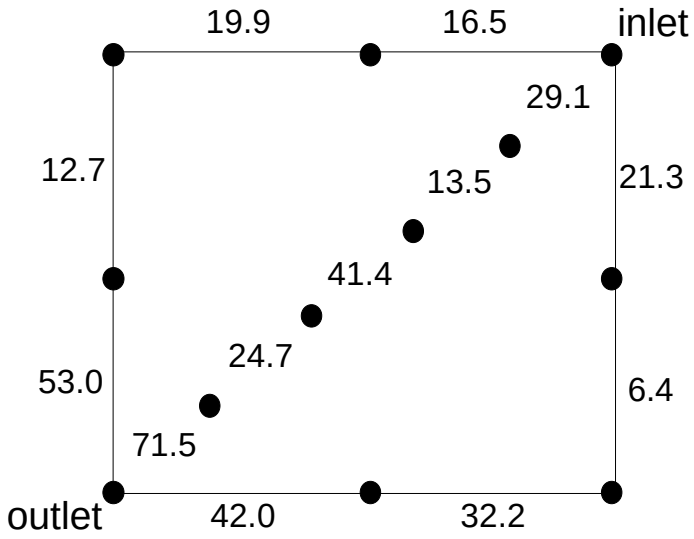

Fig. 33—Radial Fracture H3 pressure gradients (psi/ft) between pressure taps.
(During gel flow. Fracture dimensions: 12 in. x 12 in. x ~0.04 in.)

A wide variation of pressure gradients were observed between the taps—from 6.4 psi/ft to 71.5 psi/ft. The average pressure gradient for the numbers shown in Fig. 33 was 29.6 psi/ft. Interestingly, the highest pressure gradients were observed near the core outlet. A high pressure gradient was also observed in the center of the pattern—where low pressure gradients might be expected. During the final stages of gel injection, Fig. 34 plots the pressure behavior in a different form to compare the observed behavior with that predicted for linear and radial flow of Newtonian fluids. The star symbols in this figure show the behavior along the central streamline between the injection and production ports. The circle and diamond symbols show the pressure behavior along the right streamline and left streamline, respectively. The solid curve shows the

behavior predicted for Newtonian radial flow, while the dashed line shows the behavior predicted for Newtonian linear flow. Obviously, the actual pressure behavior deviated significantly from both Newtonian radial and linear flow. Interestingly, the pressure behavior along the central streamline was not significantly different than that along the right and left streamlines. We wonder whether the observed deviations from the Newtonian-linear-flow prediction might be due to variations in fracture width in this experiment.

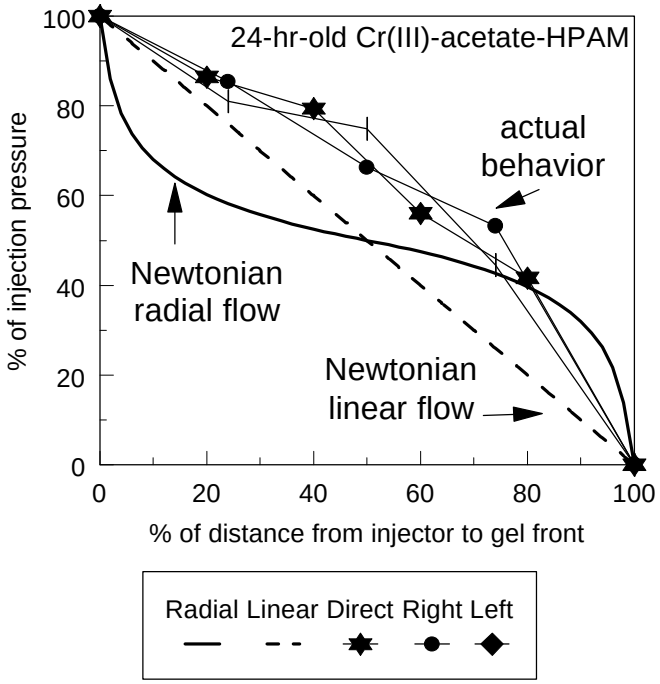

Fig. 34—Pressure behavior near the end of gel injection in Radial Fracture H3.

After gel placement, flow was stopped for one day. Then, brine was injected. Fig. 35 shows stabilized pressure gradients between the taps during brine injection at 200 cm^3/hr (the same rate used for gel placement). As shown, most of the pressure drop occurred near the injection port.

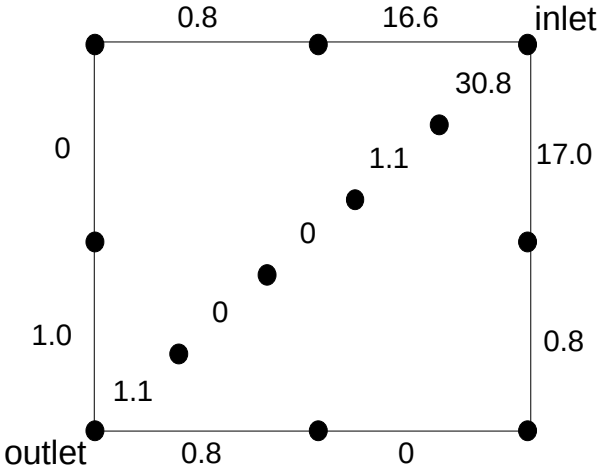

Fig. 35—Pressure gradients (psi/ft) between taps during brine injection (H3).

After this experiment was completed, Radial Fracture H3 was opened to reveal gel in the fracture. As with Radial Fracture H1, the fracture area was divided into 2-in.-by-2-in. segments and analyzed for chromium and HPAM content. Fig. 36 shows these concentrations, expressed relative to the concentrations in the original gel. On average, chromium and HPAM were concentrated by factors of 12.9 and 12.2, respectively. Chromium concentration factors ranged from 9 to 19, while HPAM concentration factors ranged from 6 to 20. The concentration factors were somewhat below average on one side of the pattern near the production port. Other than that, no relation was evident between position and the concentration factors. This finding supports the results observed with Radial Fracture H1.

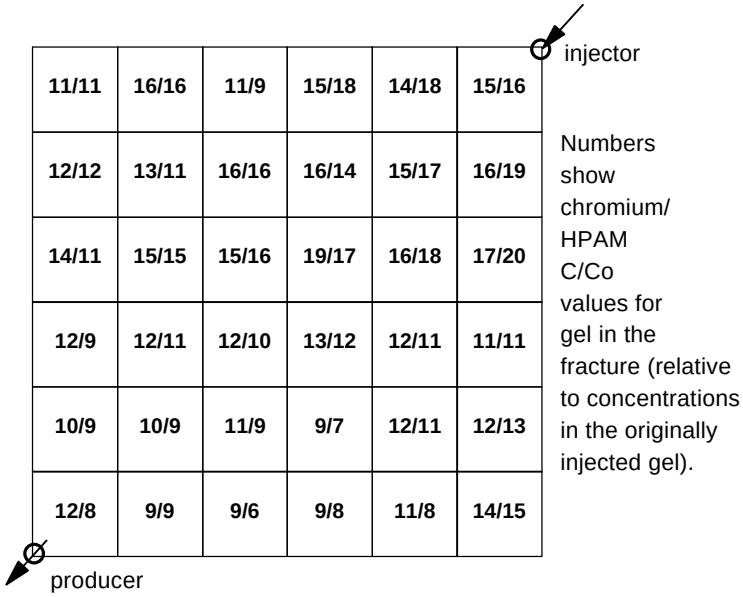

Fig. 36—Relative chromium and HPAM concentrations in Radial Fracture H3.

Radial Fracture H2. Another experiment was performed using Radial Fracture H2. This core was similar to Radial Fracture H1, except that gel was injected in the center of the areal pattern rather than at one corner. In Radial Fracture H2, the fluid was produced at the four corners of the pattern. A 24-hr-old Cr(III)-acetate-HPAM gel (our standard 1X composition) was injected using a fixed inlet pressure of 200 psi. Pressures at the outlets were atmospheric. Only 105 cm^3 (~4 fracture volumes) of gel were injected over the course of one week. About half of this volume was injected during the first 24 hours. At the end of the experiment, the fracture was opened to reveal a radial pattern of gel that extended roughly 1.5 in. from the injection port. Chemical analysis revealed that on average, the chromium and HPAM were concentrated by factors of 60 and 46, respectively.

Radial Fracture H4. Another experiment was performed using Radial Fracture H4. This core was similar to Radial Fracture H2, except that the fracture width was about 0.04 inches. Again, gel was injected in the center of the pattern and produced at the four corners. Fig. 37 shows the positions of the pressure taps, as well as the stabilized pressure gradients that were observed

between the various taps near the end of gel injection. Twenty-one fracture volumes (1,950 cm^3) of 24-hr-old Cr(III)-acetate-HPAM gel (our standard 1X composition) were injected using a fixed injection rate of 200 cm^3/hr.

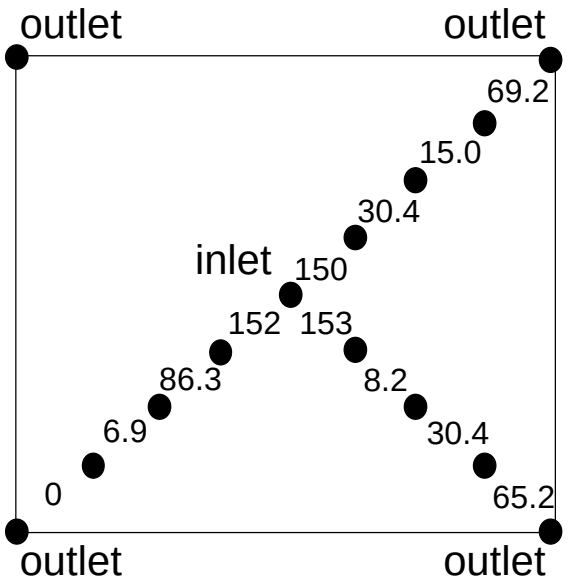

Fig. 37—Radial Fracture H4 pressure gradients (psi/ft) between pressure taps.
(During gel flow. Fracture dimensions: 12 in. x 12 in. x ~0.04 in.)

During gel injection, Fig. 38 shows the chromium and HPAM concentrations in the core effluent relative to the concentrations in the original gel. The first significant chromium and HPAM were detected in the effluent from one outlet (the outlet in Fig. 37 without a line of pressure taps) after injecting about 13 fracture volumes of gel. No significant chromium or HPAM were produced from the other three outlets.

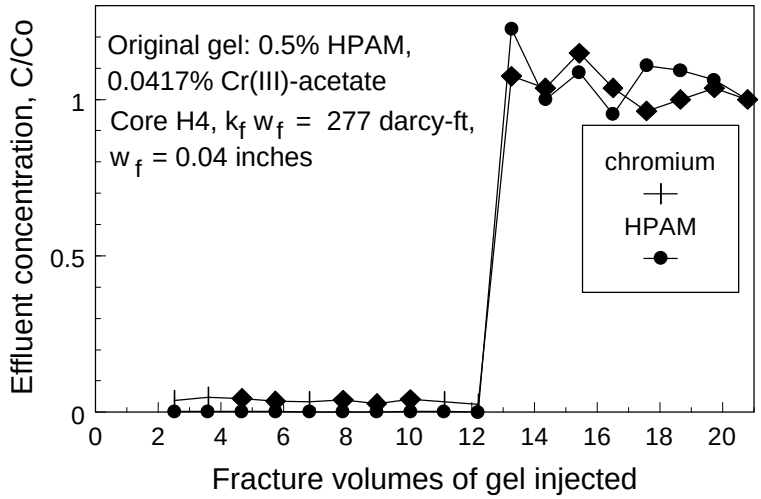

Fig. 38—Chromium and HPAM concentrations in effluent from Radial Fracture H4.

Figs. A4 to A6 in Appendix A show details of the pressure behavior for the various taps during the course of gel injection in Radial Fracture H4. The numbers between the solid circles in Fig. 37 indicate the stabilized pressure gradients that were observed between the various taps near the end of gel injection. We noted that the highest pressure gradients were observed near the inlet. Upon first consideration, one might assume that this behavior was due to radial flow near the inlet port. However, in view of our previous results, we suspect that the fracture width was narrower or "bowed inward" near the injection port because of the large weight of rock and the lack of support for that weight at the center of the areal pattern.

After this experiment was completed, Radial Fracture H4 was opened to reveal gel in the fracture. As with Radial Fractures H1 and H3, the fracture area was divided into 2-in.-by-2-in. segments and analyzed for chromium and HPAM content. Fig. 39 shows these concentrations, expressed relative to the concentrations in the original gel. On average, chromium and HPAM were concentrated by factors of 12.0 and 11.6, respectively. Chromium concentration factors ranged from 7 to 15, while HPAM concentration factors ranged from 6 to 16. Consistent with our observations with Radial Fractures H1 and H3, no relation was evident between position and the concentration factors.

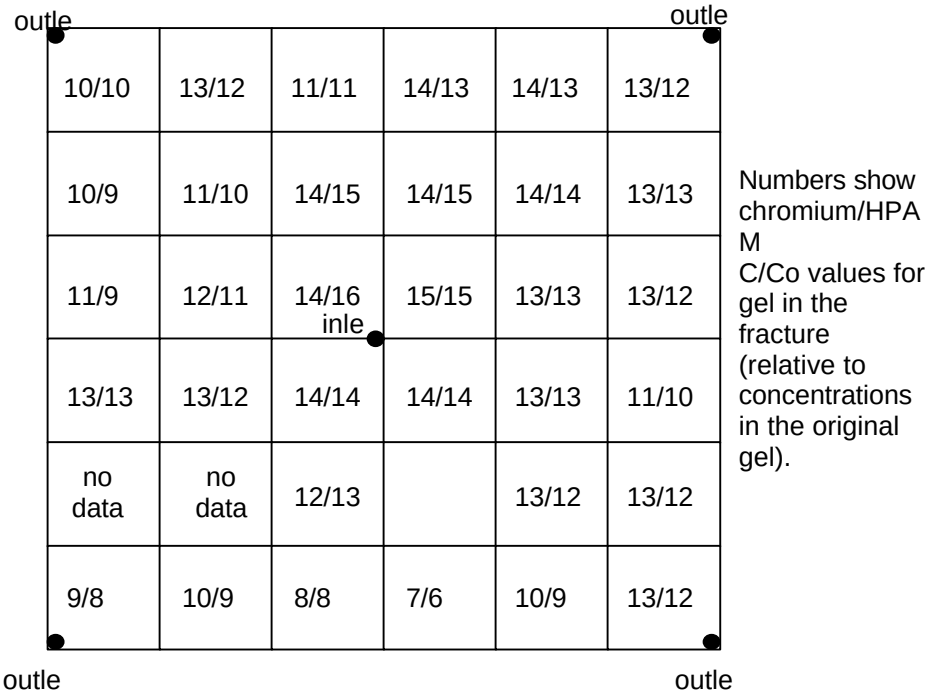

Fig. 39—Relative chromium and HPAM concentrations in Radial Fracture H4.

Radial Fracture H5. We attempted a flow visualization experiment using Radial Fracture H5. This core was very similar to Radial Fracture H3, except that one Berea sandstone "fracture face" was replaced by a piece of polycarbonate to allow gel propagation to be visualized during the placement process. Unfortunately, the polycarbonate "bowed out" during the course of gel injection. Since the fracture width clearly changed with time, this experiment was terminated.

Visualization Experiment During Linear Flow

A flow visualization experiment was performed in a 4-ft-long linear fractured core. This core was similar to our other 4-ft-long cores, except that one "fracture face" was replaced by a piece of polycarbonate to allow gel propagation to be visualized during the placement process. Also, the surface of the 650-md Berea sandstone was relatively flat and smooth (a cut surface) instead of the fractured face associated with our other 4-ft-long cores. The fracture width was about 0.04 in. and the conductivity was 277 darcy-ft. The estimated fracture volume was 46.5 cm^3. We injected 13.1 fracture volumes (620 cm^3) of 24-hr-old Cr(III)-acetate-HPAM gel (our standard 1X composition) using a flow rate of 200 cm^3/hr. Fig. 40 plots the chromium and HPAM concentrations in the effluent relative to the concentrations in the original gel. Chromium, HPAM, and gel breakthroughs were noted after injecting 9.5 fracture volumes of gel. After breakthrough, the pressure gradient stabilized at 23 psi/ft during gel extrusion.

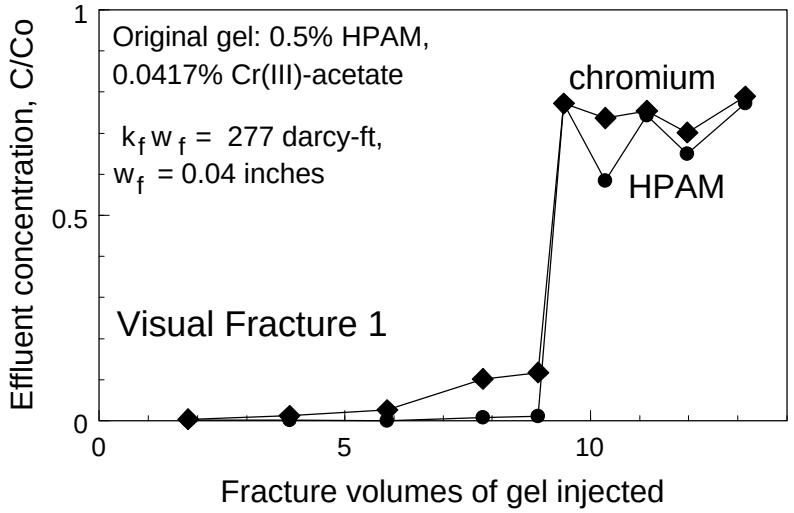

Fig. 40—Chromium and HPAM concentrations in effluent from Visual Fracture 1.

During our experiments, various sequences of dyed and undyed gel banks were injected. Also, after gel placement, various sequences of dyed and undyed water banks were injected. Unfortunately, no conclusions or insights could be drawn from our observations or video tapes.

After completing this experiment, the fracture was opened to determine the relative chromium and HPAM concentrations for gel along the length of the fracture (Fig. 41). On average, the chromium and HPAM were concentrated by factors of 9.3 and 11.5, respectively. These values are consistent with the observed gel breakthrough of 9.5 fracture volumes. We note that the gel breakthrough time, the degree of gel dehydration, and the pressure gradient for gel extrusion during this experiment were similar to those observed in our radial-flow fractures with the same fracture width (i.e., Radial Fracture H3—see Figs. 32, 33, and 34). We also note that only one fracture face was available for leakoff during this visualization experiment, while two faces were available for leakoff with Radial Fracture H3. Evidently, a single fracture face provides sufficient flow capacity for the water of dehydration to escape the fracture.

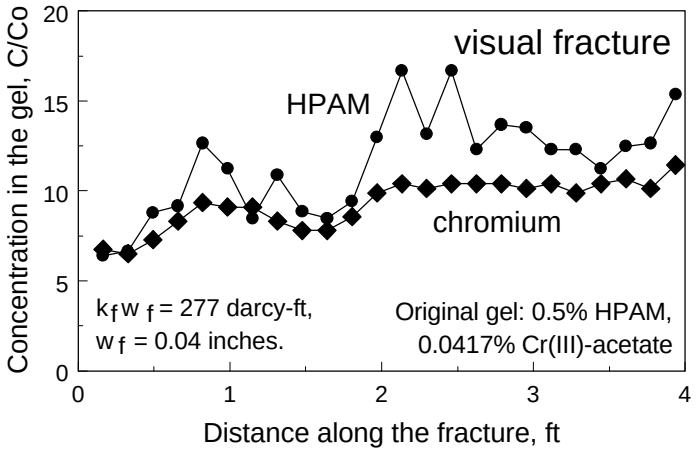

Fig. 41—Gel composition versus fracture length for Visual Fracture 1.

Nature of Effluent from Fractured Cores

In our work to date, the effluent from fractured cores consisted of the co-mingled production from the fracture and the porous rock. Only brine is produced from the porous rock. Evidence indicates that the fracture is the only conduit available for the gel. However, water also may flow through the fracture.

Since extrusion through fractures can concentrate gel by factors up to 50, one might expect the effluent from a fractured core to consist of a large ribbon of concentrated, rubbery gel along with free water. However, to date, the effluent has always appeared as a very fine dispersion of gel particles (i.e., a "colloidal-dispersion gel"). This observation suggests two possibilities. First, at the core outlet, the degree of mixing between the ribbon of extruded gel (from the fracture) and free water (from the porous rock) is sufficiently intense that a gel dispersion is created. The second possibility is that the fine dispersion of gel is indicative of the mechanism for gel transport through the fracture.

We performed an experiment in an attempt to isolate the free water produced from the porous rock from the gel produced from the fracture. A special outlet fitting was made to segregate the effluent into three parts—one from the fracture and two from the porous rock (on either side of the fracture). This polycarbonate end piece was epoxied to the core outlet as shown in Fig. 42. The core material was 650-md Berea sandstone with overall dimensions of 15.24 cm x 3.81 cm x 3.81 cm. The average fracture width was 0.04 in. or 0.1 cm (fracture conductivity: 277 darcy-ft). About 70 fracture volumes (400 cm^3) of 24-hr-old Cr(III)-acetate-HPAM gel were injected using a rate of 200 cm^3/hr. Gel arrival at the fracture outlet was noted after injecting 4 fracture volumes of gel. The physical appearance of the gel from the fracture outlet was the same as that for the injected gel. Also, the chromium and HPAM compositions of the gel from the fracture outlet were the same as those for the injected gel. Fig. 43 plots the fraction of flow from the fracture and the two matrix portions of the core during gel injection. As expected, the flow rates from the two matrix portions were identical. After injecting 70 fracture volumes of gel, flow from the fracture accounted for 80% of the total flow, while flow from the matrix accounted for 20% of the total

flow (10% from each matrix). For comparison, before gel injection, the calculated flow capacity of the fracture was 3,400 times greater than the combined flow capacity of the two matrix portions. Thus, a substantial fraction of the water that was dehydrated from the gel appeared to flow through the matrix.

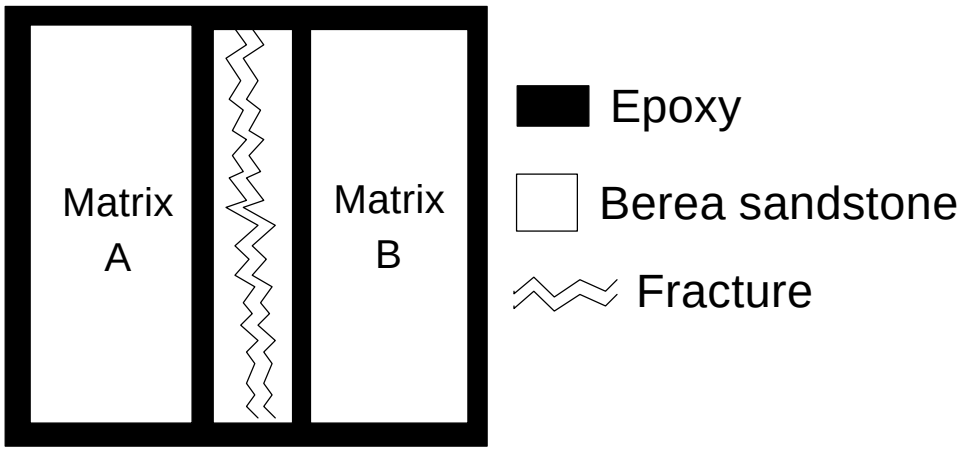

Fig. 42—Core outlet configuration to separate fracture effluent from porous-rock effluent.

The chromium concentrations are plotted in Fig. 44 for effluent samples from the fracture and the two matrix halves. Similarly, the HPAM concentrations are plotted in Fig. 45 for the effluent samples. These figures confirm that the fracture provides the only conduit for the gel. Chromium and HPAM concentrations from the matrix effluent were negligible. Also, after 10 fracture volumes of gel injection, Figs. 44 and 45 show that the composition of the effluent from the fracture was the same as that for the injected gel. Subsequent analysis of gel in the fracture revealed that chromium and HPAM were concentrated by factors of 11 and 8, respectively.

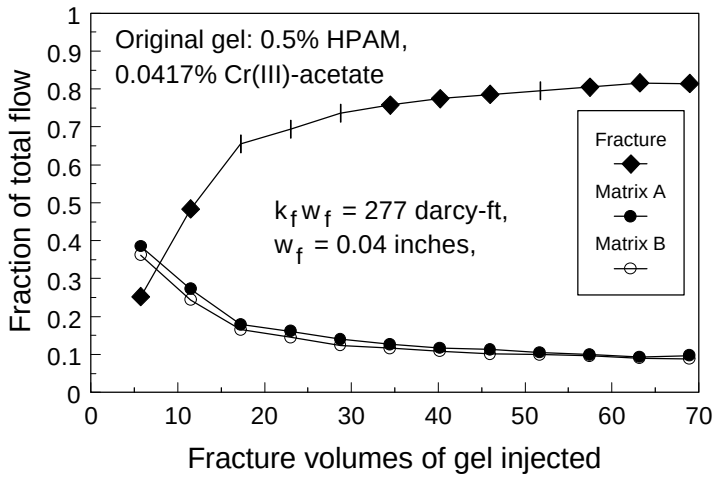

Fig. 43—Fraction of total flow in fracture versus matrix during gel injection.

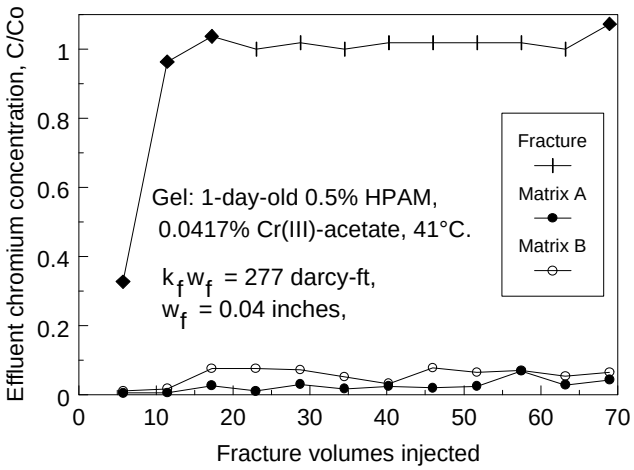

Fig. 44—Effluent chromium from fracture versus matrix during gel injection.

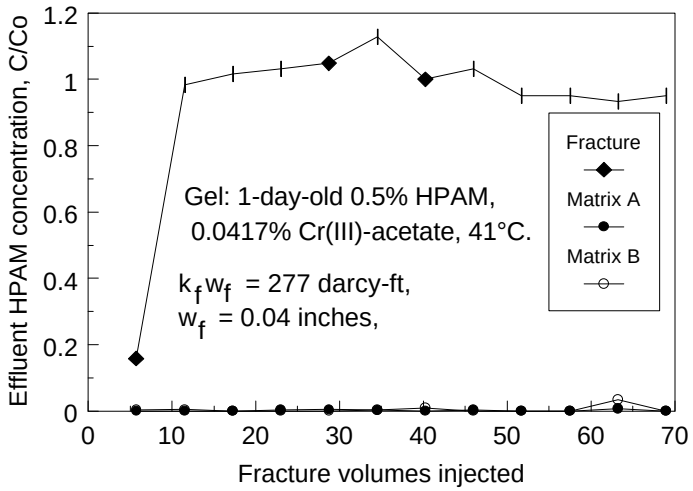

Fig. 45—Effluent HPAM from fracture versus matrix during gel injection.

Pressure Gradients in Matrix Versus Fracture

During the gel extrusion process, we wondered how the pressure gradients in the porous rock compared to those along the fracture. To address this question, a 4-ft-long fractured core (Core 34) was prepared from 650-md Berea sandstone using our standard method. The effective average fracture width was 0.04 in. (0.1 cm), and the average fracture conductivity was 277 darcy-ft. Four equally spaced internal taps were positioned to measure pressures along the length of the fracture. We also placed four equally spaced internal taps to measure pressures along the length of the porous rock. These sets of taps divided the core into five sections of equal length.

After core preparation, 17 fracture volumes (780 cm^3) of our 1X Cr(III)-acetate-HPAM gel were injected using a rate of 200 cm^3/hr. Fig. 46 shows the pressure gradients in the five core sections during gel injection. At the end of gel injection, the average pressure gradient in the fracture was 27 psi/ft. Gel was detected in the effluent after injecting 15.6 fracture volumes of gel.

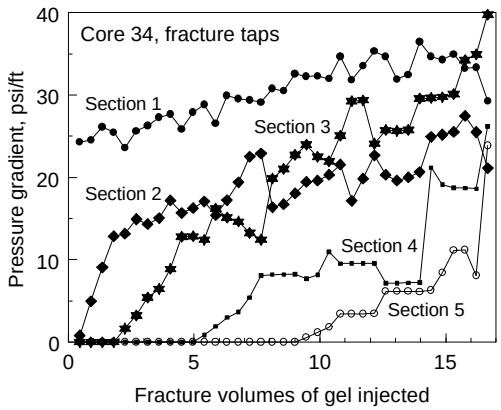

Fig. 46—Pressure gradients in the fracture during gel placement in Core 34.

During gel injection, pressure gradients in the porous rock are shown in Fig. 47 for the last four sections of the core. (Pressure gradients from the first section were not available because gel at the core inlet caused high pressures.) These pressure gradients were between 0.4 and 0.9 psi/ft—much lower than the values observed in the fracture. For a given section, the onset of a pressure response occurred at the same injection volume for both the fracture pressure gradients and the matrix pressure gradients.

Using the Darcy equation and assuming the permeability of the porous rock was 650 md, the pressure gradients in Fig. 47 can be converted to flow rates. These rates, in turn, can be converted to the fraction of total flow that occurs through the rock matrix at any given time. Fig. 48 plots the results of this conversion. For a given position along the core, Fig. 48 reveals that flow through porous rock does not become significant until the gel front reaches that position in the fracture. Shortly after arrival of the gel front in the adjacent fracture, flow in the porous rock rises to a maximum between 40% and 50% of the total flow (i.e., a minimum between 60% and 50% of the total flow occurs in the fracture). Then, the fraction of total fluid flow gradually declines.

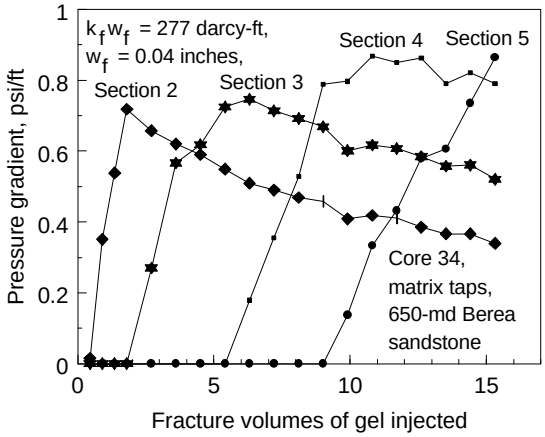

Fig. 47—Pressure gradients in the matrix during gel placement in Core 34.

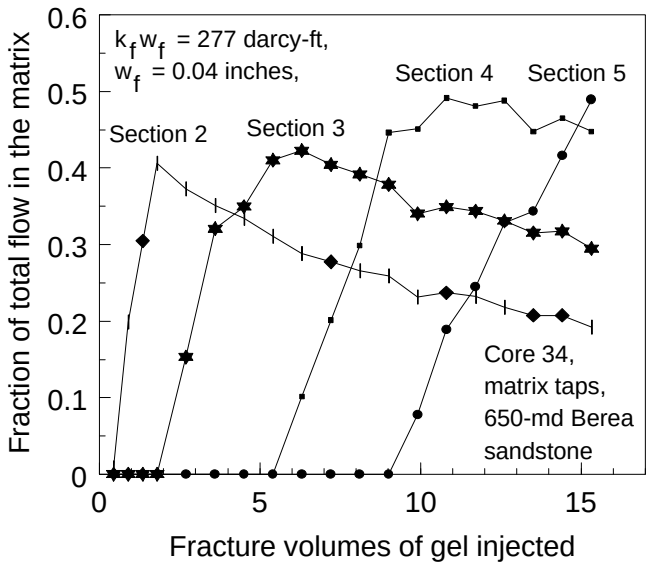

Fig. 48—Calculated flow in the matrix during gel placement in Core 34.

Utilizing a mass balance, the data in Fig. 48 can be used to determine the leakoff rate through the fracture faces for the different sections of the core. In particular, the flow rate in the matrix of a given core section is the sum of the leakoff from the fracture faces plus the flow rate from the matrix of the previous (upstream) core section. Fig. 49 plots the leakoff rate per unit of fracture face versus the fracture volumes of gel injected for the various sections of Core 34. The leakoff rates have been normalized relative to the largest leakoff rate observed during the experiment.

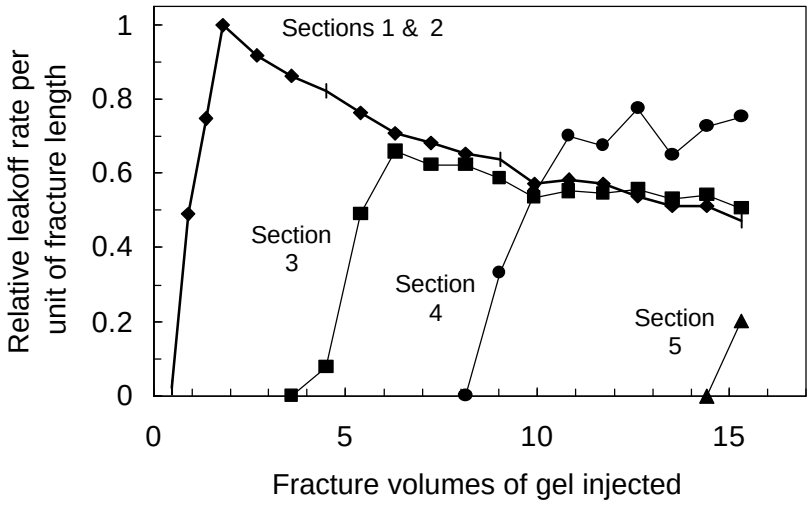

Fig. 49—Leakoff rate per unit of fracture face.

For any given section, Fig. 49 demonstrates that the leakoff rate rapidly rose to a maximum and then gradually diminished. A comparison between Figs. 46 and 49 reveals that in all but the first two sections, the onset of leakoff lagged significantly behind the arrival of the gel front in the fracture. In the fifth core section, the onset of leakoff occurred about the same time as gel arrival at the outlet of the core (i.e., 15 fracture volumes). This result implies that significant leakoff did

not begin in Section 5 until the fracture in that section was almost full. Since each core section was about 10 inches long, the onset of leakoff lagged about 10 inches behind the gel front. Careful consideration of Figs. 46 and 49 reveals that similar lags occurred in Sections 3 and 4.

The greatest leakoff rate was observed in the first two core sections after injecting about two fracture volumes of gel. In Fig. 49, this maximum rate was arbitrarily assigned a value of unity. The peak leakoff rates in Sections 3 and 4 were 66% and 77% of this value, respectively. Interestingly, after injecting 15 fracture volumes of gel, the leakoff rates in Sections 1 through 4 were reasonably similar—i.e., between 47% and 75% of the highest leakoff rate. This result suggests that water leaves the gel in a relatively uniform manner along most of the gel-filled part of the fracture. In other words, the dehydration phenomenon does not occur either primarily at the fracture entrance or primarily at the gel front.

At the end of this experiment, we opened the fracture to determine gel compositions along the length of the fracture. The results are shown in Fig. 50.

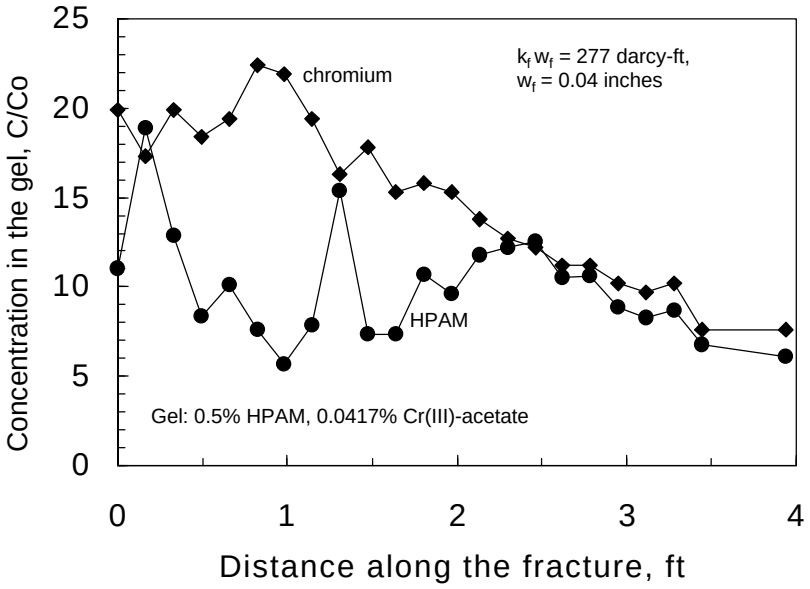

Fig. 50—Gel composition versus fracture length for Core 34.

In this experiment, the gel reached the outlet of the fracture shortly before the end of gel injection. Fig. 50 shows a gradient of gel compositions along the length of the fracture. For example, the chromium concentration (relative to that for the original gel) was about 20 near the fracture inlet and about 7 near the fracture outlet. Similar gradients of gel composition along the fracture were noted in other experiments where gel injection was stopped about the time that gel was first detected in the effluent (e.g., Figs. 25 and 26). These results might provide clues about the mechanism of gel transport through fractures. We will investigate this connection in our future work.

Gel Extrusion Through a 20-30 Mesh Sandpack

Many hydraulic fractures contain a proppant, such as a relatively coarse sand. In a propped fracture, one can argue that the gel must extrude through the porous sandpack in the fracture. What pressure gradients and degree of gel dehydration will be observed as a gel extrudes through a sandpack, and how do these properties compare to those during gel extrusion through fractures without proppant? To answer these questions, we extruded our standard 24-hour-old, 1X Cr(III)-acetate-HPAM gel through a sandpack that was made from 20-30 mesh industrial quartz (Ottawa) sand. The sandpack was 2.7-ft (82-cm) long and 2.5-inches (6.4-cm) in diameter. Four internal pressure taps were spaced equally along the pack, dividing the pack into five 6.5-inch-long sections. The permeability of the pack was 28 darcys, and the total pore volume (PV) was 1,022 cm^3. Using a capillary bundle model, the effective average pore size in the pack was estimated to be about 0.006 inches (0.015 cm).

We injected 1.6 PV (1,620 cm^3) of Cr(III)-acetate-HPAM gel using an injection rate of 200 cm^3/hr. Fig. 51 plots the pressure gradients in the first three sections of the sandpack during the gel-injection process. The pressure gradients in the fourth and fifth core sections remained near zero. In the first two sandpack sections, the pressure gradients rose to a maximum and then declined. The average pressure gradient in the first three sections of the core was roughly 200 psi/ft. This value is roughly the pressure gradient observed when extruding this gel through a 0.006-inch-wide fracture (see Fig. 1 on page 2). Of course, 200 psi/ft is a very high pressure gradient—raising doubt about the feasibility of extruding this gel through a propped fracture.

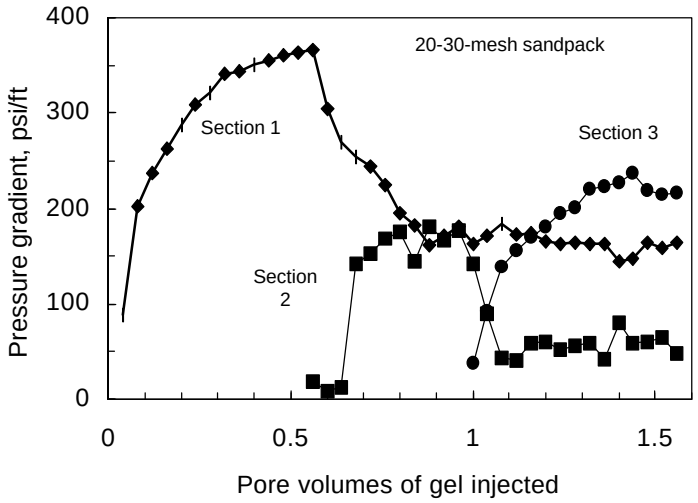

Fig. 51—Pressure gradients observed during gel injection into a sandpack.

Fig. 51 suggests that the gel front reached 40% of the distance through the sandpack after injecting one pore volume of gel. This result suggests that the extrusion process may concentrate or dehydrate the gel by a factor between two and three. However, at the end of the experiment, analysis of gel on the inlet sand face revealed that the gel was concentrated by a factor of about 10. In particular, the chromium was concentrated by a factor of 12, while the HPAM was concentrated by a factor of 9.5.

Although no gel was detected in the effluent from the sandpack, some free (apparently) chromium and uncrosslinked HPAM were found in the effluent after injecting about one pore volume of gel. This finding is shown in Fig. 52. The first chromium was detected at 0.85 PV, while the first HPAM was detected at 1.15 PV. After injecting 1.6 PV of gel, the chromium and HPAM concentrations in the effluent reached 28% and 6.6%, respectively, of the concentrations in the original gel. Thus, consistent with our observations during the filtration studies (i.e., Fig. 21), when the gel loses water, it also loses a lesser amount of chromium and even less (stoichiometrically) HPAM. This experiment represents the first time that free (apparently) chromium and uncrosslinked HPAM were produced from our core experiments significantly before gel was produced. In our previous experiments (e.g., Figs. 15, 16, 38, 40, 44, and 45), the chromium, HPAM, and gel fronts arrived at the core outlets simultaneously (through the fractures). Earlier, we suggested an explanation why free chromium and HPAM were not detected in the effluent from our fractured core experiments. In particular, any free chromium or HPAM that leaked off with water through the fracture faces in our previous experiments were probably retained by the porous rock (Berea sandstone). However, in the present sandpack experiment, chromium and HPAM retention by quartz was much less than that by Berea sandstone, so these chemicals propagated through the porous medium more effectively.

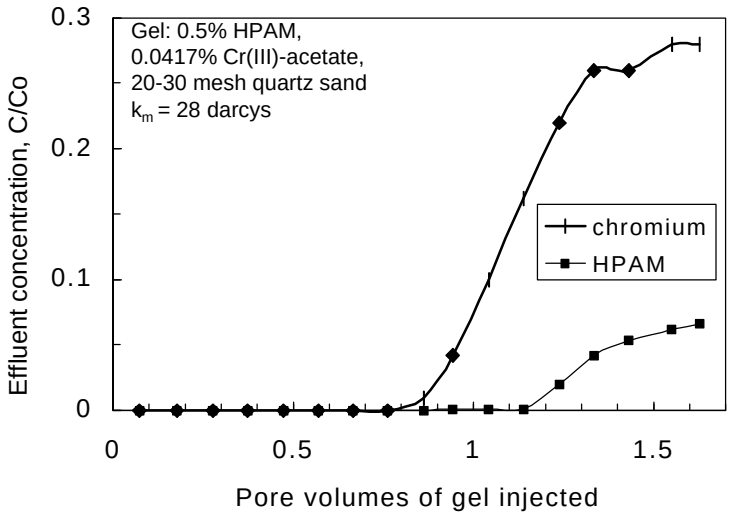

Fig. 52—Composition of the sandpack effluent.

Near the end of gel injection, we collected small samples from each of the four internal taps. Relative to the original gel, the chromium concentrations of these samples were 100%, 100%, 56%, and 49% for the first through fourth internal taps, respectively. The relative HPAM concentrations of these samples were 100%, 88%, 8.3%, and 8.0% for the first through fourth internal taps, respectively. These results suggest that at the first and second internal taps, the flowing gel had the same composition as that for the original gel. In contrast, at the third and fourth internal taps, only free chromium and uncrosslinked HPAM were flowing. More work should be performed to confirm when free chromium and uncrosslinked HPAM are flowing.

A Possible Model for Gel Propagation

Gel Propagation. At this point, we propose a possible model for gel propagation through fractures. In developing this model, a key observation is that gel produced from fractures and the first two internal sandpack taps basically had the same composition and appearance as those for the injected gel. This result was noted even though the final gels in the fractures and on the sand faces were substantially more concentrated than the injected gel. Thus, we conclude that gel of the original composition was the only form of gel that actually propagated. (In making this statement, we note that free chromium and uncrosslinked HPAM are not considered gel.)

How does the gel propagate through a fracture? We note that the original gel in our studies was a three-dimensional semi-solid structure. We propose treating the gel as an elastic solid during the extrusion process. In particular, when an element of gel moves through a fracture, it does so as a plug, with a strong "slip effect" or flow discontinuity occurring between the gel plug and the fracture faces. In other words, little or no viscous dissipation of energy occurs within the moving gel plug. This suggestion is strongly supported by the slope (~ -1) of the resistance-factor-versus-velocity curve in Fig. 14 (page 22).

To obtain a picture of how the gel might propagate, consider Fig. 53. Assume that an element of gel in a fracture is at rest and undeformed (Fig. 53a). Up to a point, application of a pressure gradient elastically deforms the gel, as shown in Fig. 53b. The shear strain, Υ, should equal the applied stress, τ, divided by the shear modulus G.[19]

$$\Upsilon = \tau/G \quad \text{.....(37)}$$

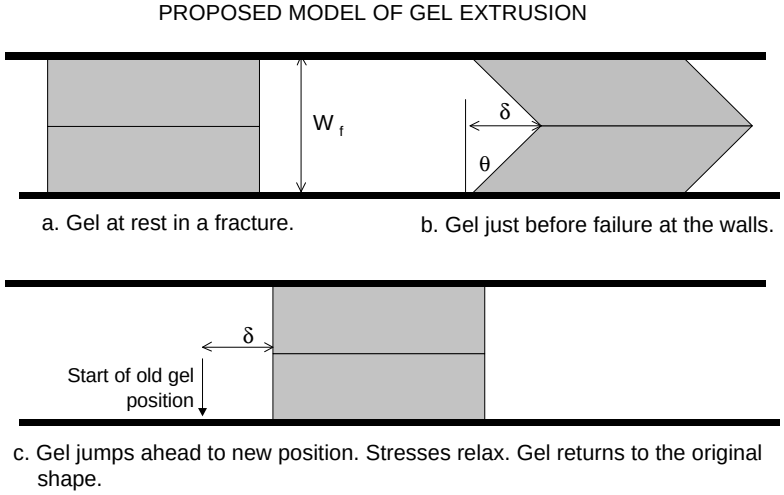

Fig. 53—Illustration of a gel extrusion model.

The shear strain is equal to the tangent of the angle of deformation, θ, in Fig. 53b.[19]

$$\Upsilon = \tan\theta = \delta/(w_f/2) \quad \text{.....(38)}$$

When a critical shear force (per unit area of fracture wall) is applied, the gel will fail at (or near) the wall, and the failed gel face will jump along the fracture (perhaps, a distance close to δ). The elastic stresses in the gel temporarily diminish (possibly, to near zero), and the gel element may temporarily approach its original shape (Fig. 53c). We suggest that gel propagates through a fracture by repeated sequences like those in Figs. 53a-53c.

Just before gel is ripped from the fracture walls, we propose that the critical shear stress at a wall, τ_c, is the sum of elastic stresses in the gel, from the wall to the center of the fracture.

$$t_c = \int_0^{w_f/2} t\,dw = G(\tan q)\int_0^{w_f/2} w\,dw = G(\tan q)\,w_f^2/8 \quad \text{.....(39)}$$

Assume that the critical shear stress, τ_c, is fixed for a given gel and fracture composition and texture. Also, assume that the stress in the gel at the center of the fracture, $G(\tan\theta)$, is directly proportional to the pressure gradient applied in the fracture, $(dp/dl)_c$.

$$(dp/dl)_c = KG(\tan q) \quad \text{.....(40)}$$

Eqs. 39 and 40 can be combined to predict that the critical pressure gradient for gel mobilization varies inversely with the square of fracture width.

$$(dp/dl)_c = 8Kt_c/w_f^2 \quad \text{.....(41)}$$

The solid line in Fig. 54 illustrates the validity of Eq. 41. (The data points are from Fig. 22).

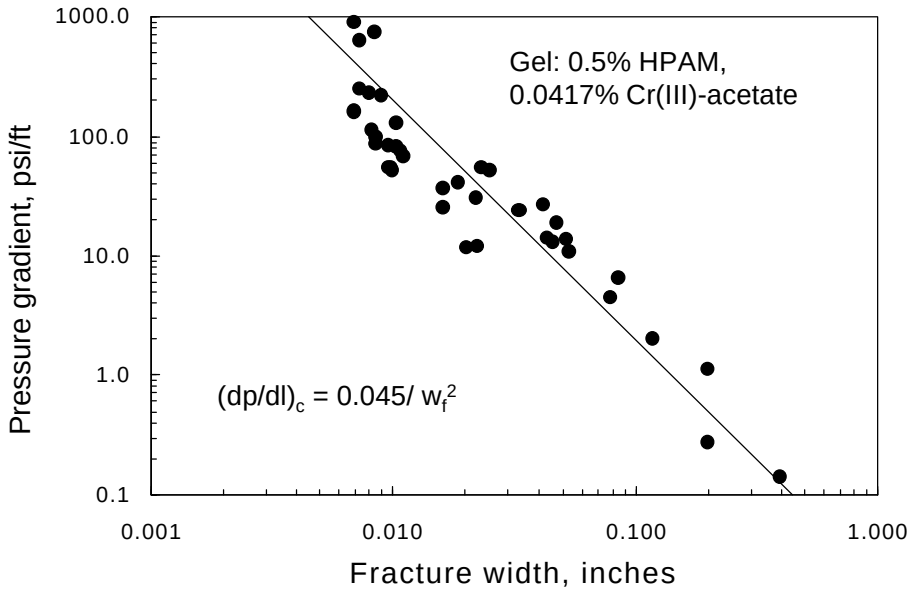

Fig. 54—Pressure gradient versus fracture width.

Gel Dehydration. The model presented above assumes that only gel with the original composition propagates through the fracture. So, how does concentrated gel form in the fracture? Fig. 49 (page 45) provides some insight into this issue. As mentioned earlier, at a given point along the fracture, the onset of leakoff may lag behind the gel front by as much as 1 ft. Of course, gel in the fracture near the front inhibits flow for gel farther upstream. Also, the pressure differences between the fracture and the matrix are greater in the early parts of the fracture than near the gel front. Thus, the upstream gel has a greater tendency to form a filter cake of concentrated gel against the fracture face.

Behind the gel front (but not close to the gel front), Fig. 49 reveals that the leakoff rate is reasonably uniform (i.e., within a factor of two) along the fracture. This observation indicates that the gel lost water along most of the gel-contacted portion of the fracture. In other words, gel dehydration did not occur all at once when the gel first enters the fracture, nor did it occur exclusively at the gel front. Our results suggest that a filter cake of concentrated gel formed gradually along the length of the fracture. We envision that the gel filter cake is formed on the fracture face because of the high pressure gradient between the fracture and the adjacent matrix.

At a given time in the gel-contacted portion of the fracture, Fig. 49 reveals that the leakoff rate gradually decreased as the fracture inlet was approached from the downstream fracture sections. This result suggests that thicker or more concentrated gel filter cakes accumulated on the fracture faces in the upstream sections of the fracture. This suggestion is supported by Fig. 50. However, other results (e.g., Figs. 17, 31, 36, 39, and 41) indicate that the final gel concentrations were fairly uniform along the fracture. More work is needed to resolve this issue.

One can envision alternative mechanisms to explain the formation of concentrated gel. For example, in our proposed gel-propagation model, the concentrated gel and the water of dehydration from the gel may be created in the region where the gel rips away from the wall. Since the gel contains more than 98% water, polymer bonds that break could release a significant amount of water (locally) and result in gel concentration near the fracture faces. This mechanism has some appeal, but it does not satisfactorily explain why so much concentrated gel formed on the inlet sand faces. On the inlet sand faces, presumably, very little gel extrusion occurs, except at the entrance to the fracture.

Final Gel Composition Versus Pressure Gradient. We wondered whether a relation exists between the pressure gradient required to extrude a gel through a fracture and the final chromium and HPAM concentrations in the gel. Table 3 lists final chromium and HPAM concentrations for gels in fractures for many of our experiments. Fig. 55 plots these results for the concentrated gels in the fractures for the data listed in Table 3. This plot includes results using our 0.5X, 1X, and 6X Cr(III)-acetate gels. Fig. 55 shows that a relationship does seem to exist between applied pressure gradient and final gel composition. In Fig. 55, the solid lines are described by Eq. 42 for chromium and Eq. 43 for HPAM.

$$\text{Final \% Cr} = 0.052\ (dp/dl)^{0.33} \quad (42)$$

$$\text{Final \% HPAM} = 1.8\ (dp/dl)^{0.33} \quad (43)$$

Table 3—Average Chromium and HPAM Concentrations Versus Pressure Gradient

Core	$k_f w_f$, darcy-ft	w_f, inches	dp/dl, psi/ft	Average HPAM in fracture	Average Cr in fracture
Injected Gel: 0.5% HPAM, 0.01% Cr (1X Gel)					
24	277,000	0.40	0.14	0.85%	0.036%
26	95,200	0.276	0.28	0.62%	0.021%
23	34,700	0.20	0.28	1.15%	0.050%
33	34,700	0.20	1.1	0.65%	0.019%
25	7,500	0.12	2.0	--	0.068%
32	2,220	0.079	4.5	2.06%	0.043%
19	242	0.038	20	5.9%	0.19%
34	277	0.040	27	4.8%	0.14%
visual	277	0.040	23	5.8%	0.092%
Short	277	0.040	--	4.0%	0.12%
H3	277	0.040	36.1	6.2%	0.13%
H4	277	0.040	63.9	5.8%	0.12%
H1	4.5	0.010	48.4	--	0.21%
31	70.5	0.025	53	12.8%	0.19%
30	5.06	0.010	131	11.4%	0.14%
15	9.5	0.013	160	8.1%	0.30%
20	1.75	0.0073	628	13%	0.44%
18	1.14	0.0063	750	3.4%	0.36%
Injected Gel: 0.25% HPAM, 0.005% Cr (0.5X Gel)					
27	58.4	0.023	55	8.5%	0.16%
Injected Gel: 3.0% HPAM, 0.06% Cr (6X Gel)					
29	17,760	0.157	70	7.6%	0.23%
28	2,220	0.079	233	16.8%	0.25%

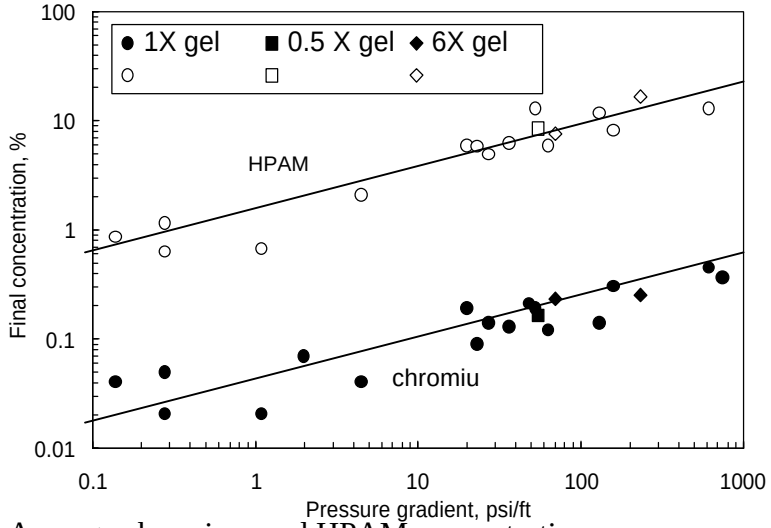

Fig. 55—Average chromium and HPAM concentrations versus pressure gradient.

The ratio of the pressure-gradient coefficients from these two equations (i.e., 1.8/0.052) was consistent with stoichiometric HPAM/chromium crosslinking, assuming that the HPAM had an 8% degree of hydrolysis and two carboxylate groups were tied to each chromium atom.

At present, we are uncertain why the final chromium and HPAM concentrations should vary with the one-third power of pressure gradient. Our first inclination was to suspect that osmotic pressure was responsible for this result. One can envision gel in a fracture as a gel against a membrane, where the fracture face acted as the membrane that separates the gel from the solvent in the porous rock. The degree of swelling or shrinking of the gel depends on the composition of the solvent, the nature of the gel, the temperature, and the pressure.[20] Therefore, we wondered if osmotic-pressure theory could explain the behavior in Fig. 55. However, the established theory predicts that gel-component concentrations should vary with the third power of pressure, instead of the one-third power.[20]

We also wondered whether gel forced against a porous medium might obey Hookes law. That is, as the gel is pressurized against the rock and water leaves the gel, the crosslinked polymer network should compress like a spring—with the distance of gel compression (in one dimension) directly proportional to the force or pressure applied. This concept predicts that the final gel-component concentrations should be directly proportional to the pressure applied. Obviously, this model does not explain the behavior in Fig. 55 either. Furthermore, as mentioned earlier, the pressure difference between the fracture and the adjacent porous rock is very high near the core inlet and very low near the core outlet. If compression or osmotic pressure were important, we might expect a consistent decrease in gel concentration along the fracture. Often, this result was not observed (e.g., see Fig. 41), especially not when significant fracture volumes of gel were produced from the fracture. Additional work is required to understand the mechanism for gel concentration in fractures.

Conclusions

The following conclusions apply to our study of a Cr(III)-acetate-HPAM gel at 41°C:

1. When compressing a gel against a filter, some free chromium and HPAM left the gel and passed through the filter along with water. However, expressed relative to the chromium and HPAM concentrations in the original gel, the relative chromium concentration in the filtrate was greater than the relative HPAM concentration.
2. The pressure gradients and dehydration factors during extrusion of gel through fractures were effectively the same for fractures in 650-md Berea sandstone as in 50-md sandstone.
3. During radial extrusion in fractures, the degree of dehydration experienced by a gel was insensitive to radial position and velocity. Pressure gradients exhibited during the extrusion process appeared to be dictated by local fracture widths, rather than by radial positions or velocities.
4. The gel effluent from a fracture had the same composition and appearance as that for the injected gel, even though a concentrated gel was found in the fracture.
5. During gel extrusion, measurements of water leakoff along a fracture suggested that a filter cake of concentrated gel formed gradually along the length of the fracture.
6. The gel could extrude through a 28-darcy (20-30 mesh) quartz sandpack, but the average pressure gradient was quite high (~200 psi/ft). Gel produced from the first two taps in the

sandpack had the same composition and appearance as that for the injected gel. In contrast, a rubbery gel was found on the inlet face of the sandpack that was about 10 times more concentrated than the injected gel.

7. A model was proposed to explain how gel propagates through fractures. Basically, this model assumed that elements of gel experience repeated sequences where the gel elements (a) elastically deform to a critical point, (b) experience failure at or near the fracture wall, and (c) after failure, jump ahead along the fracture, while the elastic forces relax. This model was shown to account for several aspects of gel behavior during extrusion through fractures.
8. A relationship was found between final gel composition in the fracture and the pressure gradient required for gel extrusion through a fracture. The final chromium and HPAM concentrations varied with the one-third power of the applied pressure gradient. For a given concentrated gel, the final HPAM/chromium concentration ratio was consistent with stoichiometric HPAM/chromium crosslinking, assuming that the HPAM had an 8% degree of hydrolysis and two carboxylate groups were tied to each chromium atom.

4. USING GELS OR FOAMS TO CONTROL CONING IN UNFRACTURED WELLS

Field experience in the Arbuckle formation in western Kansas[14] and reservoir-engineering analyses[21-23] demonstrate that gels can be very effective in treating fractured production wells with "two-dimensional" water coning. In this section, we are interested in whether gels or foams can effectively mitigate "three-dimensional" water or gas coning. Coning is a rate-sensitive phenomenon. The maximum rate at which a well can maintain water-free production is called the critical production rate. Muskat and Wyckoff [24] first proposed that an extended shale barrier near the oil-water contact could reduce water coning by preventing bottomwater from entering the well. Karp *et al.*[25] expanded this idea by proposing the placement of a horizontal barrier at the bottom of a well to suppress water coning. Specifically, they suggested inducing a horizontal fracture above the water-oil contact and then filling it with cement. The placement of horizontal barriers increases the effective wellbore radius; and thus, increases the critical production rate.[14,24]

Gels can be used as a horizontal barrier to suppress water coning. However, during placement, gelants enter all open zones, not just the water cone. Oil productivity can be damaged significantly unless the gel can reduce the permeability to water much more than that to oil.[21,22] If the gel does not significantly lower the permeability to oil, then oil can flow through the gel barrier in the upper portion of the oil zone. In contrast, when the rising water cone reaches the gel barrier, a low permeability to water impedes water influx into the well. The net effect is that the gel forms a horizontal barrier that inhibits water coning.

Following similar logic, foam has also been proposed to serve as horizontal barriers to control gas coning.[26-31]

Review of Previous Findings

In a previous study,[21] we examined the effect of gel treatments on the critical production rate using different analytical coning models. The study indicated that for gel treatments to be effective in unfractured production wells, the desired production rate should be less than 1.5 to 5 times the pretreatment critical rate. For a gel treatment to be effective, the increase in critical production rate must exceed the rate at which the well will actually be produced. However, for economic reasons, the desired production rate often is greater than the 1.5 to 5 times the critical rate. These findings suggest that gel treatments are usually not effective in suppressing water coning in unfractured production wells. In contrast, under ideal conditions, gel treatments in fractured wells could increase the critical rate by two orders of magnitude. Also, a survey of field cases revealed that the most successful gel applications have occurred in fractured wells produced by bottomwater drive.[13,14]

Objective of This Study

Several researchers[26-30] reported field results using foam as horizontal barriers to control gas coning in unfractured production wells. In one case,[26] foam was claimed to have reduced the gas-oil ratio (GOR) by more than 50%. This seems to contradict our predictions based on analytical coning models. Is it possible that the analytical coning models in our previous study do not reflect what is really happening in reservoirs? To answer this question, we reviewed several published

field cases and numerical simulation studies. The objective was to determine if gels or foams have been effective in controlling coning in unfractured production wells.

Review of Field Cases

A foam pilot test was performed in a Norwegian North-Sea field to study the effectiveness of using foam to control gas coning.[26] The pilot well was produced from a homogeneous high-permeability (2~3 darcys) sandstone formation. A gas cap covered the oil zone, and the field was developed by up-dip gas injection. Foam was generated in situ by injecting alternating slugs of surfactant (dissolved in seawater) and gas (from a neighboring well) into the top perforation. The goal was to form a foam barrier before the gas-oil contact (GOC) reached the top perforation. A series of production tests were performed before the treatment. The data from the production tests were used as base lines in a simulation study[26,27] to project the increase in GOR in the absence of a foam treatment. This projection was then compared with the actual behavior after the foam treatment. According to the simulation study, the projected GOR without foam treatment should have been more than twice the measured GOR after foam treatment. Therefore, they concluded that the foam treatment reduced the GOR by about 50%. However, a careful examination of the actual production history of the pilot well (Fig. 10 of Ref. 26) shows that the measured GOR remained relatively unchanged after treatment. In other words, the foam treatment might have stopped the increase in GOR as projected by the simulation study. However, it did not cause an actual reduction in GOR. We note that the oil-production rate after treatment was 25% lower than the pre-treatment rate. The paper did not give enough information for us to estimate the critical rate. Hence, we cannot determine how close the after-treatment oil-production rate was to the critical rate.

Lakatos *et al.*[29] used a polymer/silicate system to try to control gas coning in a Hungarian field. The two oil wells treated were in a sandstone reservoir with gas caps. They reported that both treatments failed due to hydrate formation at the well head.

In a Nigerian oil field,[30] pilot tests were performed to evaluate the potential of using foam as barriers to control gas coning and cusping. The wells treated were selected from reservoirs with a thin oil rim sandwiched between a large overlaying gas cap and a weak aquifer. A total of eight wells were selected. Most of the wells were stimulated with acid immediately before treatment to improve injectivity. Also, sand production was a serious problem for these pilot wells. Among the eight wells treated, four wells had gas-cusping problems and the other four had gas-coning problems. After treatment, only one well with gas-cusping problems showed a positive response that lasted more than 12 months. In this case, the GOR was reduced from 7,000 scf/bbl before treatment to 2,000 scf/bbl after treatment. In the mean time, the oil rate was increased from 340 bpd to 450 bpd. (The increase in oil rate was attributed to the acid treatment before foam placement.) The treatment remained effective for more than 12 months. Thus, the foam treatment appeared to be effective in treating one cusping case. Sometimes, foam treatments can be effective in treating gas cusping in layered reservoirs. During placement, foams enter all open zones. However, when the well is returned to production, the foam in the oil zones washes out quickly while the foam in the gas zones may block the gas production. With the limited information provided in the paper about the reservoir, it is difficult for us to identify the exact mechanism for the GOR reduction. One of the wells with gas coning problems showed an initial reduction in

GOR after treatment. The GOR was reduced from 5,000 scf/bbl before treatment to 1,650 scf/bbl immediately after treatment. However, the oil rate was also reduced from 600 bpd before treatment to 200 bpd after treatment. The reduction in the oil rate was attributed to near-wellbore damage due to wax formation. No long-term post-treatment results were reported. The temporary improvement in GOR could have resulted from the substantially reduced oil-production rate. Other treated wells either showed limited reduction in GOR or the reduction was short-lived.

Review of Simulation Studies

Several researchers[32-37] performed numerical simulations to study the effects of horizontal barriers on water and gas coning in unfractured production wells. Based on a numerical coning model developed by Byrne *et al.*,[38] Strickland[32,33] examined the effectiveness of placing an impermeable horizontal barrier near the oil-water contact (OWC) to suppress water coning. Results from the simulation study showed that when a well was produced below critical rates, the barriers were effective in suppressing water production until the OWC reached the barriers. The effectiveness of the barriers in delaying water production increased with increasing barrier radius. When produced above the critical rates, the water cone quickly rose to the level of the barriers and then flowed into the production well. These findings are consistent with results from our previous study[21] using analytical coning models. In the paper, Strickland also showed that even when a well is produced above the critical rate, placing a horizontal barrier can still cause a significant reduction in WOR. According to an example in the paper, placing a 100-ft barrier could cause a 50% reduction in WOR even when the well was produced at about 4 times the critical rate. In the paper, Strickland also argued that for a given amount of oil produced, the cumulative water production would be significantly less with a horizontal barrier than without the barrier. However, the comparison was based on the assumption that the barriers were placed before water breakthrough. If the barriers were placed when the well was already producing at high WOR, the saving in the total amount of water produced would have been significantly less. Results in the paper also showed that when a well was produced above the critical rate, even with a large barrier, a substantial amount of water must be produced for a given cumulative oil production. Based on an example in the paper, with a 100-ft barrier, the cumulative amount of water produced with 45% of the OOIP recovered was 10 times more when a well was produced at 4 times the critical rate than when the well was produced below the critical rate. Therefore, the high water production resulting from producing at a rate that exceeds the critical rate must be taken into account when designing water-shutoff treatments.

In reservoirs with strong bottom-water drive, Ehlig-Economides *et al.*[34] claimed that the critical-rate concept used in the analytical models neglected the movement of the OWC during production. Therefore, the analytical models cannot accurately describe the coning situation. With a black-oil simulator, they studied the effectiveness of placing a pancake-type gel barrier below the bottom perforation to control water coning. Their simulation study showed that the pancake-type gel barrier was not very effective in delaying the bottom-water breakthrough. The water quickly flowed around the barrier into the production well.

Results from the literature and our own experimental work[39-50] have shown that many polymers and gels have the ability to reduce the permeability to water much more than to oil. Thakur *et al.*[35] incorporated the disproportionate permeability reduction into his numerical coning model to

investigate the effectiveness of using polymers as barriers to control water coning in unfractured oil wells. They demonstrated that with the ability to reduce the permeability to water more than that to oil, a polymer could cause significant reduction in water saturations in the treated region. Hwan[36] expanded Thakur's study using a similar numerical coning model. Hwan showed that in unfractured wells, there existed an optimal radial penetration of polymer barriers for water-free production. With a radial penetration of the polymer barrier less than the optimal radial penetration, the water cone first rose quickly along the edge of the polymer-treated region. Then, the waterfront in the polymer-treated region moved laterally until breakthrough. In contrast, when the radial penetration of polymer barriers was more than the optimal radial penetration, a stable water cone formed below the bottom perforation. These findings are consistent with our previous study[21] with analytical coning models using the critical-rate concept. According to an example in the paper, when the radial penetration of a polymer barrier was less than the optimal radial penetration, the polymer barrier can still cause a significant reduction in water cut. However, for the same example case, switching to a smaller grid block size resulted in less reduction in water cut. Since all other simulation runs in the paper used the original coarse grid size, Hwan cautioned that the benefit of polymer treatments on water coning predicted in this paper might be too optimistic. Hwan concluded from the simulation study that polymer treatments are not effective in controlling excess water production in unfractured production wells with severe water coning problems. Also, results from Hwan's simulation study showed that an impermeable disk placed at the OWC was not any more effective in reducing the WOR than the cylindrical polymer barriers.

Ekrann and Hanssen[37] performed a numerical simulation study to evaluate the effectiveness of using foam as barriers to control coning. They suggested that for a foam barrier to be effective in controlling gas coning, a liquid foaming agent must be placed at the gas-oil contact. They proposed injecting a liquid foaming agent with a density between that of the oil phase and that of the gas phase. When the well is returned to production, the gas phase would come in contact with the foaming agent and thereby create a foam barrier to suppress gas coning. However, results from their simulation study showed that in unfractured production wells, horizontal barriers would not be effective in suppressing gas coning unless the well was produced near or below the critical production rates. This is consistent with findings in our previous study[1] using analytical models.

Conclusions

A critical examination of published field cases and simulation studies using numerical coning models revealed that gels or foam are rarely effective as horizontal barriers to suppress water or gas coning in unfractured production wells. These findings are consistent with results from our previous study using analytical coning models.

5. DISPROPORTIONATE PERMEABILITY REDUCTION

The ability of blocking agents to reduce the permeability to water much more than that to oil is critical to the success of water-shutoff treatments in production wells if hydrocarbon-productive zones cannot be protected during placement.[21,22] Results from the literature and our own experimental work[39-50,52-56] have shown that many polymers and gels exhibit this disproportionate permeability reduction. In our previous studies, we extensively examined the possible mechanisms for this disproportionate permeability reduction.[1,2,48-50,53] Although we still do not fully understand why this phenomenon occurs, many interesting leads have been generated during the course of the study. Our previous studies ruled out gravity and lubrication effects as possible mechanisms. Also, gel shrinking and swelling were unlikely to be responsible for this phenomenon.

In this chapter, we examine several other proposed mechanisms for the disproportionate permeability reduction. These mechanisms include:

1. Selective breakdown of gels in oil zones by judicious application of high pressure gradients.
2. Gel breakdown by two-phase flow.
3. Balance between capillary forces and gel elasticity.
4. Segregated oil and water pathways.
5. Wettability effects.
6. Wall effects.
7. Gel-droplet model.

Effect of Pressure Drawdown on Disproportionate Permeability Reduction

Our previous annual report[2] showed that the disproportionate permeability reduction was observed using constant-pressure displacement experiments. Can controlling the pressure drawdown maximize the disproportionate permeability reduction? To answer this question, we performed oil/water experiments using different pressure gradients to examine the effect of pressure drawdown on the disproportionate permeability reduction. For each pressure gradient, two similar oil-water experiments were performed; one with oil injected immediately after shut-in to measure oil residual resistance factor, F_{rro}, and the other with brine injected immediately after shut-in to measure water residual resistance factor, F_{rrw}. The gel contained 0.5% HPAM, 0.0417% Cr(III)-acetate, 1% NaCl, and 0.1% $CaCl_2$. Unless otherwise mentioned, this composition is the standard Cr(III)-acetate-HPAM gel throughout this report. Soltrol 130 was the oil phase. The residual resistance factors listed in Table 4 were measured immediately after shut-in. (Detailed residual-resistance-factor data are listed in Tables G.2a, G.2b, and G.2h through G.2k of Ref. 2 and Tables B11 and B12.)

In this study, we used the ratio of F_{rrw} to F_{rro} to measure disproportionate permeability reduction. Higher F_{rrw}/F_{rro} ratios indicate more pronounced disproportionate permeability reduction. Table 4 shows that the disproportionate permeability reduction decreased with increased pressure gradient above 90 psi/ft. Also, F_{rrw} decreased dramatically with increased pressure gradient. More work is needed at lower pressure gradients to study this effect.

Table 4—Effect of Pressure Drawdown on Disproportionate Permeability Reduction

Gel: 0.5% HPAM, 0.0417% Cr(III)-acetate, 1% NaCl, 0.1% $CaCl_2$
Cores: ~750-md Berea sandstone

Pressure Gradient, psi/ft	F_{rrw}	F_{rro}	F_{rrw}/F_{rro}
45	18,800	34	553
90	10,100	14	720
135	4,510	16	282
180	9	5	1.8

Gel Breakdown During Two-Phase Flow

Results from our earlier study[39] showed that significant gel breakdown occurred when switching from oil injection to water injection or when switching from water injection to oil injection. However, these experiments involved single-phase injection. In field applications, we often have zones with two-phase flow at different water/oil ratios. A material balance indicates that gels will not change the steady-state producing water/oil ratio of a single zone.[22] In other words, gels are not effective in treating a single zone where two phases are flowing.

Can simultaneous oil and water flow cause severe gel breakdown? To answer this question, we performed an experiment using different water/oil volume ratios after treatment. In this experiment, we saturated a 800-md Berea core with our standard Cr(III)-acetate-HPAM gel. After treatment, we first injected brine. After measuring the steady-state brine mobility, we switched to injection of 90% brine and 10% oil. Brine and oil mobilities were measured when a steady state was reached. This process was repeated using progressively lower brine/oil injection ratios. The results are summarized in Fig. 56, where the solid squares show brine mobilities while the solid circles show oil mobilities. After reaching a brine/oil volume ratio of 0/100, the process was reversed by injecting progressively increasing brine/oil volume ratios. In Fig. 56, the open squares and circles identify the brine and oil mobilities during this part of the experiment, respectively. (Detailed residual-resistance-factor data are listed in Table B13.)

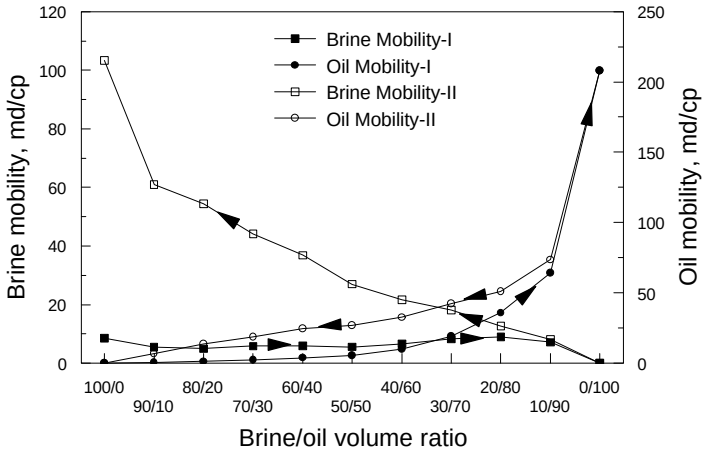

Fig. 56—Gel breakdown during two-phase flow.

If no gel breakdown occurred, the brine mobility should decrease with increasing oil fractional flow. However, this figure shows that the brine mobility remained relatively unchanged as the oil

fractional flow increased from 10% to 90%. This result indicates that the gel experienced some gel breakdown during the process. However, the breakdown was not severe. If the gel experienced severe breakdown, we should have observed a significant jump in both the brine and oil mobilities. After reaching a brine/oil volume ratio of 0/100, the process was reversed by decreasing oil fractional flow. The oil and brine curves show that both the brine and oil mobilities were significantly higher than before. In other words, the gel experienced severe gel breakdown during the process. Does this result imply that high oil fractional flow is more damaging to the gel then low oil fractional flow? Is it possible that the gel breakdown was simply a result of the large amount of fluid throughput? To answer these questions, we will perform a similar experiment where high oil fractional flows are applied first.

Balance Between Capillary Forces and Gel Elasticity

After viewing the results from the micromodel experiments of Dawe and Zhang,[52] we wondered whether capillary forces and gel elasticity might contribute to the disproportionate permeability reduction.[49,53] In a video from Dawe and Zhang, we observed that during oil injection, oil drops squeezed through an elastic, aqueous gel. During water injection, most of the water flowed through the pathways created by oil, however, the pathways were more constricted. Dawe and Zhang[52] reported that the gel reduced the permeability to water significantly more than that to oil. We suspected that a balance between capillary forces and gel elasticity caused the disproportionate permeability reduction. As illustrated in Fig. 57, when an oil droplet extrudes through an aqueous gel, two opposing forces act. On the one hand, a capillary force acts to maintain a minimum droplet radius, which in turn, forces open a channel through the gel. On the other hand, the gel exerts an elastic confining force to close the channel. The final radius of the oil droplet and the size of the oil pathway depend on the balance between the two forces. The effective permeability to oil increases with increasing radius of the flow path around the oil droplet. In contrast, when water flows through the same channel, no capillary force acts to open the channel. Therefore, the effective permeability to water should be less than that to oil.

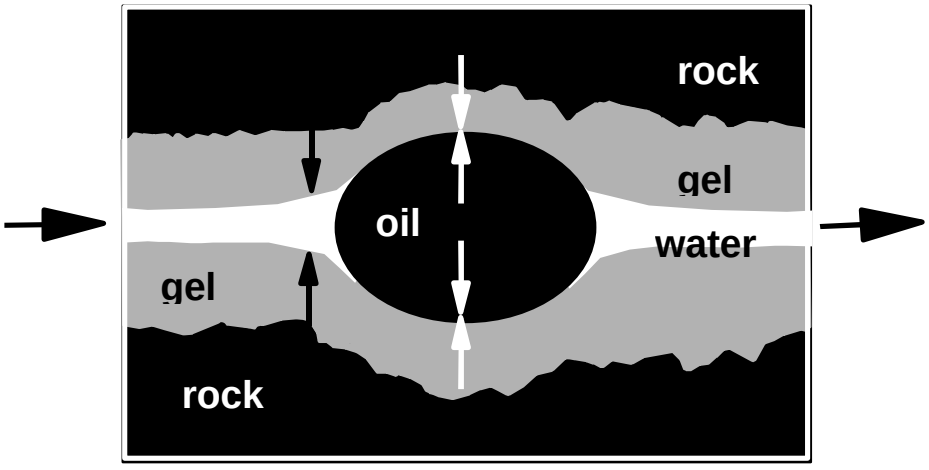

Fig. 57—Balance between capillary forces and gel elasticity.

Review of Previous Work. Two possible methods exist to test this theory: (1) vary the capillary force and (2) change the gel elasticity. In a previous study,[1,53] we performed oil-water

experiments in small glass conduits (3 cm × 0.5 cm × 0.05 cm) to reproduce our observation from the micromodel experiments of Dawe and Zhang.[52] A Cr(III)-acetate-HPAM gel reduced the permeability to water more than that to oil in small glass conduits.

In a small glass conduit that was filled with a Cr(III)-acetate-HPAM gel, lowering the oil water interfacial tension from 42.5 dyne/cm to 8 dyne/cm resulted in a decreased permeability to oil.[1,53] This finding supports the theory that capillary forces and gel elasticity contribute to the disproportionate permeability reduction. However, a similar experiment in a Berea sandstone core did not show a decrease in permeability to oil when the oil-water interfacial tension was reduced.[1,53] Thus, we suspect that a capillary-elastic-force balance may not be the dominant mechanism in porous rock.

In Berea sandstone, the disproportionate permeability reduction was very similar for a Cr(III)-acetate-HPAM gel and a Cr(III)-acetate-HPAM-nitrogen gelled foam.[49,53] This finding does not support the theory that capillary forces and gel elasticity contribute to the disproportionate permeability reduction in porous rock. However, we recognize that gelled foams may not be a good analogy for studying the elastic mechanism. To address this concern, we must find another way to change the gel elasticity. Therefore, we attempted to control the elasticity of a Cr(III)-acetate-HPAM gel by varying the Cr(III)/acetate ratio.

Varying Cr(III)/Acetate Ratio to Control Elasticity of a Cr(III)-Acetate-HPAM Gel. For a Cr(III)-acetate-HPAM gel, the gel elasticity decreases with decreasing Cr(III)/acetate ratio. Adding more acetate in the gelant results in a weaker, more pliable gel. In this study, we attempted to vary gel elasticity by incorporating different amounts of sodium acetate into the gelant. For each sodium-acetate concentration, two similar experiments were performed; one with oil injected immediately after shut-in to measure F_{rro} and the other with brine injected immediately after shut-in to measure F_{rrw}. Table 5 shows F_{rrw} and F_{rrw}/F_{rro} decreased with increased acetate concentration. However, because the gel obviously experienced significant gel breakdown when excess acetate was present (because of the low F_{rrw}-values), conclusions about the effect of gel elasticity cannot be drawn. We suspect that a more definitive test would increase the gel elasticity by increasing the Cr(III)/acetate ratio. One way to accomplish that is to adjust the proportions of Cr(III)-acetate and $CrCl_3$ in the gelant to achieve the desired Cr(III) concentration. We hope to perform this experiment in the future. (Detailed residual-resistance-factor data are listed in Table A.2b of Ref. 1 and Tables B14 and B15.)

Table 5—Effect of Acetate on Disproportionate Permeability Reduction
Gel: 0.5% HPAM, 0.0417% Cr(III)-acetate, 1% NaCl, 0.1% $CaCl_2$
Cores: ~850 Berea sandstone

[Na-acetate], M	F_{rrw}	F_{rro}	F_{rrw}/F_{rro}
0	2,450	42	58
0.025	43	6	7
0.05	13	8	1.6

Segregated Oil and Water Pathways

In our previous studies,[48,49,53] we proposed that the disproportionate permeability reduction might be caused by water and oil following segregated pathways. If (on a microscopic scale) a water-

based gelant follows primarily the pathways available to water, many of the oil pathways could remain open (relatively gel-free) after treatment while most of the water pathways would be blocked by the gel (Fig. 58). In this way, the water-based gel could reduce permeability to water more than to oil.

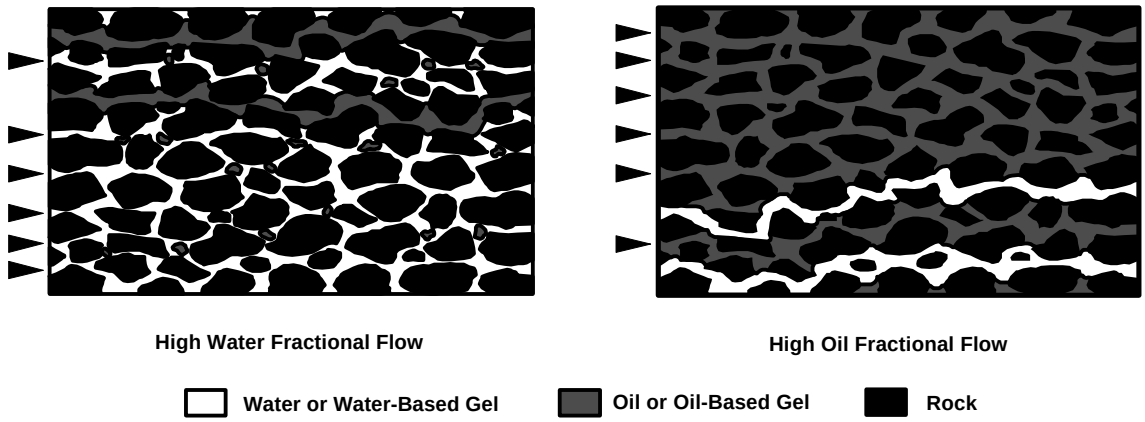

Fig. 58—Segregated oil and water pathways.

Following the same logic, during high oil fractional flow, if an oil-based gel follows primarily the pathways available to oil on a microscopic scale, many of the water pathways could remain open after treatment while most of the oil pathways would be blocked by the gel.

If this segregated-pathway theory is valid, we speculated that the disproportionate permeability reduction could be enhanced by simultaneously injecting oil with a water-based gelant or water with an oil-based gelant. Presumably, simultaneous injection of oil and a water-based gelant should allow a larger fraction of oil pathways to remain open than if a water-based gelant is injected by itself. Using similar logic, simultaneous injection of water and an oil-based gelant should allow a larger fraction of water pathways to remain open than if an oil-based gelant is injected alone.

Review of Previous Work. In previous studies, [48,49,53] we found that an oil-based gel (12-hydroxystearic acid in Soltrol 130) reduced permeability to oil much more than to water. Also, simultaneous injection of water with an oil-based gel (using a 50/50 gelant/water volume ratio) in Berea sandstone enhanced the disproportionate permeability reduction. These findings support the segregated-oil-and-water-pathway theory. In contrast, our previous annual report[2] showed that simultaneous injection of oil with an aqueous gel (using gelant/oil volume ratios of 100/0, 95/5, 50/50, 30/70) did not enhance the disproportionate permeability reduction. These findings do not support the theory. However, the report[2] also showed that if the gelant/oil ratio was high enough (95/5), continuous oil injection during the gelation period could enhance the disproportionate permeability reduction. Why did the simultaneous injection of oil with an aqueous gelant fail to enhance the disproportionate permeability reduction? One possible explanation was that the capillary redistribution of fluids closed the open oil channels during the shut-in period.

Capillary Redistribution of Fluids During Shut-In. For a water-based gelant, viscous forces may keep oil pathways open during simultaneous gelant/oil injection in a strongly water-wet rock.

During the shut-in period, capillary forces may allow the water-based gelant to imbibe into and block some of the open oil pathways. In contrast, in a strongly water-wet rock, capillary forces would not allow an oil-based gelant to imbibe into the open pathways during shut-in. This mechanism might explain why simultaneous injection of water with an oil-based gel in Berea sandstone enhanced the disproportionate permeability reduction while simultaneous injection of oil with a water-based gel failed to do so.[2] The best way to test this theory is to use a water-based gel in a strongly oil-wet porous medium. Since oil is the wetting phase, capillary forces should not cause a water-based gelant to block the open oil pathways during the shut-in period.

Effect of Gelant/Oil Volume Ratio During Placement on Disproportionate Permeability Reduction in Strongly Oil-Wet Porous Media. To test the capillary-redistribution theory, we conducted oil/water experiments in strongly oil-wet cores using our standard water-based Cr(III)-acetate-HPAM gel. Soltrol 130 was the oil phase. The oil-wet cores were artificial polyethylene cores. The cores had an absolute water permeability of 7 darcys. Table 6 shows that simultaneous injection of oil with a water-based gelant using a 50/50 volume ratio did not enhance the disproportionate permeability reduction in strongly oil-wet cores. This finding does not support the capillary-redistribution theory. More experiments using higher gelant/oil volume ratios are underway to study this phenomenon. (Detailed residual-resistance-factor data are listed in Tables B16 and B17.)

Table 6—F_{rrw} and F_{rro} Values for a Water-Based Gel in Strongly Oil-Wet Core
Gel: 0.5% HPAM, 0.0417% Cr(III)-acetate, 1% NaCl, 0.1% $CaCl_2$
Cores: ~7-darcy artificial polyethylene cores

Gelant/oil volume ratio	F_{rrw}	F_{rro}	F_{rrw}/F_{rro}
100/0	25,000	192	130
50/50	670	23	29

Wettability Effect

In our previous studies,[39,48,53] cases were observed where the disproportionate permeability reduction was more pronounced in cores of intermediate wettability than in water-wet cores. Thus, we suspect that wettability may play an important role in the disproportionate permeability reduction.

Disproportionate Permeability Reduction in Strongly Oil-Wet Cores. To study the wettability effect, we conducted an oil/water experiment in a strongly oil-wet artificial polyethylene core using our standard Cr(III)-acetate-HPAM gel. Soltrol 130 was the oil phase. The core had an absolute permeability to water of 15 darcys. Table 7 shows that the gel reduced the permeability to water significantly more than that to oil in the oil-wet core. Also, mechanical gel breakdown was observed during the multiple oil/water injection cycles (Table 7). These observations were similar to the behavior in strongly water-wet cores.[39,48,53] During the second oil and the third water injection, residual resistance factors were measured using different flow velocities. The residual resistance for oil, F_{rro}, was flow-rate independent. The residual resistance factor for water, F_{rrw}, was weakly dependent on the flow rate, with a power-law exponent of -0.19 (sixth column of Table 7). This result contrasts with the strong shear-thinning behavior of

F_{rrw} observed in strongly water-wet cores using the same gel.[39,48,53] (Detailed residual-resistance-factor data are listed in Table B18.)

Table 7—Summary of F_{rrw} and F_{rro} After a Water-Based Gel Treatment
Core: oil-wet artificial polyethylene core
Gel: 0.5% HPAM, 0.0417% Cr(III)-acetate, 1% NaCl, 0.1% $CaCl_2$

k_w	1st F_{rrw}	1st F_{rro}	2nd F_{rrw}	2nd F_{rro}	3rd F_{rrw}
15 darcy	90,000	375	47,000	345	$11{,}128\ u^{-0.19}$

A similar experiment was conducted using an oil-based gel. Results in Table 8 show that the oil-based gel reduced the permeability to oil more than that to water in an oil-wet polyethylene core. Residual resistance factors were measured using different velocities during the second oil and third water injection. Both the F_{rrw} and the F_{rro} were flow-rate independent. These observations were similar to the behavior in strongly water-wet cores using the same gel.[39,48,53] (Detailed residual-resistance-factor data are listed in Table B19.)

Table 8—Summary of F_{rrw} and F_{rro} After an Oil-Based Gel Treatment
Core: oil-wet artificial polyethylene core
Gel: 18% 12-hydroxystearic acid in Soltrol 130

k_w	1st F_{rrw}	1st F_{rro}	2nd F_{rrw}	2nd F_{rro}	3rd F_{rrw}
15 darcy	85	375	80	353	68

Effect of Permeability on Disproportionate Permeability Reduction. In a previous study,[53] the disproportionate permeability reduction decreased with decreased absolute permeability in strongly water-wet cores. We performed additional experiments using our standard Cr(III)-acetate-HPAM gel in strongly oil-wet cores. Table 9 shows that the F_{rrw}/F_{rro} ratio in a 15-darcy polyethylene core was almost twice as high as that in a 7-darcy polyethylene core. The results suggest that the disproportionate permeability reduction decreased with decreased absolute permeability in strongly oil-wet cores. This finding is consistent with the behavior in strongly water-wet cores.[53] (Detailed residual-resistance-factor data are listed in Tables B16 and B18.)

For the standard Cr(III)-acetate-HPAM gel, Table 9 shows that the disproportionate permeability reduction was more pronounced in a 15-darcy oil-wet polyethylene core than in a 745-md water-wet Berea core. However, the trend was reversed between a 7-darcy oil-wet polyethylene core and the 745-md water-wet Berea core. Perhaps, the effect of permeability on the disproportionate permeability reduction played a role here. More work is needed to understand this phenomenon. (Detailed residual-resistance-factor data are listed in Tables B16, B18, and B20.)

Table 9—Effect of Permeability on Disproportionate Permeability Reduction
Gel: 0.5% HPAM, 0.0417% Cr(III)-acetate, 1% NaCl, 0.1% $CaCl_2$

Core Type	1st F_{rrw}	1st F_{rro}	F_{rrw}/F_{rro}
15-darcy polyethylene core (oil wet)	90,000	375	240
7-darcy polyethylene core (oil wet)	25,000	192	130

745-md Berea core (water-wet)	10,100	59	171

Wall Effects

Zaitoun *et al*.[55] reported that disproportionate permeability reduction was observed in both oil- and water-wet cores using a nonionic polyacrylamide polymer. They attributed the disproportionate permeability reduction to wall effects resulting from an adsorbed polymer layer on the pore walls. Fig. 59 shows that in a strongly water-wet system, the presence of residual oil droplets at the center of the pores can significantly reduce the effective width of the water channels during waterflooding. In contrast, this restriction may not exist during oilflooding. Therefore, for a given thickness of an adsorbed polymer layer, the permeability reduction for water during waterflooding is greater than that for oil during oilflooding. In an oil-wet system, they proposed that the polymer could still cover most of the rock surface by anchoring on the small part of the rock surface that remains water-wet. The layer of polymer covering the oil-wet surface would shift the wettability toward water-wet. In this way, the polymer could reduce the permeability to water more than that to oil in an oil-wet core. Zaitoun *et al*.[55] reported that the capillary pressure of a silane-treated oil-wet sandstone core shifted from negative before treatment to positive after treatment. Also, the polymer reduced the permeability to water more than that to oil in the oil-wet core. Based on these findings, they concluded that the adsorbed polymer layer was responsible for the disproportionate permeability reduction in both the oil- and water-wet cores.

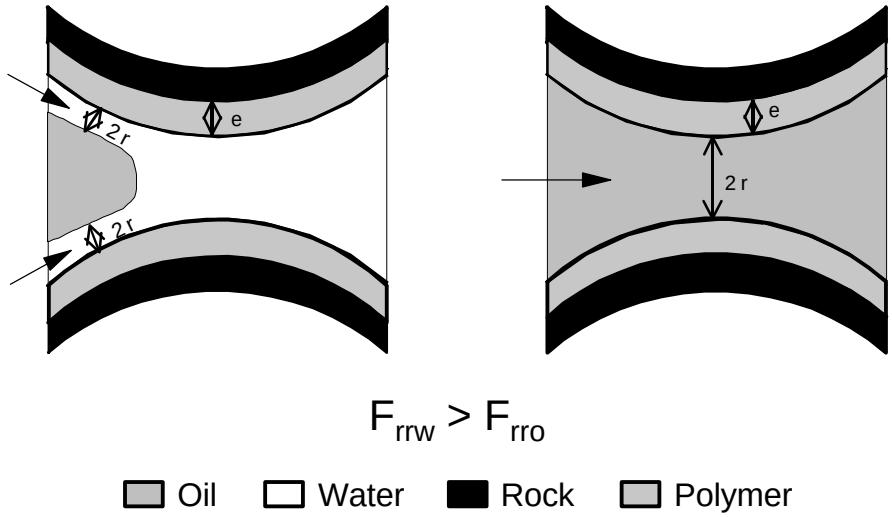

Fig. 59—Wall-effect model proposed by Zaitoun *et al.*[55]

If this theory is correct, the disproportionate permeability reduction should vanish in strongly oil-wet polyethylene cores where there is no water-wet surface for the polymer molecules to anchor on. However, Table 7 shows that a water-based gel reduced the permeability to water much more than that to oil in an oil-wet polyethylene core. This finding does not support the wall-effect theory. Also, the wall-effect model can not explain why an oil-based gel reduced the permeability to oil more than that to water in a strongly water-wet system.[48,49,53] (It is unlikely that the oil-based gel would adsorb onto the strongly water-wet pore walls.) As will be demonstrated in the

next section, the gel-droplet model proposed by Nilsson *et al*.[56] could provide an explanation for the observations that could not be explained by the wall-effect model.

Gel-Droplet Model

Nilsson *et al*.[56] performed a mechanistic study of the disproportionate permeability reduction. They used quartz sand and Teflon powder to simulate strongly water-wet and oil-wet porous media, respectively. Results from their experiments showed that a water-based HPAM gel reduced the permeability to water significantly more than that to oil in a strongly oil-wet porous medium. The same gel, however, completely blocked a strongly water-wet porous medium. Based on these findings, they proposed that the mechanism for the disproportionate permeability reduction is that water and oil flow more easily in some channels than in others.

Fig. 60 shows that when water flows through an oil-wet pore, the only restriction to the water flow is a thin film of oil on the pore wall. In contrast, when oil flows through the same pore, a residual water droplet in the pore restricts the oil flow. (This explains why the endpoint permeability of the wetting phase is always lower than that of the non-wetting phase.) During placement, a water-based gelant flows through the center of the oil-wet core. After gelation, a gel droplet forms at the center of the pore replacing the residual water droplet. Fig. 60 shows that if the size of the gel droplet is the same as that of the residual water droplet, the volume fraction of the pore available to oil flow remains the same as before treatment. However, Fig. 60 also shows that the presence of the gel droplet significantly reduces the volume fraction of the pore available to water flow. (Recall that the only restriction to water flow before treatment was the thin film of oil on the pore wall.) Thus, the gel could reduce the permeability to water without affecting the permeability to oil. Of course, if the gel droplet is larger than the residual water droplet, the permeability to oil will be reduced. Also, the disproportionate permeability reduction diminishes when the size of the gel droplet falls below that of the residual water droplet. Following similar logic, an oil-based gel should reduce the permeability to oil more than that to water in a strongly water-wet system. In support of this theory, results from our previous study showed that an oil-based gel reduced the permeability to oil more than that to water in a strongly water-wet system.[48,49,53] The authors pointed out that some gels are susceptible to syneresis after gelation. Since the size of the gel droplet decreases with increasing degree of syneresis, gel syneresis is predicted to have a strong influence on the disproportionate permeability reduction.

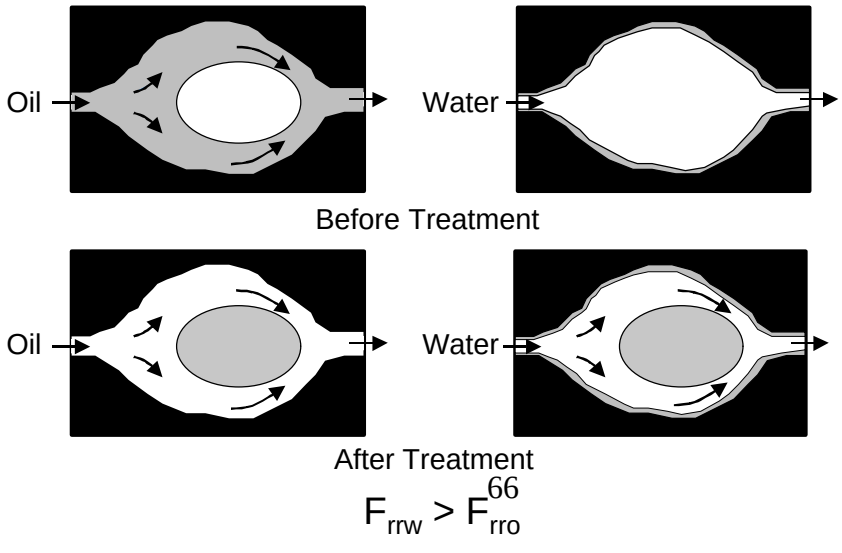

Fig. 60—Gel-droplet model proposed by Nilsson *et al.*[56]

In a strongly water-wet system, the model predicts that a strong water-based gel could block the pores completely by encapsulating the residual oil droplets. In support of the theory, our previous study showed that a strong water-based gel encapsulated the residual oil saturation and rendered it immobile after treatment.[39] Even with syneresis, the authors argued that the gel droplet could still occupy a significant volume fraction of the pore, thereby causing significant permeability reduction to both water and oil. However, this gel-droplet model could not explain why a water-based gel reduced the permeability to water much more than that to oil in a strongly water-wet system.[39,48,53] Also, this model cannot explain why an oil-based gel reduced the permeability to oil more than that to water in an oil-wet system (Table 8).

However, with minor modifications, the wall-effect model proposed by Zaitoun *et al.*[55] could provide satisfactorily explanations for these observations. In a modified wall-effect model, we assume that in a strongly water-wet system, the adsorbed layer on the pore walls after treatment can either be a polymer or a water-based gel. As discussed in the previous section, the presence of residual oil droplets at the center of the pores in a strongly water-wet system can significantly reduce the effective radius of the water channels during waterflooding. However, this restriction may not exist during oilflooding. Therefore, for a given thickness of an adsorbed polymer or gel layer, the permeability reduction for water during waterflooding is greater than that for oil during oilflooding.

Following similar logic, an oil-based gel could form a gel layer on the pore walls of a strongly oil-wet system. In this case, the presence of residual water droplets at the center of the pores could significantly reduce the effective width of the oil channels during oilflooding. However, this restriction may not exist during waterflooding. Therefore, for a given thickness of an adsorbed layer of the oil-based gel, the permeability reduction for oil during oilflooding is greater than that for water during waterflooding. This explains why an oil-based gel reduced the permeability to oil more than that to water in an oil-wet system (Table 8).

Summary. Our analyses demonstrated that if a gelant is the wetting phase, the wall-effect model proposed by Zaitoun *et al.*[55] could explain why the disproportionate permeability reduction occurs. In contrast, when the gelant is the non-wetting phase, the gel-droplet model proposed by Nilsson *et al.*[56] could be used to explain the disproportionate permeability reduction. However, this combined model is still highly idealized. Some issues remain unresolved, so more work is needed to test this model.

Conclusions

1. Results from our oil/water core experiments showed that the disproportionate permeability reduction decreased with increasing pressure gradient above 90 psi/ft. Also, the F_{rrw} decreased dramatically with increasing pressure gradient. More work is needed at even lower pressure gradients to study this effect.
2. Simultaneous gelant-oil injection in an oil-wet polyethylene core did not enhance the disproportionate permeability reduction. This finding does not support the segregated-pathway theory.

3. A Cr(III)-acetate-HPAM gel reduced the permeability to water significantly more than that to oil in oil-wet polyethylene cores. The residual resistance factor for oil, F_{rro}, was flow-rate independent. However, the residual resistance factor for water, F_{rrw}, was only weakly dependent on the flow rate. This result contrasts with the strong flow-rate dependent behavior of F_{rrw} observed in strongly water-wet cores using the same gel.[39,48,53]
4. An oil-based gel reduced the permeability to oil more than that to water in an oil-wet polyethylene core. Both the F_{rrw} and the F_{rro} were flow-rate independent. These observations are consistent with the behavior in strongly water-wet cores using the same gel.[39,48,53]
5. In oil-wet polyethylene cores, the disproportionate permeability reduction decreased with decreased absolute permeability. This observation is consistent with the behavior in strongly water-wet cores.[53]
6. With a Cr(III)-acetate-HPAM gel, the disproportionate permeability reduction was more pronounced in a 15-darcy oil-wet polyethylene core than in a 745-md water-wet Berea core. However, the trend was reversed between a 7-darcy oil-wet polyethylene core and the 745-md water-wet Berea core.
7. Our analyses suggest that if a gelant is the wetting phase, the wall-effect model proposed by Zaitoun *et al.*[55] could explain why the disproportionate permeability reduction occurs. In contrast, when the gelant is the non-wetting phase, the gel-droplet model proposed by Nilsson *et al.*[56] could be used to explain the disproportionate permeability reduction. However, this combined model is still highly idealized. Some issues remain unresolved, so more work is needed to test this model.

NOMENCLATURE

C = produced tracer concentration, g/m^3
C_o = injected tracer concentration, g/m^3
c_a = constant in Eq. 34
F_{dx} = gel dehydration factor for *x*-direction fractures
F_{dy} = gel dehydration factor for *y*-direction fractures
F_r = gel resistance factor (brine mobility before gel placement divided by gel mobility)
F_{rro} = oil residual resistance factor (oil mobility before gel divided by oil mobility after gel)
F_{rrw} = water residual resistance factor (water mobility before gel divided by that after gel)
G = shear modulus, psi [Pa]
h_f = fracture height, ft [m]
I_x = integer defined by Eq. 23
I_y = integer defined by Eq. 19
K = constant in Eq. 40
k_f = fracture permeability, darcys [μm^2]
k_{fx} = permeability of fractures oriented in the *x*-direction, darcys [μm^2]
k_{fy} = permeability of fractures oriented in the *y*-direction, darcys [μm^2]
k_w = relative permeability to water, darcys [μm^2]
L_x = distance of gel penetration along an *x*-direction fracture, ft [m]
DL_x = distance between adjacent *y*-direction fractures along the *x*-direction, ft [m]
L_{xo} = distance of gel penetration along the most-direct fracture, ft [m]
L_{xm} = distance of gel penetration along the m^{th} *x*-direction fracture, ft [m]
L_y = distance of gel penetration along an *y*-direction fracture, ft [m]
DL_y = distance between adjacent *x*-direction fractures along the *y*-direction, ft [m]
L_{yn} = distance of gel penetration along the n^{th} *y*-direction fracture, ft [m]
m = counting integer in Eq. 11 for *x*-direction fractures
m_{max} = counting integer defined in Eq. 15
n = counting integer in Eq. 9 for *y*-direction fractures; velocity exponent in Eq. 31
dp/dl = pressure gradient, psi/ft [Pa/m]
$(dp/dl)_c$ = critical pressure gradient for gel extrusion, psi/ft [Pa/m]
$(dp/dl)_x$ = pressure gradient required to extrude gel through *x*-direction fractures, psi/ft [Pa/m]
$(dp/dl)_y$ = pressure gradient required to extrude gel through *y*-direction fractures, psi/ft [Pa/m]
Dp = pressure drop, psi [Pa]
Dp_x = pressure drop along the *x*-direction, psi [Pa]
Dp_y = pressure drop along the *y*-direction, psi [Pa]
R = fracture conductivity ratio defined by Eq. 2
u = superficial velocity, ft/d, [m/s]
V_T = total volume of gel injected, bbl [m^3]
V_x = volume of *x*-direction fractures occupied by gel, bbl [m^3]
V_y = volume of *y*-direction fractures occupied by gel, bbl [m^3]
w_f = fracture width, ft [m]
w_{fx} = width of fractures oriented in the *x*-direction, ft [m]
w_{fy} = width of fractures oriented in the *y*-direction, ft [m]
x = abscissa
y = ordinate

Υ = shear strain
δ = distance of deformation, ft [m]
θ = angle, degrees
ϕ_f = effective porosity in a fracture
τ = shear stress, psi [Pa]
τ_c = critical shear stress for gel separation from the fracture wall, psi [Pa]

REFERENCES

1. Seright, R.S.: "Improved Methods for Water Shutoff," DOE Report DOE/PC/91008-1, Contract No. DE-AC22-94PC91008, BDM-Oklahoma Subcontract No. G4S60330, U.S. Department of Energy (Aug. 1997).
2. Seright, R.S.: "Improved Methods for Water Shutoff," Annual Technical Progress Report (U.S. DOE Report DOE/PC/91008-4), U.S. DOE Contract DE-AC22-94PC91008, BDM-Oklahoma Subcontract G4S60330 (Nov. 1997).
3. Sydansk, R.D. and Moore, P.E.: "Gel Conformance Treatments Increase Oil Production in Wyoming," *Oil & Gas J.* (Jan. 20, 1992) 40-45.
4. Borling, D.C.: "Injection Conformance Control Case Histories Using Gels at the Wertz Field CO_2 Teriary Flood in Wyoming, USA," paper SPE 27825 presented at the 1994 SPE/DOE Symposium on Improved Oil Recovery, April 17-20.
5. Hild, G.P., and Wackowski, R.K.: "Results of the Injection Well Polymer Gel Treatment Program at the Rangely Weber Sand Unit, Rangely, Colorado" paper SPE/DOE 39612 presented at the 1998 SPE/DOE Symposium on Improved Oil Recovery, Tulsa, April 19-22.
6. Tweidt, L.I. *et al.*: "Improving Sweep Efficiency in the Norman Wells Naturally Fractured Reservoir Through the Use of Polymer Gels: A Field Case History," paper SPE 38901 presented at the 1997 SPE Annual Technical Conference and Exhibition, San Antonio, Oct. 5-8.
7. Hughes, T.L. *et al.*: "Large-Volume Foam-Gel Treatments to Improve Conformance of the Rangely CO_2 Flood" paper SPE/DOE 39649 presented at the 1998 SPE/DOE Symposium on Improved Oil Recovery, Tulsa, April 19-22.
8. Seright, R.S.: "Gel Placement in Fractured Systems," *SPEPF* (Nov. 1995), 241-248.
9. Seright, R.S.: "Use of Preformed Gels for Conformance Control in Fractured Systems," *SPEPF* (Feb. 1997) 59-65.
10. Seright, R.S: "Gel Dehydration During Extrusion Through Fractures," paper SPE 39957 presented at the 1998 Rocky Mountain Regional Meeting/Low-Permeability Reservoirs Symposium, Denver, April 5-8.
11. Seright, R.S. and Lee, Robert: "Gel Treatments for Reducing Channeling Through Naturally Fractured Reservoirs," paper SPE 39802 presented at the 1998 SPE Permian Basin Oil and Gas Recovery Conference, Midland, March 23-26.
12. Vela, S., Peaceman, D.W., and Sandvik, E.I.: "Evaluation of Polymer Flooding in a Layered Reservoir With Crossflow, Retention, and Degradation," *SPEJ* (April 1976) 82-96.
13. Seright, R.S. and Liang, J.: "A Survey of Field Applications of Gel Treatments for Water Shutoff," paper SPE 26991 presented at the 1994 SPE III Latin American & Caribbean Petroleum Engineering Conference, Buenos Aires, April 27-29.
14. Moffitt, P.D.: "Long-Term Production Results of Polymer Treatments on Producing Wells in Western Kansas," *JPT* (April 1993) 356-362.
15. Kintzele, M.J.: "Polymer Treatments Brighten Production Profiles of Rocky Mountain Wells," American Oil & Gas Reporter (Feb. 1998) 109-119.
16. Sanders, G.S., Chambers, M.J., and Lane, R.H.: "Successful Gas Shutoff with Polymer Gel Using Temperature Modeling and Selective Placement in the Prudhoe Bay Field," paper SPE 28502 presented at the 1994 SPE Annual Technical Conference and Exhibition, New Orleans, Sept. 25-28.
17. Odorisio, V.G. and Curtis, S.C.: "Operational Advances from Field Application of Short-

Radius Horizontal Drilling in the Yates Field Unit," paper SPE 24612 presented at the 1992 SPE Annual Technical Conference and Exhibition, Washington, D.C., Oct. 4-7.
18. Shaw, D.J.: *Introduction to Colloid and Surface Chemistry, 2nd Ed.*, Butterworths, London (1970) 193.
19. Aklonis, J.J., and MacKnight, W.J.: *Introduction to Polymer Viscoelasticity, 2nd Ed.*, Wiley-Interscience, New York (1983) 9.
20. Schroder, U.P. and W. Opermann, "Properties of Polyelectrolyte Gels," in *Physical Properties of Polymeric Gels*, J.P. Cohen Addad, *ed.*, Wiley (1996) 19-38.
21. Seright, R.S., Liang, J., and Sun, H.: "Gel Treatments in Production Wells with Water Coning Problems," *In Situ* (1993) **17**, No.3, 243-272.
22. Liang, J., Lee, R.L., and Seright, R.S.: "Placement of Gels in Production Wells," *SPE Production & Facilities* (Nov. 1993) 276-284; *Transactions* AIME **295**.
23. Seright, R.S., Seldal, M., and Liang, J.: "Sizing Gelant Treatments in Hydraulically Fractured Production Wells," *SPEPF* (Nov. 1998).
24. Muskat, M. and R.D. Wycoff: "An Approximate Theory of Water-Coning in Oil Production," *Trans.*, AIME (1935) **114**, 144-161.
25. Karp, J.C., D.K. Lowe, and N. Marusov: "Horizontal Barriers for Controlling Water Coning," *JPT* (July 1962) 783.
26. Aarra, M.G., Skauge, A., Søgnesand, S., and Stenhaug, M.: "A Foam Pilot Test Aimed at Reducing Gas Inflow in a Production Well at the Oseberg Field," *Petroleum Geoscience*, (1996) **2**, 125-132.
27. Surguchev, L.M. and Hanssen, J.E.: "Foam Application in North Sea Reservoirs, I: Design and Technical Support of Field Trials," paper SPE 35371 presented at the 1996 SPE/DOE Symposium on Improved Oil Recovery, Tulsa, April 21-24.
28. Aarra, M.G. and Skauge, A.: "A Foam Pilot in a North Sear Oil Reservoir: Preparation for a Production Well Treatment," paper SPE 28599 presented at the 1994 SPE Annual Technical Conference and Exhibition, New Orleans, Sept. 25-28.
29. Lakatos, I., Lakatos-Szabó, J., Kosztin, B., Trömböczky, S., Bodola, M., and Palásthy, G.: "Selective Fluid Shutoff Treatments at the Algyõ Field, Hungary," paper presented at the 9th European Symposium on Improved Oil Recovery, The Hague, Oct. 20-22, 1997.
30. Chukwueke, V.O., Bouts, M.N., and Dijkum, V.: "Gas Shut-off Foam Treatments," paper SPE 39650 presented at the 1998 SPE/DOE Symposium on Improved Oil Recovery, Tulsa, April 19-22.
31. Dalland, M. and Hanssen, E.: "Foam Barriers for Thin Oil Rims: Gas Blockage with Hydrocarbon Foams," paper presented at the 7th European Symposium on Improved Oil Recovery, The Hague, Oct. 20-22, 1993.
32. Strickland, R.F.: "Artificial Barriers May Control Water Coning–1," *Oil & Gas J.* (Oct. 7, 1974) 61.
33. Strickland, R.F.: "Artificial Barriers May Control Water Coning–2," *Oil & Gas J.* (Oct. 14, 1974) 110.
34. Ehlig-Economides, C.A., Chan, K.S., and Spath, J.B.: "Production Enhancement Strategies for Strong Bottom Water Drive Reservoirs," paper SPE 36613 presented the 1996 SPE Annual Technical Conference and Exhibition, Denver, Oct. 6-9.
35. Thakur, G.C. and Thachuk, A.R.: "Retardation of Water Coning in Oil Wells Using Polymers–A Reservoir Simulation Application," paper number 374027 presented at the 25th

Annual Technical Meeting, Petroleum Society of CIM, Calgary, May 7-10, 1974.
36. Hwan, R-N.R.: "Numerical Simulation Study of Water Shutoff Treatment Using Polymers," paper SPE 25854 presented at the 1993 SPE Rock Mountain Regional/Low Permeability Reservoirs Symposium, Denver, April 12-14.
37. Ekrann, S. and Hanssen, J.E.: "Well Treatments Against Gas Coning Must Exploit Gravity Effects," paper presented at the IEA Collaborative Project on Enhanced Oil Recovery, Workshop and Symposium Banff, Sept. 1992.
38. Byrne, W.B. and Morse, R.A.: "Water Coning May Not Be Harmful–1," *Oil & Gas J.* (Sept. 3, 1973) 66.
39. Liang, J., Sun, H., Seright, R.S.: "Reduction of Oil and Water Permeabilities Using Gels," paper SPE 24195 presented at the 1992 SPE/DOE Symposium on Enhanced Oil Recovery, Tulsa, April 22-24.
40. Needham, R.B., Threlkeld, C.B., and Gall, J.W.: "Control of Water Mobility Using Polymers and Multivalent Cations," paper SPE 4747 presented at the 1974 SPE-AIME Improved Oil Recovery Symposium, Tulsa, April 22-24.
41. Avery, M.R. and Wells, T.A.: "Field Evaluation of a New Gelant for Water Control in Production Wells," paper SPE 18201 presented at the 1988 SPE Annual Technical Conference and Exhibition, Houston, Oct. 2-5.
42. Sandiford, B.B. and Graham, G.A.: "Injection of Polymer Solutions in Producing Wells," AIChE Symposium Series, (1973) **69**, No. 127, 38.
43. Schneider, F.N. and Owens, W.W.: "Steady-State Measurements of Relative Permeability for Polymer/Oil Systems," *SPEJ* (Feb. 1982) 79.
44. Sparlin, D.D.: "An Evaluation of Polyacrylamides for Reducing Water Production," *JPT* (Aug. 1976) 906-914.
45. White, J.L., Goddard, J.E., and Phillips, H.M.: "Use of Polymers To Control Water Production in Oil Wells," *JPT* (Feb. 1973) 143-150.
46. Zaitoun, A. and Kohler N.: "Two-Phase Flow Through Porous Media: Effect of an Adsorbed Polymer Layer," paper SPE 18085 presented at the 1988 SPE Annual Technical Conference and Exhibition, Houston, Oct. 2-5.
47. Zaitoun, A. and Kohler N.: "Thin Polyacrylamide Gels for Water Control in High-Permeability Production Wells" paper SPE 22785 presented at the 1991 SPE Annual Technical Conference and Exhibition, Dallas, Oct. 6-9.
48. Liang, J., Sun, H., Seright, R.S.: "Why Do Gels Reduce Water Permeability More Than Oil Permeability?," *SPERE* (Nov. 1995) 282-286.
49. Seright, R.S.: "Improved Techniques for Fluid Diversion in Oil Recovery Processes," final report, DOE/BC/14880-15, U.S. DOE (Jan. 1996) 62-89.
50. Seright, R.S.: "Reduction of Gas and Water Permeabilities Using Gels," *SPEPF* (Nov. 1995) 103-108.
51. Elphick, J. and Seright, R.S.: "A Classification of Water Production Problems"presented at the 3rd International Conference on Reservoir Conformance, Profile Control, and Water and Gas Shutoff, Houston, (Aug. 1997).
52. Dawe, R.A. and Zhang, Y.: "Mechanistic Study of the Selective Action of Oil and Water Penetrating into a Gel Emplaced in a Porous Medium," *Journal of Petroleum Science and Engineering* (1994) **12**, 113-125.
53. Liang, J. and Seright, R.S.: "Further Investigations of Why Gels Reduce k_w More Than k_o,"

SPEPF (Nov. 1997).
54. Seright, R.S. and Martin, F.D.: “Fluid Diversion and Sweep Improvement with Chemical Gels in Oil Recovery Processes,” final report, DOE/BC/14447-15, U.S. DOE (Sept. 1992) 28-58.
55. Zaitoun, A., Bertin, H., and Lasseux, D.: “Two-Phase Flow Property Modifications by Polymer Adsorption,” paper SPE 39631 presented at the 1998 SPE/DOE Improved Oil Recovery Symposium, Tulsa, April 19-22.
56. Nilsson, S., Stavland, A. and Jonsbraten, H. C.: “Mechanistic Study of Disproportionate Permeability Reduction” paper SPE 39635 presented at the 1998 SPE/DOE Improved Oil Recovery Symposium, Tulsa, April 19-22.

APPENDIX A: Data Supplement to Chapter 3

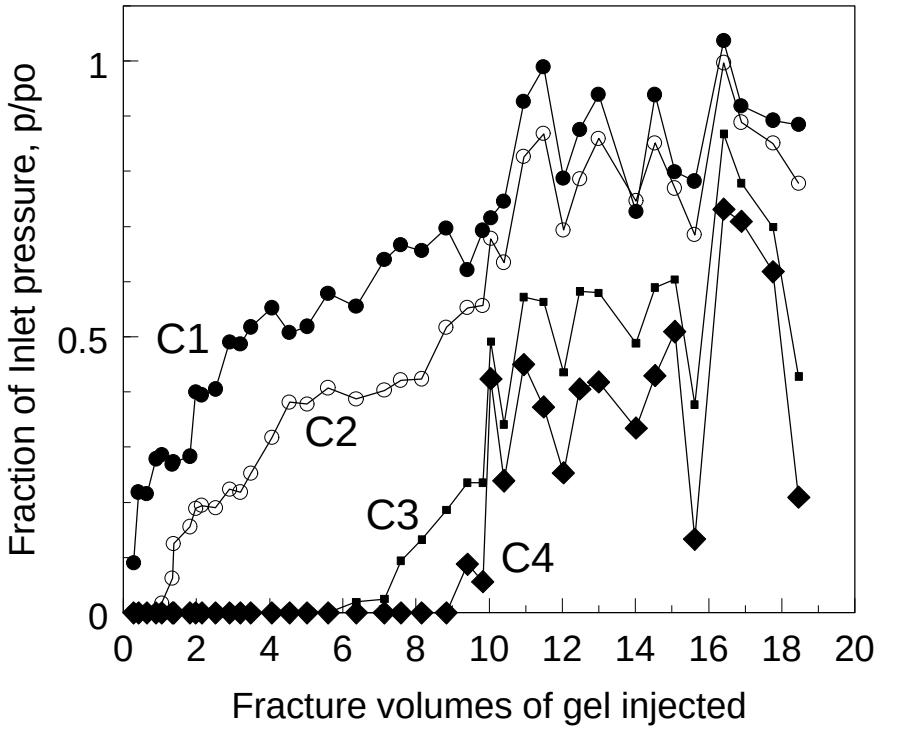

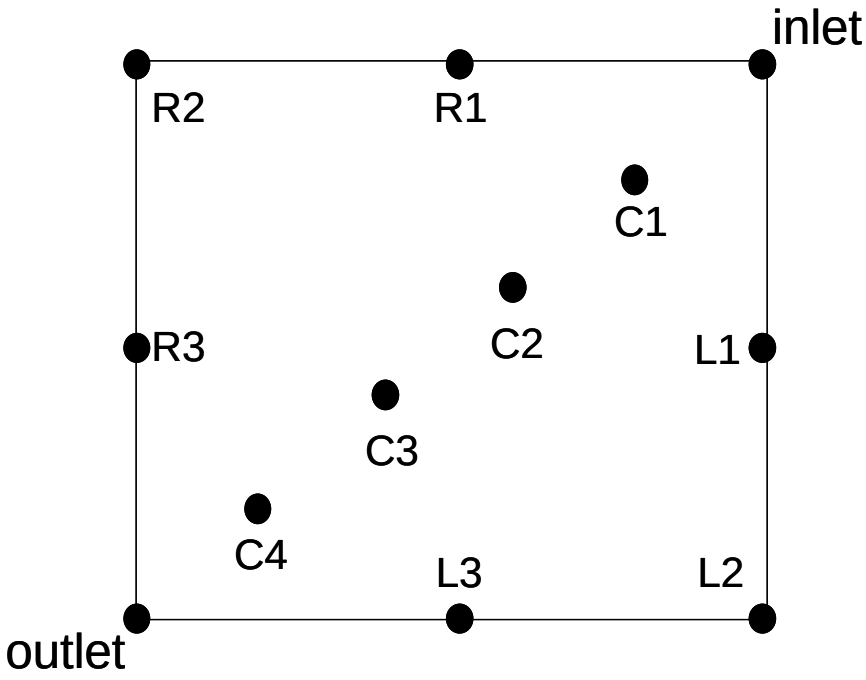

Pressure tap locations for Radial Fracture H3

Fig. A1—Radial Fracture H3 pressure behavior along the central streamline. (During gel injection. Fracture dimensions: 12 in. x 12 in. x ~0.04 in.)

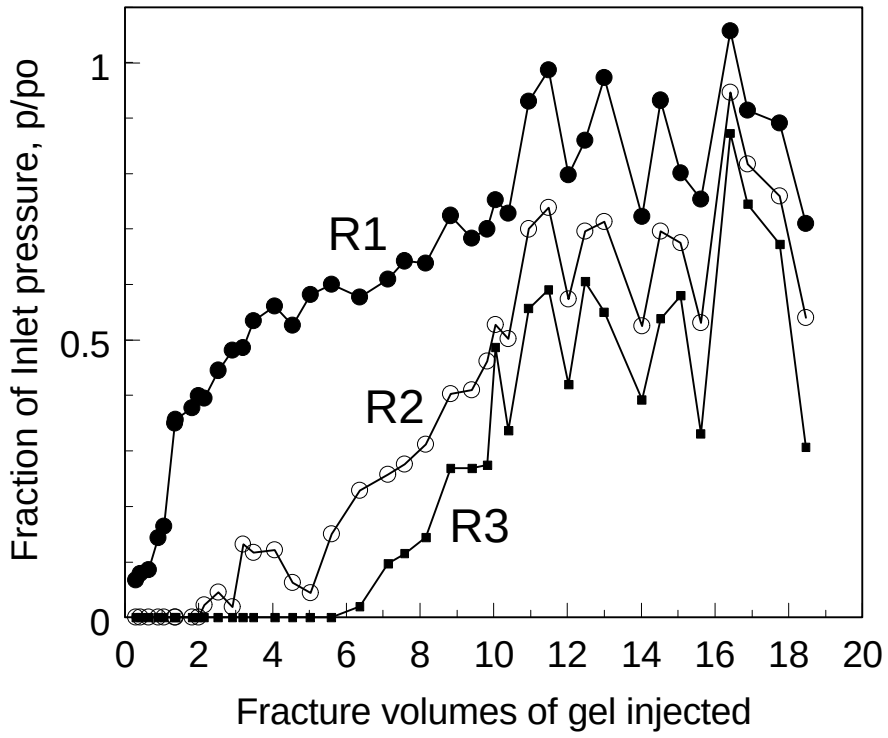

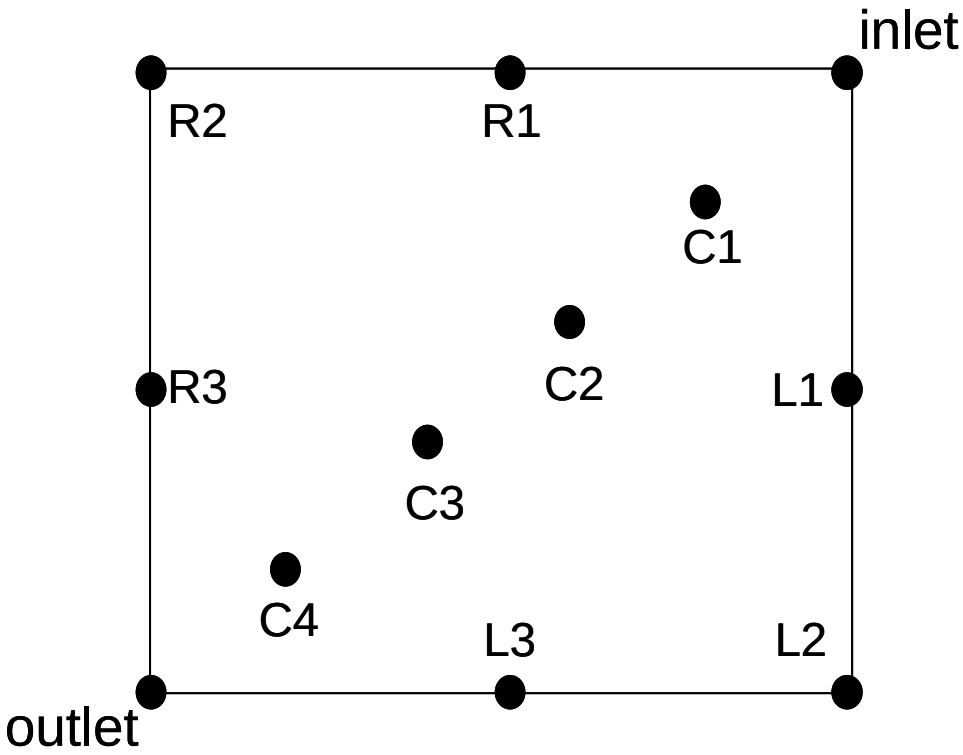

Pressure tap locations for Radial Fracture H3

Fig. A2—Radial Fracture H3 pressure behavior along the right streamline. (During gel injection. Fracture dimensions: 12 in. x 12 in. x ~0.04 in.)

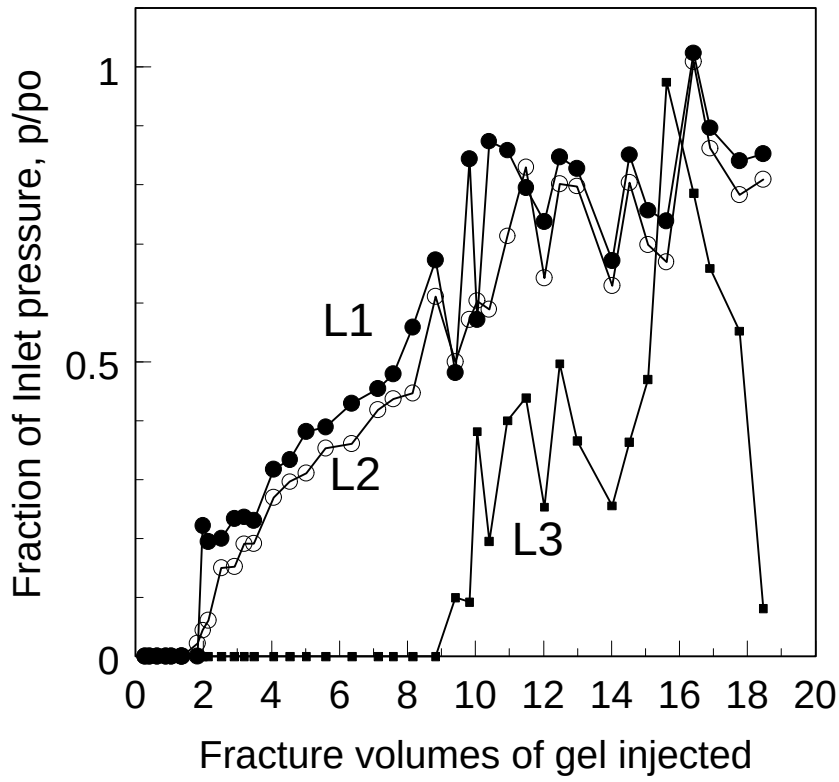

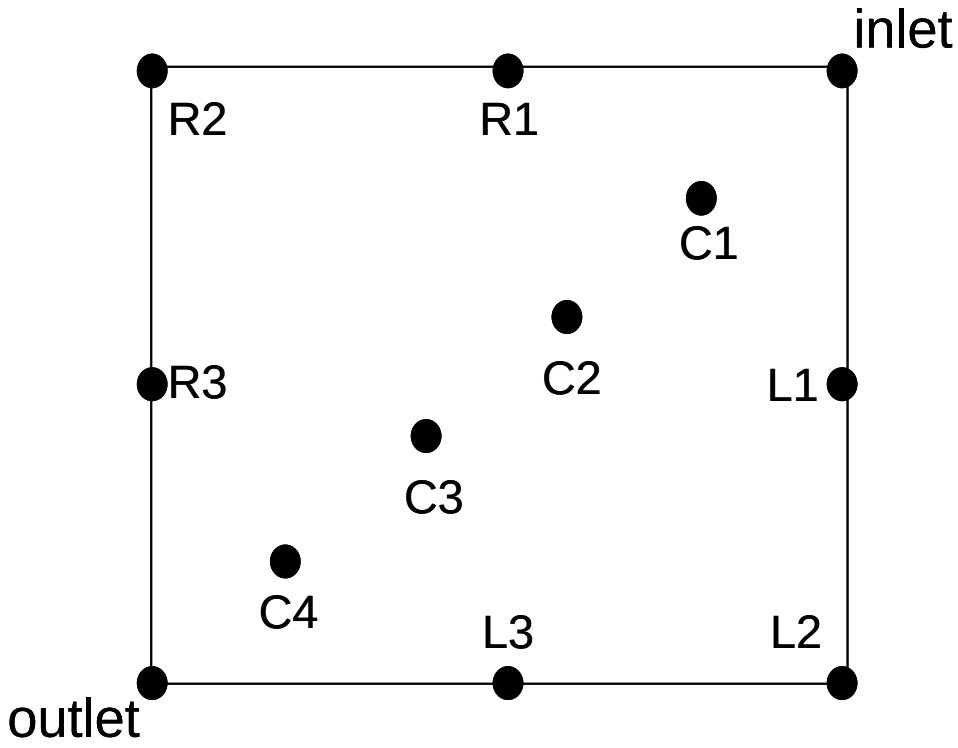

Pressure tap locations for Radial Fracture H3

Fig. A3—Radial Fracture H3 pressure behavior along the left streamline. (During gel injection. Fracture dimensions: 12 in. x 12 in. x ~0.04 in.)

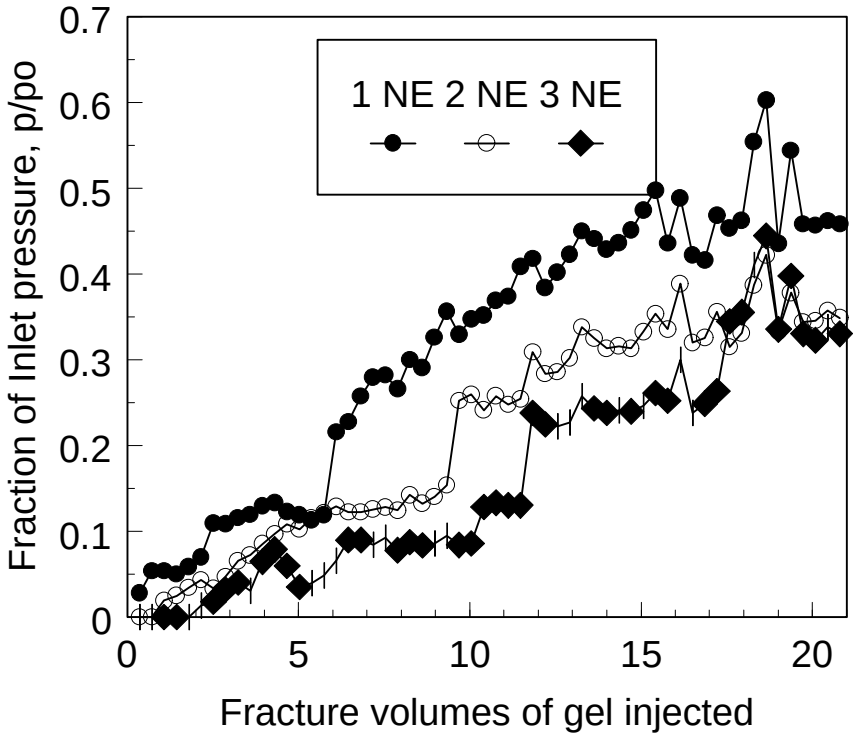

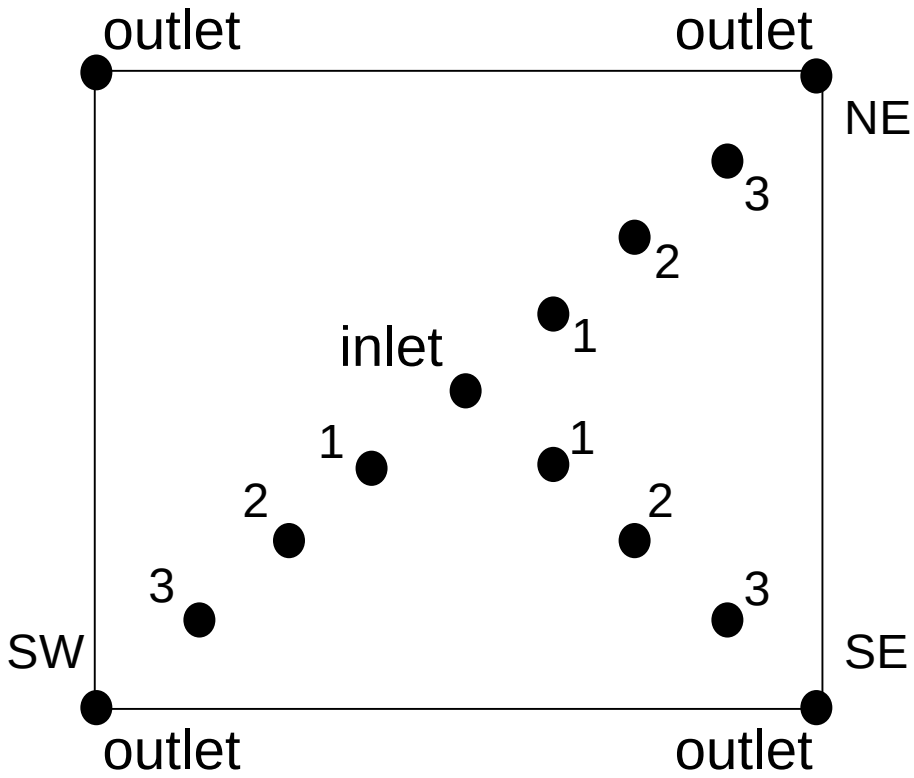

Fig. A4—Radial Fracture H4 pressure behavior along the NE streamline. (During gel injection. Fracture dimensions: 12 in. x 12 in. x ~0.04 in.)

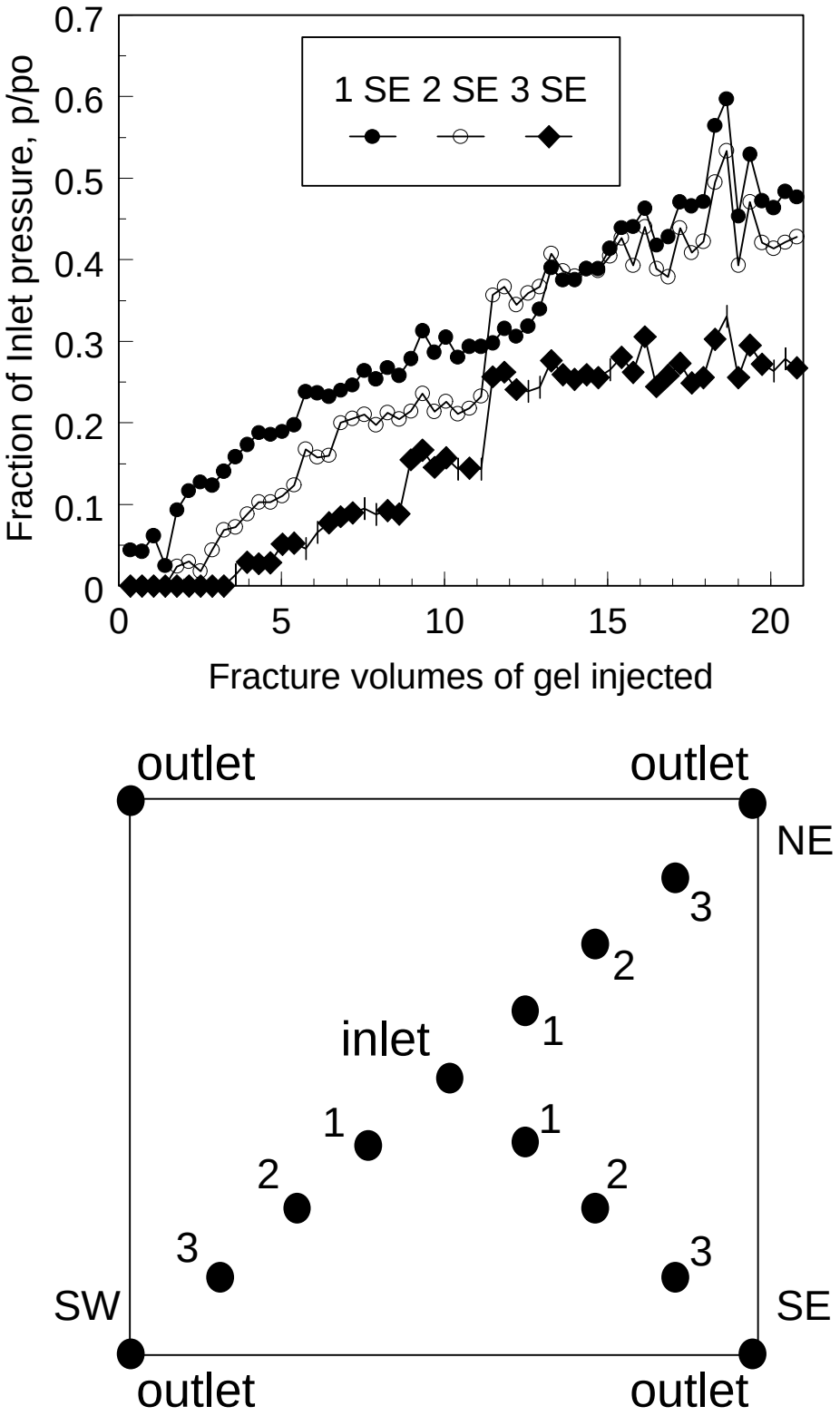

Fig. A5—Radial Fracture H4 pressure behavior along the SE streamline.
(During gel injection. Fracture dimensions: 12 in. x 12 in. x ~0.04 in.)

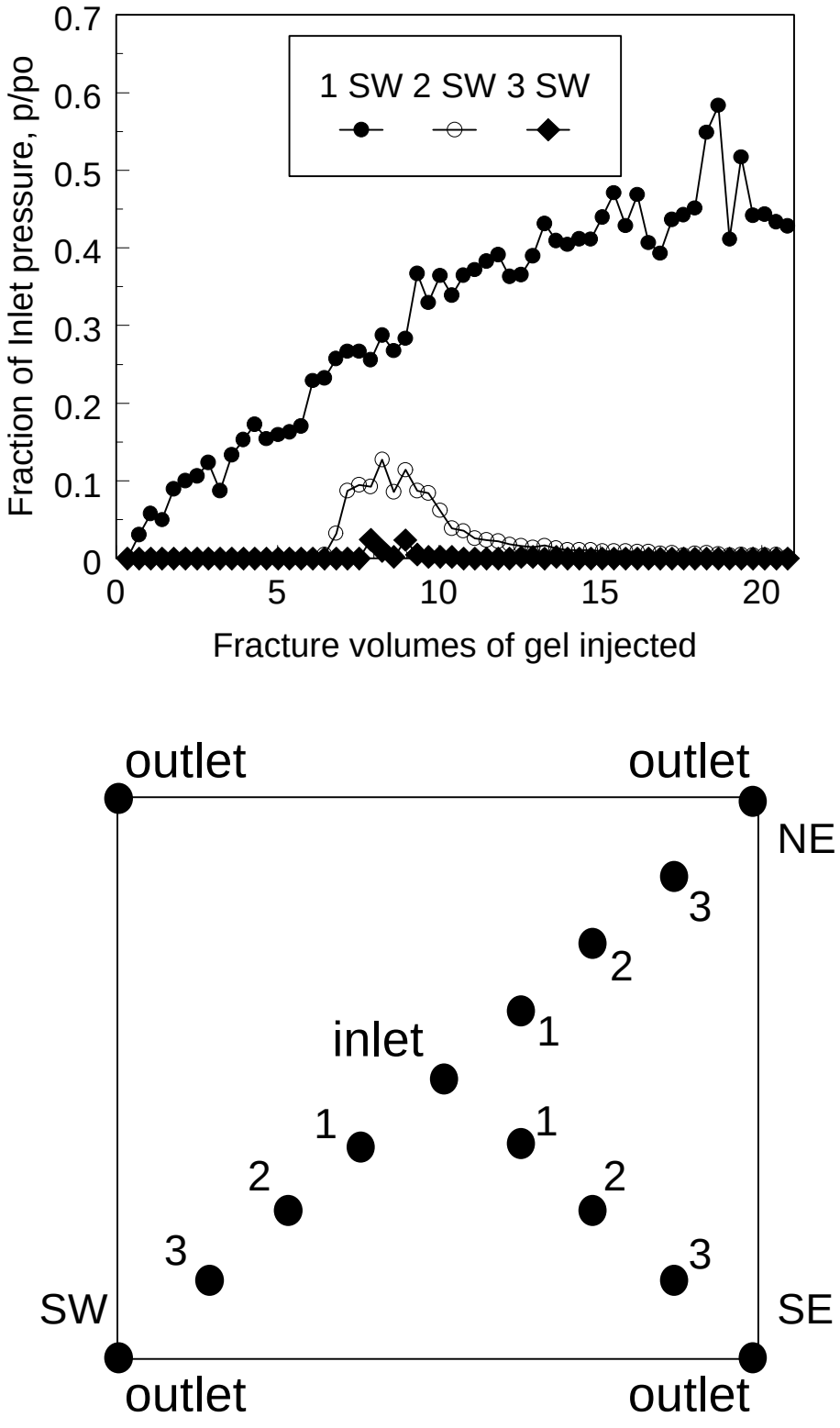

Fig. A6—Radial Fracture H4 pressure behavior along the SW streamline.
(During gel injection. Fracture dimensions: 12 in. x 12 in. x ~0.04 in.)

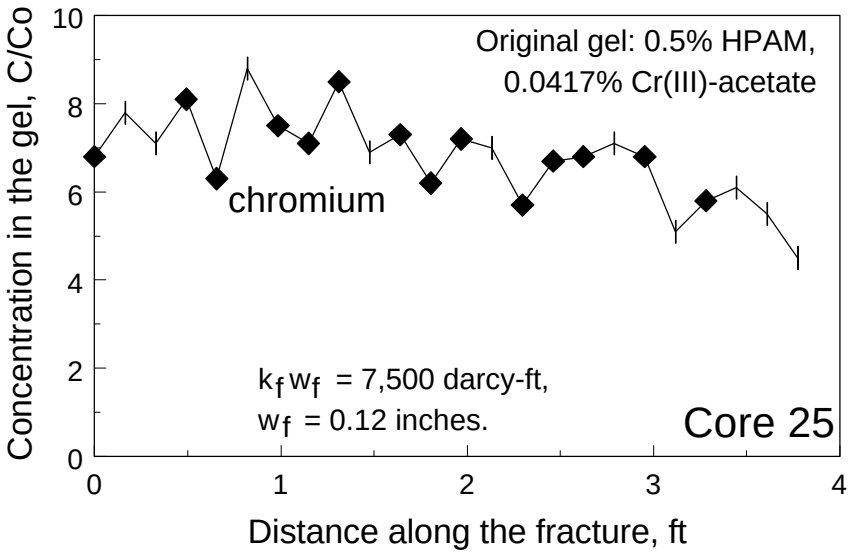

Fig. A7—Chromium concentration versus fracture length for Core 25.

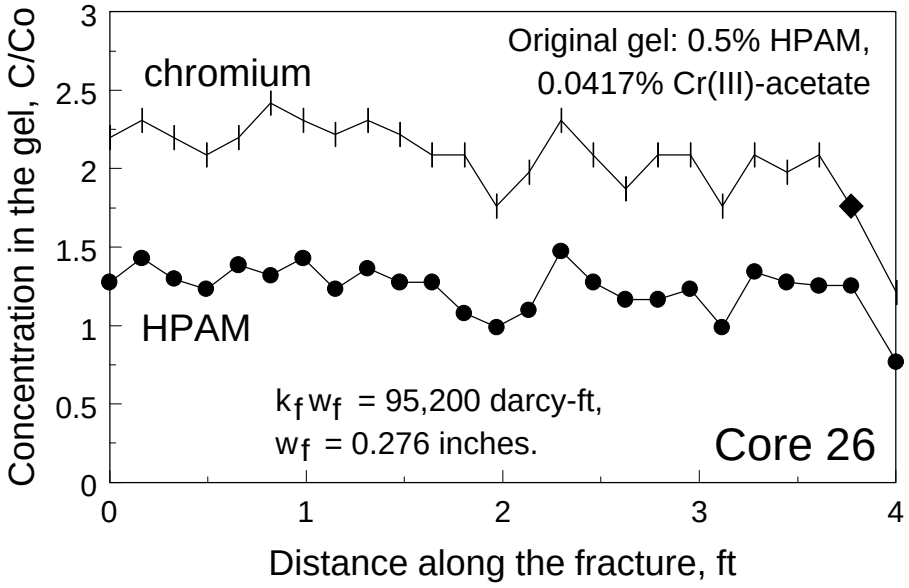

Fig. A8—Gel composition versus fracture length for Core 26.

APPENDIX B: Data Supplement for Chapter 5

Table B1—Summary of Water and Oil Mobilities Before Gel Treatment
(Core SSH-184, High-permeability Berea sandstone, 41°C)

$(k/\mu)_w$, md/cp @ S_w=1.0	$(k/\mu)_o$, md/cp @ S_{wr}=0.28	$(k/\mu)_w$, md/cp @ S_{or}=0.24
1,244	700	403

Table B2—Summary of Water and Oil Mobilities Before Gel Treatment
(Core SSH-173, High-permeability Berea sandstone, 41°C)

$(k/\mu)_w$, md/cp @ S_w=1.0	$(k/\mu)_o$, md/cp @ S_{wr}=0.28	$(k/\mu)_w$, md/cp @ S_{or}=0.24
1,028	570	279

Table B3—Summary of Water and Oil Mobilities Before Gel Treatment
(Core SSH-182, High-permeability Berea sandstone, 41°C)

$(k/\mu)_w$, md/cp @ S_w=1.0	$(k/\mu)_o$, md/cp @ S_{wr}=0.30	$(k/\mu)_w$, md/cp @ S_{or}=0.22
1,194	631	382

Table B4—Summary of Water and Oil Mobilities Before Gel Treatment
(Core SSH-183, High-permeability Berea sandstone, 41°C)

$(k/\mu)_w$, md/cp @ S_w=1.0	$(k/\mu)_o$, md/cp @ S_{wr}=0.28	$(k/\mu)_w$, md/cp @ S_{or}=0.24
1,327	695	438

Table B5—Summary of Water and Oil Mobilities Before Gel Treatment
(Core SSH-185, High-permeability Berea sandstone, 41°C)

$(k/\mu)_w$, md/cp @ S_w=1.0	$(k/\mu)_o$, md/cp @ S_{wr}=0.28	$(k/\mu)_w$, md/cp @ S_{or}=0.24
1,193	651	350

Table B6—Summary of Water and Oil Mobilities Before Gel Treatment
(Core PE-205, Artificial polyethylene core, 41°C)

$(k/\mu)_w$, md/cp @ S_w=1.0	$(k/\mu)_o$, md/cp @ S_{wr}=0.14	$(k/\mu)_w$, md/cp @ S_{or}=0.31
10,370	1,806	4,010

Table B7—Summary of Water and Oil Mobilities Before Gel Treatment
(Core PE-208, Artificial polyethylene core, 41°C)

$(k/\mu)_w$, md/cp @ S_w=1.0	$(k/\mu)_o$, md/cp @ S_{wr}=0.14	$(k/\mu)_w$, md/cp @ S_{or}=0.28
10,900	2,033	4,080

Table B8—Summary of Water and Oil Mobilities Before Gel Treatment
(Core PE-201, Artificial polyethylene core, 41°C)

$(k/\mu)_w$, md/cp @ S_w=1.0	$(k/\mu)_o$, md/cp @ S_{wr}=0.18	$(k/\mu)_w$, md/cp @ S_{or}=0.25
22,800	4,540	10,000

Table B9—Summary of Water and Oil Mobilities Before Gel Treatment
(Core PE-202, Artificial polyethylene core, 41°C)

$(k/\mu)_w$, md/cp @ S_w=1.0	$(k/\mu)_o$, md/cp @ S_{wr}=0.28	$(k/\mu)_w$, md/cp @ S_{or}=0.12
22,200	5,000	7,930

Table B10—Summary of Water and Oil Mobilities Before Gel Treatment
(Core SSH-197, Berea sandstone, 41°C)

$(k/\mu)_w$, md/cp @ S_w=1.0	$(k/\mu)_o$, md/cp @ S_{wr}=0.32	$(k/\mu)_w$, md/cp @ S_{or}=0.20
1,113	640	391

Table B11—Summary of Residual Resistance Factors-Core SSH-184
Core: 834-md Berea sandstone
Gel: 0.5% HPAM, 0.0417% Cr(III)-acetate, 1% NaCl, 0.1% $CaCl_2$

1st Waterflood		
Flux, ft/d	F_{rrw} (1st short core segment)	F_{rrw} (center core segment)
0.025	2,975	10,950
1st Oilflood		
Flux, ft/d	F_{rro} (1st short core segment)	F_{rro} (center core segment)
0.787	39	217
2nd Waterflood		
Flux, ft/d	F_{rrw} (1st short core segment)	F_{rrw} (center core segment)
0.025	1,600	11,600
2nd Oilflood		
Flux, ft/d	F_{rro} (1st short core segment)	F_{rro} (center core segment)
0.787	50	305
3rd Waterflood		
Flux, ft/d	F_{rrw} (1st short core segment)	F_{rrw} (center core segment)
0.0061 (45 psi/ft)	2,310	18,830
0.025	1,540	11,900
0.050	1,170	8,000
0.025	1,560	10,250
0.101	870	5,120
0.050	1,320	7,330
0.025	1,790	9,950
F_{rrw} (center segment)= 1,900 $u^{-0.459}$, r = 0.984		

Table B12—Summary of Residual Resistance Factors-Core SSH-173
Core: 689-md Berea sandstone
Gel: 0.5% HPAM, 0.0417% Cr(III)-acetate, 1% NaCl, 0.1% $CaCl_2$

1st Oilflood		
Pressure gradient, psi/ft	F_{rro} (1st short core segment)	F_{rro} (center core segment)
45	4	34
1st Waterflood		
Pressure gradient, psi/ft	F_{rrw} (1st short core segment)	F_{rrw} (center core segment)
45	279	4713
2nd Oilflood		
Pressure gradient, psi/ft	F_{rro} (1st short core segment)	F_{rro} (center core segment)
45	1.4	24

Table B13—Summary of Residual Resistance Factors-Core SSH-182
Core: 800-md Berea sandstone
Gel: 0.5% HPAM, 0.0417% Cr(III)-acetate, 1% NaCl, 0.1% $CaCl_2$

Brine/Oil Volume Ratio	Brine Mobility, md/cp	Oil Mobility, md/cp
100/0	8.62	0
90/10	5.56	0.62
80/20	4.96	1.24
70/30	5.86	2.51
60/40	5.88	3.92
50/50	5.6	5.6
40/60	6.69	10.04
30/70	8.24	19.23
20/80	8.97	35.87
10/90	7.13	64.15
0/100	0	207.88
10/90	8.17	73.55
20/80	12.75	51.02
30/70	18.17	42.41
40/60	21.73	32.60
50/50	27.01	27.01
60/40	36.85	24.56
70/30	44.13	18.91
80/20	54.48	13.62
90/10	60.94	6.77
100/0	103.35	0

Table B14—Summary of Residual Resistance Factors-Core SSH-183
Core: 889-md Berea sandstone
Gel: 0.5% HPAM, 0.0417% Cr(III)-acetate, 0.05 M Na-acetate, 1% NaCl, 0.1% $CaCl_2$

1st Oilflood		
Flux, ft/d	F_{rro} (1st short core segment)	F_{rro} (center core segment)
25.2	5	8
1st Waterflood		
Flux, ft/d	F_{rrw} (1st short core segment)	F_{rrw} (center core segment)
6.3	32	13
2nd Oilflood		
Flux, ft/d	F_{rro} (1st short core segment)	F_{rro} (center core segment)
25.2	3	5

Table B15—Summary of Residual Resistance Factors-Core SSH-185
Core: 800-md Berea sandstone.
Gel: 0.5% HPAM, 0.0417% Cr(III)-acetate, 0.025 M Na-acetate, 1% NaCl, 0.1% $CaCl_2$

1st Oilflood		
Flux, ft/d	F_{rro} (1st short core segment)	F_{rro} (center core segment)
25.2	2	6
1st Waterflood		
Flux, ft/d	F_{rrw} (1st short core segment)	F_{rrw} (center core segment)
1.575	73	43
2nd Oilflood		
Flux, ft/d	F_{rro} (1st short core segment)	F_{rro} (center core segment)
25.2	4	4
3rd Waterflood		
Flux, ft/d	F_{rrw} (1st short core segment)	F_{rrw} (center core segment)
6.3	23	13

Table B16—Summary of Residual Resistance Factors-Core PE-205
Core: 6,950-md artificial polyethylene core. Gelant/oil ratio: 100/0.
Gel: 0.5% HPAM, 0.0417% Cr(III)-acetate, 1% NaCl, 0.1% $CaCl_2$

1st Waterflood		
Flux, ft/d	F_{rrw} (1st short core segment)	F_{rrw} (center core segment)
0.033 (ΔP_{center} = 10 psi)	24,000	25,000
1st Oilflood		
Flux, ft/d	F_{rro} (1st short core segment)	F_{rro} (center core segment)
1.918 (ΔP_{center} = 10 psi)	83	192
2nd Waterflood		
Flux, ft/d	F_{rrw} (1st short core segment)	F_{rrw} (center core segment)
0.021 (ΔP_{center} = 9 psi)	57,000	35,300
2nd Oilflood		
Flux, ft/d	F_{rro} (1st short core segment)	F_{rro} (center core segment)
1.588 (ΔP_{center} = 10 psi)	57	235
3rd Waterflood		
Flux, ft/d	F_{rrw} (1st short core segment)	F_{rrw} (center core segment)
0.028 (ΔP_{center} = 9.5 psi)	12,800	27,000

Table B17—Summary of Residual Resistance Factors-Core PE-208
Core: 7,303-md artificial polyethylene core. Gelant/oil ratio: 50/50.
Gel: 0.5% HPAM, 0.0417% Cr(III)-acetate, 1% NaCl, 0.1% $CaCl_2$

1st Waterflood		
Flux, ft/d	F_{rrw} (1st short core segment)	F_{rrw} (center core segment)
1.191 (ΔP_{center} = 10 psi)	180	670
1st Oilflood		
Flux, ft/d	F_{rro} (1st short core segment)	F_{rro} (center core segment)
15.55 (ΔP_{center} = 9.5 psi)	11	23
2nd Waterflood		
Flux, ft/d	F_{rrw} (1st short core segment)	F_{rrw} (center core segment)
9.264 (ΔP_{center} = 10 psi)	11	83
2nd Oilflood		
Flux, ft/d	F_{rro} (1st short core segment)	F_{rro} (center core segment)
54.59 (ΔP_{center} = 10 psi)	3	7

Table B18—Summary of Residual Resistance Factors-Core PE-201
Core: 15,276-md artificial polyethylene core
Gel: 0.5% HPAM, 0.0417% Cr(III)-acetate, 1% NaCl, 0.1% $CaCl_2$

1st Waterflood		
Flux, ft/d	F_{rrw} (1st short core segment)	F_{rrw} (center core segment)
0.021 (ΔP_{center} = 10 psi)	5,000	90,000
1st Oilflood		
Flux, ft/d	F_{rro} (1st short core segment)	F_{rro} (center core segment)
2.669 (ΔP_{center} = 11 psi)	21	375
2nd Waterflood		
Flux, ft/d	F_{rrw} (1st short core segment)	F_{rrw} (center core segment)
0.021 (ΔP_{center} = 5.5 psi)	1,550	47,000
2nd Oilflood		
Flux, ft/d	F_{rro} (1st short core segment)	F_{rro} (center core segment)
2.669 (ΔP_{center} = 10 psi)	2	345
1.335	6	299
0.667	12	273
2.669	1	209
3rd Waterflood		
Flux, ft/d	F_{rrw} (1st short core segment)	F_{rrw} (center core segment)
0.120 (ΔP_{center} = 10 psi)	1,140	16,500
0.085	1,600	17,800
0.043	2,300	20,000
0.021	4,200	23,000
F_{rrw} (center segment) = 11,128 $u^{-0.19}$, r = 0.999		

Table B19—Summary of Residual Resistance Factors-Core PE-205
Core: 14,874-md artificial polyethylene core
Gel: 18% 12-hydroxystearic acid in Soltrol-130

1st Waterflood		
Flux, ft/d	F_{rrw} (1st short core segment)	F_{rrw} (center core segment)
15.014 (ΔP_{center} = 8.5 psi)	22	85
1st Oilflood		
Flux, ft/d	F_{rro} (1st short core segment)	F_{rro} (center core segment)
2.669 (ΔP_{center} = 10 psi)	75	375
2nd Waterflood		
Flux, ft/d	F_{rrw} (1st short core segment)	F_{rrw} (center core segment)
15.014 (ΔP_{center} = 8 psi)	11	80
2nd Oilflood		
Flux, ft/d	F_{rro} (1st short core segment)	F_{rro} (center core segment)
2.669 (ΔP_{center} = 10 psi)	40	338
1.335	39	342
0.667	46	345
0.334	49	390
Avg. F_{rro} (center segment) = 354		
3rd Waterflood		
Flux, ft/d	F_{rrw} (1st short core segment)	F_{rrw} (center core segment)
21.353 (ΔP_{center} = 10 psi)	1	73
10.667	1	66
5.338	2	65
2.669	5	66
Avg. F_{rrw} (center segment) = 68		

Table B20—Summary of Residual Resistance Factors-Core SSH-197
Core: 745-md Berea sandstone
Gel: 0.5% HPAM, 0.0417% Cr(III)-acetate, 1% NaCl, 0.1% $CaCl_2$

1st Waterflood		
Flux, ft/d	F_{rrw} (1st short core segment)	F_{rrw} (center core segment)
0.011	685	10,100
1st Oilflood		
Flux, ft/d	F_{rro} (1st short core segment)	F_{rro} (center core segment)
2.787	7	59
2nd Waterflood		
Flux, ft/d	F_{rrw} (1st short core segment)	F_{rrw} (center core segment)
0.089	55	1,390
2nd Oilflood		
Flux, ft/d	F_{rro} (1st short core segment)	F_{rro} (center core segment)
2.787	6	56
3rd Waterflood		
Flux, ft/d	F_{rrw} (1st short core segment)	F_{rrw} (center core segment)
0.089	36	1,265

APPENDIX C: Technology Transfer

Presentations

On October 6 and 7, 1998, we held a project review in Socorro, NM.

On August 10, 1998, we presented the talk, "Where Will the Disproportionate Permeability Reduction Be Most Useful in Field Applications?," at the 4th International Conference on Reservoir Conformance, Profile Control, and Water and Gas Shutoff in Houston, Texas.

On August 6, 1998, we presented the talk, "Placement of Blocking Agents in Heterogeneous Reservoirs," at the Gordon Research Conference in Andover, NH.

On June 8, 1998, we presented the talk, "Water-Shutoff Treatments in North America" at the European Union's Water Control in Oil and Gas Production Workshop in Leipzig, Germany.

On May 2, 1998, we presented the talk, "An Overview of Water-Shutoff Treatments," at the ONGC Round Table Conference on Water and Gas Control, Bombay, India.

On April 18, 1998, we presented the one-day short course, "Water Shutoff" at the 1998 SPE/DOE Improved Oil Recovery Symposium in Tulsa, OK.

On April 7, 1998, we presented SPE paper 39957, "Gel Dehydration During Extrusion Through Fractures," at the 1998 Rocky Mountain Regional Meeting/Low-Permeability Reservoirs Symposium in Denver, CO.

On March 25, 1998, we presented SPE paper 39802, "Gel Treatments for Reducing Channeling Through Naturally Fractured Reservoirs," at the 1998 SPE Permian Basin Oil and Gas Recovery Conference in Midland, TX.

On January 28 and 29, 1998, we held a project review in Socorro, NM. The review was attended by 26 people (not including New Mexico Tech personnel) representing 16 different organizations.

On November 18, 1997, we presented the talk, "Candidate Selection Criteria," at the Water Shutoff/Water Management Meeting in Plano, Texas.

On October 21, 1997, we presented the talk, "Engineering Approach for Water-Shutoff Treatment Design," at the Best-Practices Forum in Calgary, Alberta, Canada.

On October 8, 1997, we presented SPE paper 38835 and the talk, "Sizing Gelant Treatments in Hydraulically Fractured Production Wells," at the 1997 SPE Annual Technical Conference and Exhibition in San Antonio, Texas.

On September 29, 1997, we presented the poster, "Engineering Approach for Water-Shutoff

Treatment Design," at the MOBPTECH Water Management Forum in Houston.

On August 6, 1997, we presented the talk, "The Importance of Reducing Water Permeability More than Oil Permeability Through the Use of Gels," at the 3rd International Conference on Reservoir Conformance, Profile Control, and Water and Gas Shutoff in Houston, Texas.

On August 5, 1997, we presented the talk, "Engineering Approach for Water-Shutoff Treatment Design," at the North Slope Water Management Meeting in Anchorage, Alaska.

On June 19, 1997, we presented an overview of our project at the DOE's Contractor Review Meeting in Houston, Texas.

On May 20, 1997, we presented the talk, "A Strategy for Diagnosing and Attacking Water-Shutoff Problems," at the SPE Applied Technology Workshop in Dunkeld, Scotland.

From May 19 to 23, 1997, we presented "Water-Shutoff and Conformance Control Using Polymers and Gels," at the University of Petroleum, Beijing, China.

On April 29 and 30, 1997, we held a project review in Socorro, NM. The review was attended by 28 people (not including New Mexico Tech personnel) representing 16 different organizations.

On February 18, 1997, we presented SPE paper 37249 and the talk, "Further Investigations of Why Gels Reduce k_w More Than k_o," at the 1997 SPE International Symposium on Oilfield Chemistry in Houston, Texas.

On September 24, 1996, we presented the talk, "Issues Involved with Sizing Gel Treatments," at the 2nd Annual Subsurface Fluid Control Symposium and Exhibition that was held in Houston, Texas.

On August 19, 1996, we presented the paper, "What Gels Can and Cannot Do," at the 2nd International Conference on Reservoir Conformance, Profile Control, and Water and Gas Shutoff in Houston, Texas.

From July 1 to 12, 1996, we presented "Water-Shutoff in Gas Reservoirs Using Polymers and Gels," at the Chinese Petroleum Corporation in Miaoli, Taiwan.

On June 4 and 5, 1996, we held a project review in Socorro, NM. The review was attended by 27 people (not including New Mexico Tech personnel) representing 18 different organizations.

Internet Postings on the Project and Software to Download

A description of the project can be found at the following New Mexico PRRC web site: http://baervan.nmt.edu/ResSweepEffic/reservoir.htm

This web site also allows downloading of software for sizing gelant treatments in hydraulically fractured production wells.

Papers and Publications:

Seright, R.S., Seldal, M., and Liang, J.: “Sizing Gelant Treatments in Hydraulically Fractured Production Wells,” *SPE Production & Facilities* (Nov. 1998).

Seright, R.S: “Gel Dehydration During Extrusion Through Fractures,” paper SPE 39957 presented at the 1998 Rocky Mountain Regional Meeting/Low-Permeability Reservoirs Symposium, Denver, CO, April 5-8.

Seright, R.S. and Lee, Robert: “Gel Treatments for Reducing Channeling Through Naturally Fractured Reservoirs,” paper SPE 39802 presented at the 1998 SPE Permian Basin Oil and Gas Recovery Conference, Midland, TX, March 23-26.

Liang, J-T. and Seright, R.S.: “Further Investigations of Why Gels Reduce k_w More Than k_o,” *SPE Production & Facilities* (Nov. 1997) 225-230.

Seright, R.S.: “Improved Methods for Water Shutoff,” Annual Technical Progress Report (U.S. DOE Report DOE/PC/91008-4), U.S. DOE Contract DE-AC22-94PC91008, BDM-Oklahoma Subcontract G4S60330 (Nov. 1997).

Seright, R.S., Seldal, M., and Liang, J.: “Sizing Gelant Treatments in Hydraulically Fractured Production Wells,” SPE paper 38835 presented at the 1997 SPE Annual Technical Conference and Exhibition, San Antonio, Texas.

Taber, J.J., Martin, F.D., and Seright, R.S.: "EOR Screening Criteria Revisited—Part 1: Introduction to Screening Criteria and Enhanced Recovery Field Projects," *SPE Reservoir Engineering* (Aug. 1997) 189-198.

Taber, J.J., Martin, F.D., and Seright, R.S.: "EOR Screening Criteria Revisited—Part 2: Applications and Impact of Oil Prices," *SPE Reservoir Engineering* (Aug. 1997) 199-205.

Seright, R.S.: “Improved Methods for Water Shutoff,” DOE Report DOE/PC/91008-1, Contract No. DE-AC22-94PC91008, BDM-Oklahoma Subcontract No. G4S60330, U.S. Department of Energy (Aug. 1997).

Seright, R.S.: "Use of Preformed Gels for Conformance Control in Fractured Systems," *SPE Production & Facilities* (Feb. 1997) 59-65.